Synthesis and Biological Evaluation of Artificial Metalloproteases Based on Amphiphilic Cyclen Derivatives

Inaugural-Dissertation to obtain the academic degree
Doctor rerum naturalium (Dr. rer. nat.)
submitted to the Department of Biology, Chemistry and Pharmacy of
Freie Universiät Berlin

by

Chrischani Perera-Bobusch (M. Sc.)
from Berlin.

2015

The present work was carried out under the supervision of Prof. Dr. Nora Kulak from August 2012 to December 2015 at the Institute of Chemistry and Biochemistry, at Freie Universität Berlin.

First Referee: Prof. Dr. Nora Kulak

Second Referee: Prof. Dr. Biprajit Sarkar

Date of Defense: 24.02.2016

— “Back off me, I’m a scientist!” —

Dr. Peter Venkman, Ghostbusters

Vorwort

Zuerst möchte ich mich bei Prof. Dr. Nora Kulak bedanken für die Themenstellung dieser Arbeit und für viele interessante Diskussionen, Anregungen und Ratschläge.

Prof Dr. Biprajit Sarkar möchte ich herzlich für die Ãœbernahme des Zweitgutachtens danken.

Dr. Stefanie Wedepohl und Dr. Jens Dernedde danke ich für die Durchführung der Cytotoxizitätsstudien.

Prof. Dr. Michael Gradzielski möchte ich für Einführung in die â€žPyren 1:3 ratioâ€œ Methode danken und für die Hilfe bei der Auswertung der Daten.

Chris Weise möchte ich ganz besonders danken, nicht nur für die Aufnahme etlicher MALDI-Spektren sondern auch für viele gute Ratschläge.

Dr .Kai Licha danke ich für die großzügigen Cyclen-Spenden. Dr. Larissa Müller danke ich für die ICP-MS-Messungen. Mein Dank gilt auch den Mitarbeitern der Service Abteilungen für die schnelle und gewissenhafte Bearbeitung meiner Aufträge danken.

Den Studenten die mich im Laufe meiner Promotion unterstützt haben möchte ich für ihre Arbeit und ihre Ideen danken.

Großer Dank gilt der gesamten Arbeitsgruppe Kulak. In den letzten Jahren sind aus Kollegen Freunde geworden und die Unterstützung und Diskussionen in dieser Zeit haben nicht nur meinen Arbeitsalltag bereichert.

Meinen Freunden möchte ich für die Motivation in den letzten Monaten danken. Mir war bisher nicht klar wieviel ein paar nette Worte manchmal ausmachen können! Meiner Familie danke ich für ihr Interesse und ihre Unterstützung.

Meinem Mann, Bernhard Bobusch, möchte für so vieles danken: Du hast mir in den letzten Monaten immer den Rücken freigehalten, mich unterstützt und wieder aufgebaut, wenn es mal nicht so lief. Ich kann dir nicht genug danken, versuche es an dieser Stelle aber trotzdem. LARF!

Zusammenfassung

Zahlreiche Krankheiten, wie z.B die Parkinson-Krankheit, die Alzheimer-Krankheit und Diabetes mellitus Typ II, werden durch die **Fehlfaltung** spezifischer Proteine und der daraus resultierenden Bildung von Aggregaten ausgelöst. Besonders die **Alzheimer-Krankheit** hat in den letzten Jahren ein ansteigendes wissenschaftliches Interesse erfahren, ausgelöst durch neue Einblicke in die Entstehung dieser komplexen Erkrankung.

Für die Behandlung der Alzheimer-Krankheit wurden verschiedene Strategien entwickelt. Die Spaltung der pathogenen, fehlgefalteten Proteine und ihrer Aggregate mit Metallkomplexen als **künstliche Proteasen** ist eine dieser Strategien. Für die **Cu(II)- und Co(III)-Komplexe des Cyclens** konnte proteolytische Aktivität nachgewiesen werden. Zahlreiche Derivate wurden seitdem basierend auf dem Cyclen-Grundgerüst untersucht, um diese Aktivität zu steigern.

Im Rahmen der vorliegenden Arbeit wurden monoalkylierte Derivate des Cyclens und entsprechende Oxa- und Dioxa-Analoga dargestellt. Mit Komplexen dieser amphiphilen Verbindungen wurde der Einfluss von **Mizellenbildung** auf die Spaltaktivität gegenüber verschiedenen Modell-Proteinen untersucht. Fünf amphiphile Liganden und deren Cu(II) Komplexe konnten synthetisiert werden. Zwei Co(III) Komplexe basierend auf den dargestellten Liganden konnten ebenfalls synthetisiert werden.

Die proteolytische Aktivität wurde mittels SDS-PAGE (sodium dodecyl sulfate polyacrylamide gel electrophoresis) mit verschiedenen Proteinen untersucht. Ein Anstieg um mindestens **zwei Größenordnungen** konnte mit allen Komplexen im Vergleich zu Cu(II)-Cyclen nachgewiesen werden.

Ein Vergleich von Cyclen-Derivaten mit unterschiedlicher Kettenlänge zeigte die Abhängigkeit der Aktivität von der Anzahl der CH_2-Gruppen in der Alkylkette, wobei das Derivat mit dem längsten Alkylrest die höchste Aktivität zeigte. Obwohl ein Anstieg der Aktivität für die Oxa-Spezies erwartet wurde, konnte die höchste Aktivität aller Komplexe für Co(III)-Hexadecylcyclen nachgewiesen werden.

Bemerkenswert war die proteolytische Aktivität der Liganden, die vergleichbar war mit der Aktivität der Komplexe. Weitere Nachforschungen sind notwendig, um Metallspuren als Quelle dieser Aktivität auszuschließen. Für Hämproteine zeigte sich ein Abfall der proteolytischen Aktivität ab einer bestimmten Komplexkonzentration, wohingegen die Spaltaktivität gegenüber Proteinen ohne Hämgruppe mit der Konzentration der spaltenden Spezies steigt. Um diesen Sachverhalt zu klären, werden derzeit Molecular Modeling-Studien durchgeführt.

Fragmente der Spaltung von Myoglobin konnten mittels MALDI-TOF (Matrix-assisted laser desorption/ionization time-of-flight) Massenspektrometrie nachgewiesen werden. Eines dieser Fragmente kann einer Spaltung nahe der Hämgruppe zugeordnet werden. Die entsprechende Spaltstelle wurde bereits in der Literatur mit einem anderen Cyclen-Derivat als erste

Schnittstelle im Spaltprozess zugeordnet. Die Ergebnisse dieser Untersuchungen lassen eine Schlüsselrolle für die Hämgruppe bei der Spaltung von Hämproteinen vermuten.

Cytotoxizitätsstudien mittels MTT (3-(4,5-Dimethylthiazol-2-yl)-2,5-diphenyltetrazoliumbromid)-Assay zeigten einen deutlichen Anstieg der **Toxizität** der Komplexe von 1-Dodecylcyclen im Vergleich mit den entsprechenden Cyclen-Komplexen. Jedoch ist die Toxizität vergleichbar mit anderen Spezies, die derzeit als mögliche Alzheimer-Therapeutika untersucht werden.

Die **kritische Mizellenkonzentration** der Komplexe wurde mit der „Pyren 1:3-Methode“ untersucht, einer auf Fluoreszenz basierenden Methode. Die ermittelten Werte liegen zwischen **0.04-0.47 mM**. Die hier dargestellten Ergebnisse, insbesondere die hervorragende Spaltaktivität der untersuchten Komplexe, legen weitere Studien mit amphiphilen Cyclenderivaten nahe. Die alkylierten Cyclenkomplexe weisen eine deutlich weniger komplexe Struktur auf als die meisten anderen künstlichen Proteasen, zeigen aber eine vergleichbare proteolytische Aktivität auf. Die gezielte Spaltung pathogener Proteine könnte in Zukunft durch die Einführung selektiver Gruppen ermöglicht werden.

Abstract

Numerous diseases are caused by the **misfolding** of specific proteins and the subsequent formation of aggregates, for example Parkinson's disease, type II diabetes and **Alzheimer's disease** (AD).

In the last years the scientific interest in AD has grown remarkably due to new insights into the development of this complex disorder. Numerous therapeutic strategies have been developed for the treatment of AD. Cleavage of pathogenic misfolded proteins and their aggregates with small metal complexes acting as **artificial proteases** is one of them.

Cu(II) and Co(III) complexes of the macrocycle **cyclen** were shown to cleave proteins and numerous derivatives have already been synthesized to improve the proteolytic activity.

In the scope of the present thesis monoalkylated derivatives of cyclen and its oxa and dioxa analoga were synthesized. Amphiphilic metal complexes of these ligands were generated to investigate the influence of **micelle formation** on the proteolytic activity of cyclen. Five ligands and their Cu(II) complexes as well as two Co(III) complexes were synthesized.

The protein cleavage ability was investigated *via* SDS-PAGE (sodium dodecyl sulfate polyacrylamide gel electrophoresis) with various model proteins. An increase of at least **two orders of magnitude** was observed with all seven complexes compared to the corresponding cyclen compounds. A comparison of the cyclen complexes of varying alkyl chain length could show that the proteolytic activity depends on the number of CH_2 groups in the chain with the longest alkyl moiety being the most effective cleavage agent. The highest activity of all complexes could be detected with the Co(III) complex of 1-hexadecylcyclen, even though an improvement of the activity was expected for the oxa analoga of the same chain length.

Remarkably, the ligands alone exhibited a comparable proteolytic activity to the complexes. Further investigations are necessary to exclude traces of metal as origin for this activity. An interesting finding was the decrease of the proteolytic activity above a certain complex concentration towards **heme proteins**, whereas non-heme protein cleavage increases consistently with the complex concentration. Molecular modeling studies are underway to further investigate these results.

Fragments of the cleavage process were detected by MALDI-TOF (Matrix-assisted laser desorption/ionization time-of-flight) mass spectrometry. One of the fragments found in these studies reflects a specific cleavage site in proximity to the heme group of myoglobin already established in the literature as initial cleavage site of another cyclen derivative. These findings suggest a key role for the heme group in the cleavage process of heme proteins.

Cytotoxicity studies *via* MTT (3-(4,5-dimethylthiazol-2-yl)-2,5-diphenyltetrazolium bromide) assay showed a drastic increase of the **cytotoxicity** for the complexes of 1-dodecylcyclen compared to cyclen. However, in comparison with other compounds currently under investigation for the treatment of AD the cytotoxicity is moderate. The **critical micellar**

concentration of the complexes was observed with the "pyrene 1:3 ratio" method, a technique based on fluorescence, and the values range from **0.04 - 0.47 mM**. No distinct relation could be found for the formation of micelles and the cleavage activity.

The results presented in this work, in particular the outstanding proteolytic activity of the complexes, suggest further studies with amphiphilic cyclen derivatives. The alkylated complexes have a rather simple structure compared to other artificial proteases but exhibit a comparable cleavage activity towards all model proteins. Targeted cleavage of pathogenic proteins might be achieved by introduction of recognition sites to the amphiphile.

Contents

List of Figures

List of Schemes

List of Acronyms

AD	Alzheimer's Disease
APP	Amyloid Precursor Protein
BSA	Bovine Serum Albumin
C'	C-terminus
CA	Carbonic Anhydrase
cmc	critical micelle concentration
cyclen	1,4,7,10-tetraazacyclododecane
d	dublet
DCM	Dichloromethane
DMAP	4-Dimethylaminopyridine
DMF	Dimethylformamide
DOTA	1,4,7,10-tetraazacyclododecane-1,4,7,10-tetraacetic acid
EDTA	Ethylenediaminetetraacetic acid
f.l.t.r.	from left to right
FRET	Förster Resonance Energy Transfer
m	multiplet
MALDI	Matrix-assisted Laser Desorption/Ionization

MTT	3-(4,5-Dimethylthiazol-2-yl)-2,5-diphenyltetrazolium bromide
N'	N-terminus
oxacyclen	1-oxa-4,7,10-tetraazacyclododecane
PCD	Poly(chloromethylstyrene-co-divinylbenzene)
ppm	parts per million
ROS	Reactive Oxygen Species
s	singlet
SDS-PAGE	Sodium Dodecyl Sulfate Polyacrylamide Gel Electrophoresis
SEM	Standard Error of the Mean
t	triplet
tacn	1,4,7-triazacyclononane
THF	Tetrahydrofurane
TOF	Time Of Flight

CHAPTER 1

Introduction

1.1 Proteins and proteases

Proteins, like nucleic acids and polysaccharides, are essential building blocks of life occurring in all organisms. These macromolecules are made from amino acids connected by peptide bonds as shown examplarily on a tripeptide in Fig. 1.1.

Fig. 1.1: A tripeptide with peptide bonds shown in red.

Proteins have uncountable functions, ranging from signal transduction over enzymatic and immunoregulatory reactions to structural features. Biosynthesis of proteins takes place at the ribosomes with the information about the amino acid sequence derived from DNA *via* mRNA. Degradation of proteins is necessary for regulatory processes and to regenerate amino acids for protein synthesis. The half life of an amide bond ranges from 160 – 600 years.[1–3] To accelerate the cleavage of peptide bonds specific enzymes, namely proteases and peptidases, are necessary. Two main pathways are known for the intracellular degradation of proteins in eukaryotic cells.

For the lysosomal pathway the proteins are enclosed in lysosomes (membrane enclosed vesicles) and are degraded by a number of different proteases which are active under the acidic conditions inside the lysosome (Scheme 1.1, left). Lysosomal

degradation depends on the proteins destined for degradation and other participants like autophagosomes and endosomes.[4]

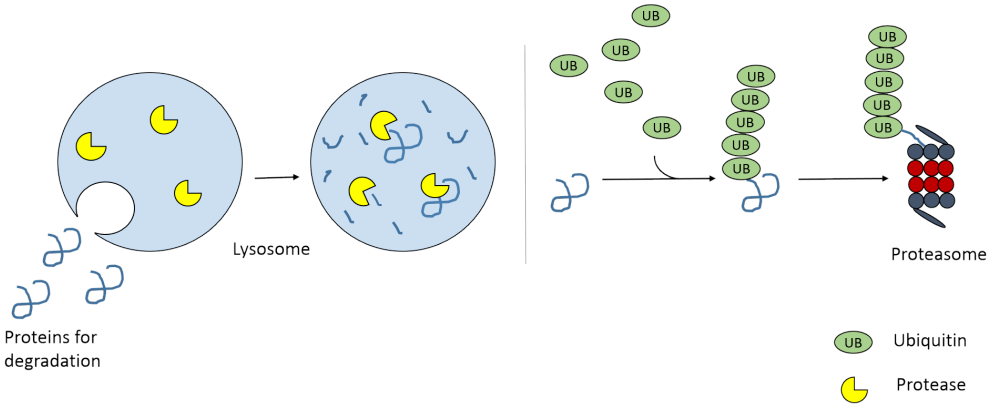

Scheme 1.1: Degradation of proteins in eukaryotic cells by the lysosomal (left) and ubiquitin-mediated pathway (right).

The ubiquitin-mediated pathway is, in contrast to lysosomal degradation, a specific process. Proteins are tagged with ubiquitin in an enzymatic reaction by formation of a covalent bond. This process repeats itself resulting in an polyubiquitin chain at the protein. This motif activates the proteasome, a large protein complex which hydrolyzes the peptide bonds of the tagged proteins (Scheme 1.1, right).[5]

Proteases are not only active in protein regulation but also in protein-protein interactions, signal transduction, protein activation and many other processes. The variety of proteases can be divided into endo- and exoproteases. Exoproteases target their substrates from the C- and N-termini all proteins have in common, whereas endoproteases cleave internal peptide bonds. Another classification distinguishes proteases into six classes according to the functional group introducing cleavage. Cysteine, serine and threonine proteases induce hydrolysis with the side chain of the eponymous amino acid as nucleophile. Aspartic, glutamic and metalloproteases apply an activated water molecule as nucleophile. This diversity in the action of proteases and the variety of applications has led to an enormous scientific interest in this substance class.[6]

1.2 Proteins and disease

The folding of proteins is a very complex process which is not fully understood to date. During or after their synthesis, proteins fold themselves caused by interactions of the amino acids in order to obtain their functional three-dimensional structure. The folding takes place in split seconds to afford the protein in its native state.[7] Often chaperones or enzymes are necessary to help the protein finding its kinetically favourable state and in some cases they do not find it at all. It is assumed that at least 30% of all proteins are misfolded.[8]

Misfolding occurs due to mistakes in transcription or translation or environmental effects like oxidative stress, extreme pH or temperature. Ageing appears to be another factor promoting misfolding since most related diseases occur predominantely with elderly patients.

Misfolding or partial unfolding of proteins can cause the loss of their function and moreover generate toxic species. In many cases misfolded proteins are recognized and degraded by the cell's protein quality control but in some cases misfolded proteins are not detected and can cause diseases.[9] Alzheimer's, Parkinson's and Huntington's diseases as well as type II diabetes and prion disease are just some of the maladies caused by the misfolding of a specific protein. Disease can be caused simply by the loss of the protein's functionality but in many cases aggregation of misfolded proteins causes pathogenic species.

Misfolded proteins are often much more aggregation-prone compared to their native state analoga. The aggregation process consists of a nucleation and an elongation phase (Scheme 1.2). The misfolding of the monomers and the formation of oligomers are energetically unfavorable. Hence, the equilibrium of the reaction is shifted to the native state monomer in a healthy organism and the nucleation is the rate-determining step in the aggregation process. The formation of protofibrils introduces the elongation phase and is energetically more favorable. The generation of fibrils from protofibrils is the final step of the elongation phase and has the lowest energy. The equilibrium is completely shifted to the generation of fibrils.[10]

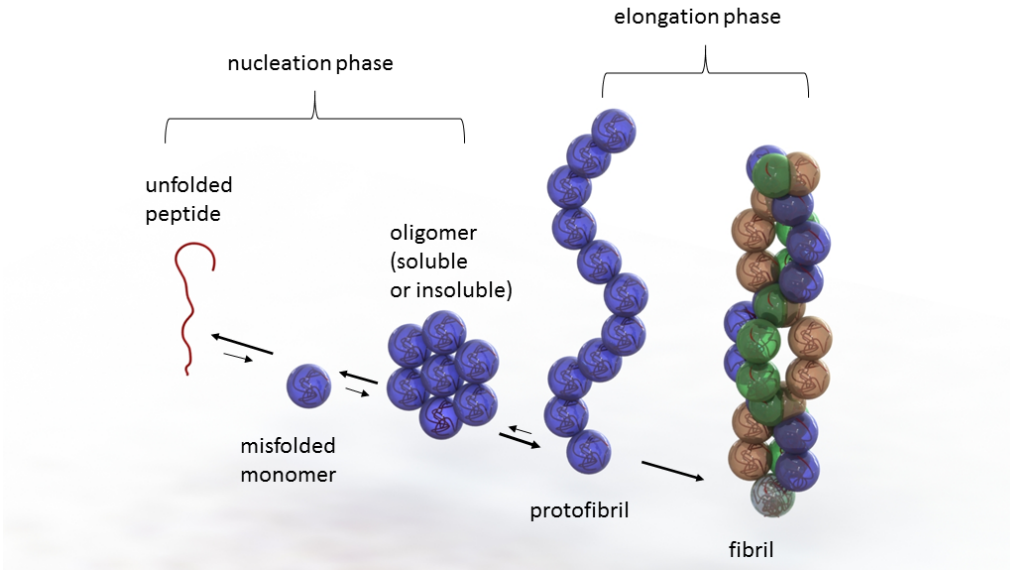

Scheme 1.2: Aggregation process of misfolded proteins.

Those fibrils have a diameter of about 10 nm and can have a length of several 100 μm. They constitute deposits like the characteristic extracellular plaques found in the brains of patients suffering from Alzheimer's disease (AD). The misfolded proteins exhibit an increased amount of β-sheet structures which pile up forming fibrils.[10] For a long time the fibrils were expected to be the most pathogenic species in the development of AD but increasing evidence suggest that soluble oligomeric species are more toxic.[11]

Different strategies were developed for the treatment of protein misfolding diseases.[12] **Stabilization of the native state** with small molecules could prevent the formation of aggregates.[13] Moreover, small molecules could be applied to **inhibit growth of aggregates** by binding to oligomers or fibrils.[14] **Gene therapy** could be applied to reduce the propensity of a specific protein to aggregate *via* mutation.[15] The **inhibition of proteases** which generate aggregation-prone peptides from precursor proteins is another therapeutic strategy under investigation.[16,17] Examples for such proteases are β and γ-secretase which cleave the amyloid precursor protein (APP) to the aggragation-prone peptides Aβ40 and Aβ42. Both peptides are related to Alzheimer's disease. Finally, **dissolving aggregates of misfolded proteins** might lead to symptom alleviation or even curing of the corresponding diseases. For

this strategy **antibodies** have proven succesful in clearing Aβ deposits *in vivo*.[18,19] Another strategy is the cleavage of aggregation products with **artificial proteases**, organic or metal complexes, cleaving the amide bonds of the proteins backbone. This promising strategy will be further discussed in the upcoming sections.

1.3 Alzheimer's disease

Alzheimer's disease is the most common cause of dementia.[20] With a worldwide rising life expectancy more and more people suffer from this age-related disorder. Today, over 46 million people are affected by dementia and, according to estimates, this number will almost triple to 131.5 million in 2050. The worldwide annual costs of dementia are estimated to 818 billion US $.[21] Therefore, AD is not only a personal burden for those who are affected by the disease and their families but also underway to become an economical disaster.

Alzheimer's disease is a multifactorial disorder. Consequently, a number of factors have to be taken into account to find a therapy and not all parts of the puzzle have been found yet. Various hypotheses have been proposed about the development of Alzheimer's disease with the amyloid cascade hypothesis being the most prominent. According to this theory deposits of the misfolded Aβ peptide are the cause for AD. The Aβ peptides with a length of 40 (Aβ40) and 42 (Aβ42) amino acids are the main peptides generated from the cleavage of APP by β- and γ-secretase and can be found in high concentrations in amyloid aggregates. In healthy brains Aβ peptides are present in solution and Aβ40 is the more prevalent form. In AD-affected brains soluble and insoluble oligomers of Aβ can be found. In the deposits Aβ42 is particularly enriched .[22] The longer of the two peptides has two additional hydrophobic amino acid residues, alanine and isoleucine, and is more aggregation-prone and toxic towards neurons .[23,24] Cleavage of the misfolded peptides by increasing the activity of natural proteases or by the application of specific artificial proteases could dissolve the deposits and is one of the strategies pursued to find a cure for AD.

The fact that Aβ aggregates are focal and not distributed all over the brain although the peptides are ubiquitously expressed gave rise to doubts on the amyloid cascade hypothesis. An increased concentration of Aβ alone could not be the single cause for AD. Moreover, the concentration of Aβ does not increase with age although AD is an age-dependent disease, whereas the brain serum concentration of copper

increases throughout life .[25] Therefore, Bush and Tanzi hypothesized that a disturbed metal homeostatis might influence the aggregation of Aβ[26]. Copper, zinc and iron ions were found in high concentrations in amyloid plaques and these transition metals were shown to promote Aβ aggregation.[27–30] Moreover, metal chelators were shown to dissolve amyloid deposits.[31,32] It has been assumed that reduction of the metal ions by Aβ peptides could trigger oxidative stress and generate reactive oxygen species (ROS), particularly H_2O_2 and ·OH in a Fenton-type reaction.[33] ROS can cause lipid peroxidation, protein carbonyl modifications and DNA oxidation adducts. This assumption is supported by studies which have shown that the antioxidants Vitamine E and curcumin had a neuroprotective effect in animal models and could reduce the level of insoluble Aβ peptides or prevent their formation.[34,35] A bimodal approach with a chelator with antioxidant properties exhibited promising results in preventing copper-induced amyloid aggregation and in dissolving aggregates.[36]

1.4 Artificial proteases

Naturally occuring proteases can be divided into metallo- and non-metalloproteases with the latter gaining their proteolytic activity from amino acid side chains. Only a small fraction of their artificial mimicry is based on organic functional groups.[37–39] The advantage of metal complexes is their versatility. Multiple roles of the proteolytic reaction can be adopted by the metal ion and its aqua and hydroxido ligands in aqueous solution. The precise interaction of two or more organic functional groups would be necessary to perform these functions without a metal ion. The redox activity or Lewis acidity of the metal ion can be exploited. Throughout the reaction it can polarize the carbonyl group of the peptide bond due to the latter property, induce strain into the reaction center and serve as a template to convert an intermolecular into an intramolecular reaction.[40] Moreover, a hydroxyl group bound to the metal center can act as nucleophile and a coordinated water molecule as a general acid.[41] In general, two modes of action can be distinguished for metal-induced cleavage: oxidative and hydrolytic reactions.

For oxidative cleavage, the oxidation state of the metal changes throughout the reaction in the presence of a reducing agent. The generation of H_2O_2 from O_2 is catalyzed by the reduced metal and subsequently other ROS such as ·OH are formed.

These species abstract the proton at C_α (Scheme 1.3, shown in red) followed by oxidation of the same carbon atom.

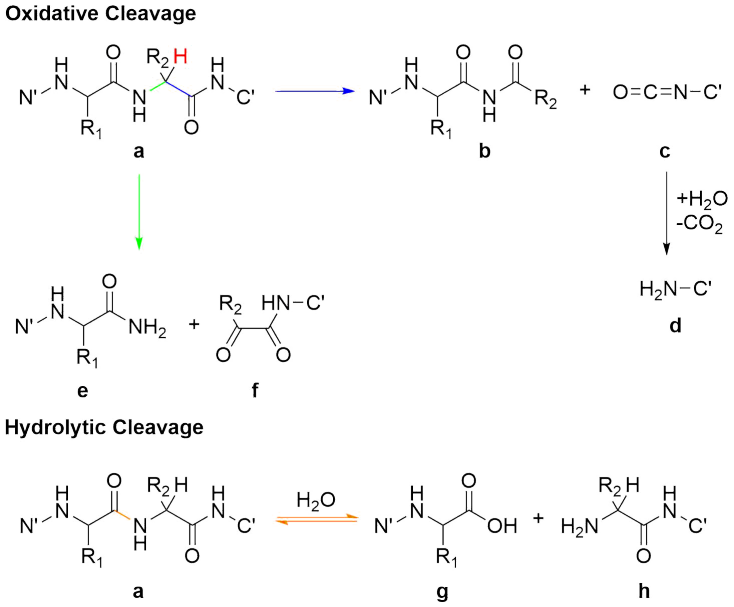

Scheme 1.3: Mechanisms of cleavage exploited by artificial proteases.

The actual bond cleavage can occur between C_α and the adjacent nitrogen atom (Scheme 1.3, shown in green) giving a N-terminal (N') fragment **e** with a C-terminal amine and a C-terminal (C') fragment **f** with a blocked N-terminus. Another site for oxidative cleavage is the bond between C_α and the adjacent carbonyl C-atom (Scheme 1.3, shown in blue) resulting in a N-terminal fragment **b** with a C-terminal acyl amide and a proposed unstable intermediate **c** which is hydrolyzed to a C-terminal fragment **d** with a free N-terminus and carbon dioxide.[42] Fragments of hydrolytic cleavage are an N-terminal species **g** with a free carboxy terminus and a C-terminal species **h** with a free amino terminus (Scheme 1.3, shown in orange). The generation of two new peptides makes this approach particularly attractive. The proposed mechanism for hydrolytic cleavage will be illustrated on a specific example in the following section.

The development of metal-based artificial proteases began with the finding that several metal ions (e.g. Ce(IV), Zn(II), Co(II), Ni(II) and Cu(II)) exhibit the ability to catalyse the hydrolysis of peptide bonds.[43,44,45] In many cases only specific

peptide bonds were cleaved and the rates were moderate. The introduction of defined metal complexes instead of metal salts can enhance solubility and stability and moreover, organic functional groups in the ligand sphere can interact with the peptides and enhance the proteolytic activity. Hence, small molecules based on metal complexes might represent a promising alternative for natural enzymes. Complexes were generated from numerous ligands and metal ions (e. g. Co(III), Cu(II), Fe(II), Ni(II), Pd(II), Pt(II) and Zn(II)).[46]

Collman and Buckingham investigated the cleavage activity of a Co(III) complex of trien, β $[Co(trien)OH(H_2O)]^{2+}$, towards small peptides (Fig. 1.2).

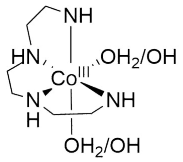

A

Fig. 1.2: Co(III)trien **A**, an artificial protease.

Cleavage occurs at the N-terminus of the peptide and conjugates of the complex with amino acids could be detected.[47] Hence, complex **A** does not act catalytically which would be preferable for various applications.

Several studies were performed with Fe(II) EDTA derivatives as oxidative cleavage agents.

With complex **B** selective cleavage of calmodulin could be accomplished. Trifluoperazine, as a calmoduline antagonist, served as recognition site whereas EDTA was induced as iron chelator (Fig. 1.3).[48]

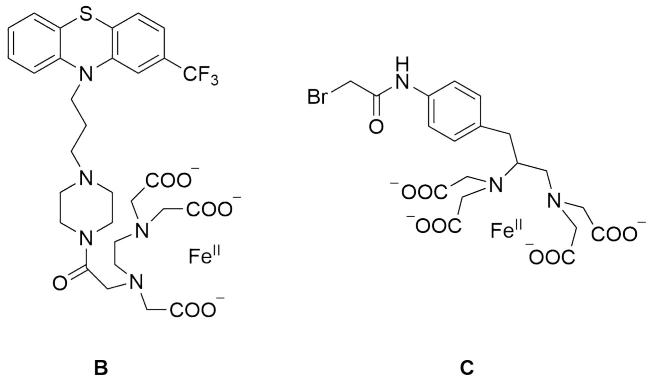

Fig. 1.3: Fe(II) EDTA complexes for protein cleavage.

Similarly, BSA was cleaved at two specific bonds by complex **C**, Fe(II) 1-(*p*-bromoacetamidobenzyl)-EDTA.[49] In both cases reducing agents had to be added to induce cleavage.

Hydrolytic cleavage of sulfur-containing peptides could be detected with palladium aqua complexes, cisplatin (*cis*-$[PtCl_2(NH_3)_2]$) and molybdocene dichloride.[50–52] The complexes bind to the sulfur group of cystein or methionine and cleave peptide bonds in proximity to their anchoring site. For the platinum and molybdenum species cleavage was not catalytic and high concentrations of the cleavage agents were necessary for the palladium complex.

Copper is the most prominent metal applied for artificial proteases. With a high redox activity and Lewis acidity complexes of copper can perform oxidative as well as hydrolytic cleavage reactions.

Kito *et al.* were able to show that Cu(II) phenanthroline **D** cleaves proteins in presence of β-mercaptoethanol (Fig. 1.4).[53]

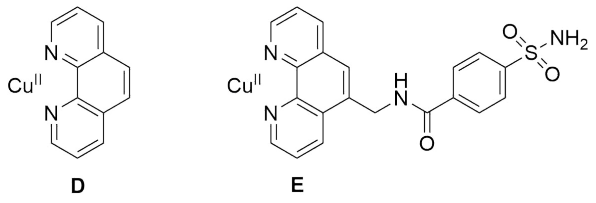

Fig. 1.4: Cu(II) phenanthroline complexes with proteolytic activity.

Sigman *et al.* introduced a known inhibitor of the metalloenzyme carbonic anhydrase (CA), namely 4-carboxybenzene-1-sulfonamide, to Cu(II) phenanthroline and detected a discrete set of CA fragments in the presence of ascorbate.[42]

Hydrolytic cleavage of BSA without any reducing agents near pathological pH was detected with the Cu(II) complex of 1,4,7-triazacyclononane (tacn) **F** but the reaction was remarkably slow (Fig. 1.5). To cleave about 15% of the protein 13 days of incubation at 50 °C were necessary.[54]

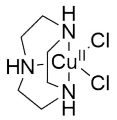

F

Fig. 1.5: Cu(II) complex of 1,4,7-triazacyclononane for protein cleavage.

A new level of activity was achieved by Suh *et al.* with derivatives of the Cu(II) and Co(III) complexes of cyclen (1,4,7,10-tetraazacyclododecane). Whereas complexes of the bare macrocycles exhibit a comparable activity to Cu(II) tacn, various derivatives of cyclen exhibit a proteolytic activity increased by multiple orders of magnitude.[55] The simple substitution of one nitrogen atom with oxygen in the macrocyle induced a remarkable increase of the cleavage activity towards multiple proteins.[56,57] This improvement was explained with the enhanced Lewis aciditity of the metal ion with the oxacyclen ligand **2** compared to cyclen **1** (Fig. 1.6).

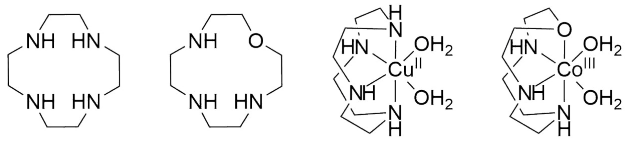

1 **2** Cu(II) **1** Co(III) **2**

Fig. 1.6: Cyclen and oxacyclen and its Cu(II) and Co(III) complexes.

Moreover, a reduction of steric strain for the tetrahedral intermediate generated in the course of the hydrolytic reaction (see mechanism in section 1.5) might have a beneficial influence on the proteolytic activity.

Two other strategies to improve the cleavage activity of cyclen were the linking of the macrocycle to PCD (Poly(chloromethylstyrene-co-divinylbenzene)) and the introduction of aldehyde groups in proximity to the macrocycle.[41,58,59] With a

combination of both approaches complex **G** with a remarkable proteolytic activity could be generated (Fig. 1.7).[60]

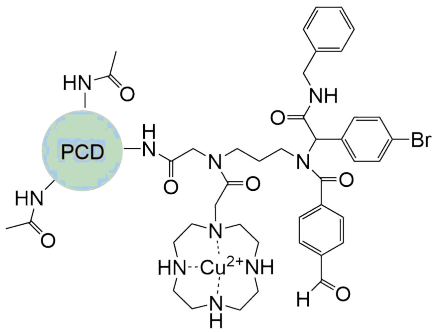

G

Fig. 1.7: Cyclen derivative with PCD backbone and aldehyde group.

The hydrophobic microenvironment of the polymer was supposed to enhance polar interactions of the enzyme-substrate complex and therefore stabilize the transition state.[61] The aldehyde group was introduced as binding site for ε-amino groups of lysine residues and is supposed to facilitate the approach of the complex to the protein.[60]

The first small molecules acting as artificial proteases selective towards pathogenic compounds (h-IAPP, the misfolded species in type II diabetes, and Aβ42) were prepared with cyclen complexes as catalytic cleavage moieties and aromatic moieties as recognition sites (Fig. 1.8). Selectivity was confirmed by the absent proteolytic activity towards several non-pathogenic peptides.[62–64]

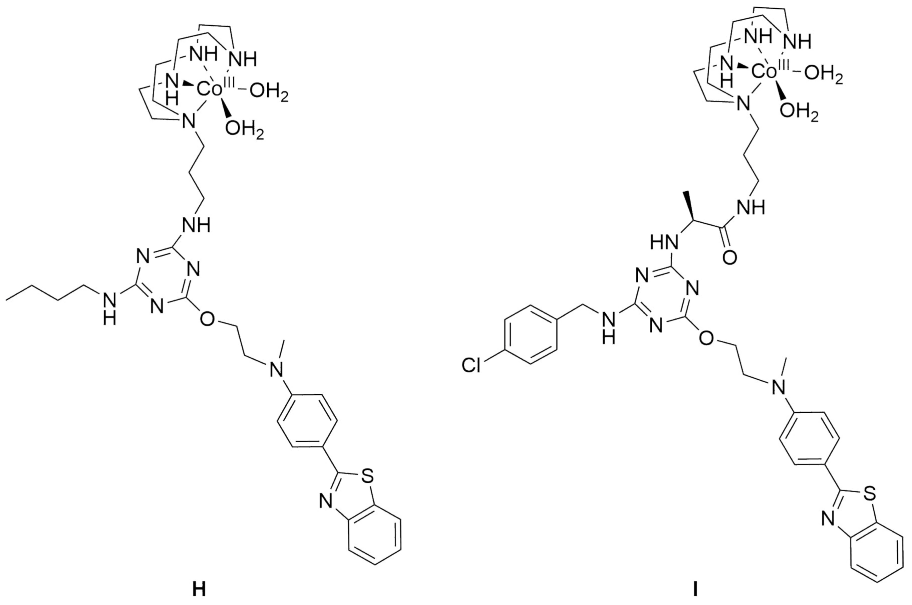

Fig. 1.8: Selective artificial proteases for h-IAPP (left) and Aβ (right) based on the cyclen moiety.

A bimodal approach for AD treatment applies a cyclen bearing ligand to sequester copper ions from Aβ deposits. The generation of the copper complex activates the peptide cleaving species.[65] A short peptide sequence was applied as recognition site.

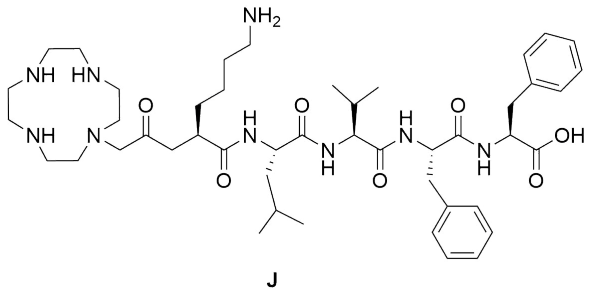

Fig. 1.9: Ligand for the sequestration of Cu from Aβ with subsequent activation of the generated protease.

The results of this study confirmed that cyclen derivatives are promising candidates as AD therapeutics.

1.5 Cyclen-mediated protein cleavage

The mechanism of protein cleavage by cyclen complexes was detected as catalytic hydrolysis reaction.

Experiments propose polarization of a carbonyl bond of the peptide backbone by the metal ion to induce the cleavage reaction for Co(III) complexes of cyclen shown in Scheme 1.4.[66,67] The nucleophilic attack on the same bond by a metal-bound hydroxide ion leads to the formation of a tetrahedral intermediate. A proton is transferred to the amine group and the four-membered ring collapses. Cleavage products are two fragments with an amine and a carboxy-terminus, respectively, whereas the complex is regenerated.

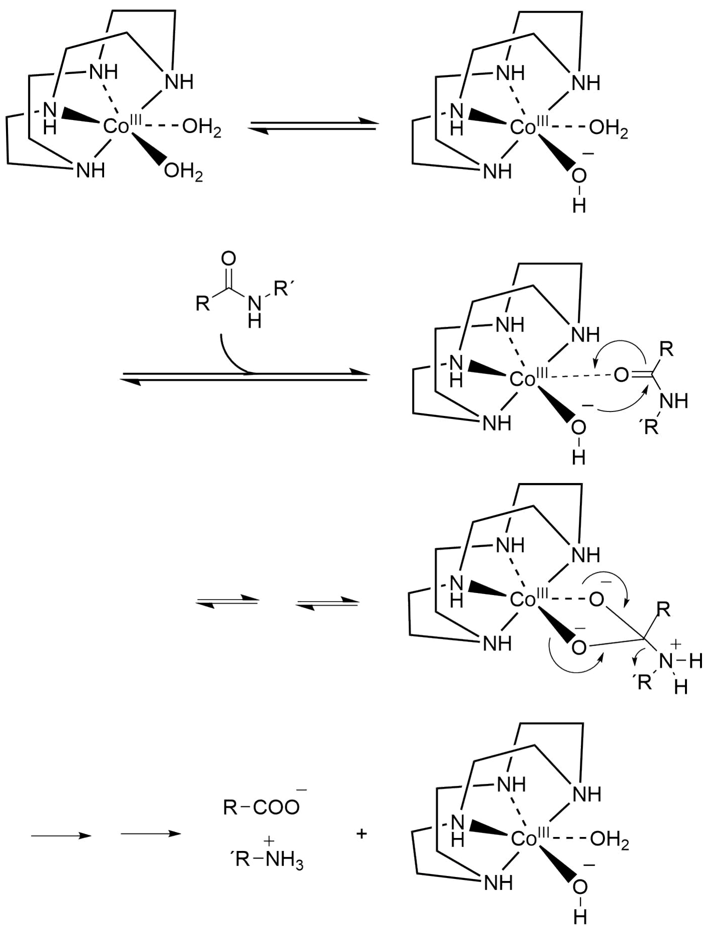

Scheme 1.4: Proposed mechanism for protein cleavage by Co(III) cyclen. Adapted from [68].

The stability of the four-membered ring was proposed to be rate-determining and is dependent on the Lewis acidity of the metal ion and the geometry of the complex formed with the substrate.[68]

1.6 Applications for artificial proteases

About 60% of all enzymes sold worldwide are proteases, particularly because this substance class is vital for the detergent and dairy industry[69,70]. Moreover, proteases are necessary for various biotechnological applications such as protein sequencing, protein engineering and protein footprinting.[71–75]

Disadvantages of natural proteases for industrial and biotechnological purposes are low thermal and chemical stabilities, strong pH dependence, and high expenses. Small molecule mimicry could be designed to overcome these limiting factors.

For pharmaceutical applications a catalytic mode of action is not only more economic but also allows lower dosage. Whereas conventional drugs targeting disease-related proteins such as receptors or enzymes have to be administered stoichiometrically to inhibit their target's action, catalytic drugs allow lower dosage and therefore minimize side effects (Fig. 1.10).

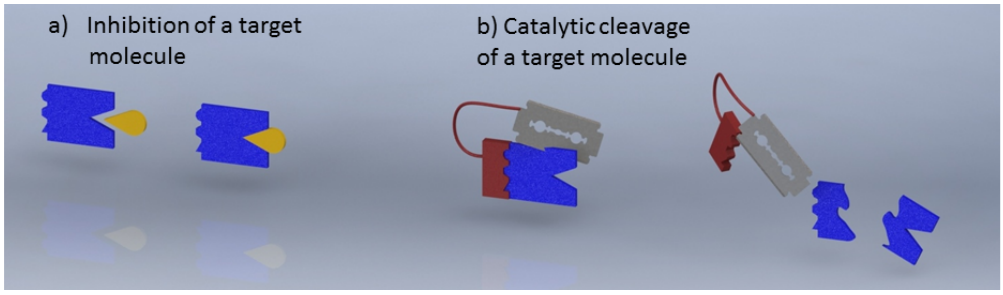

Fig. 1.10: Comparison of inhibition (a) and cleavage (b) of a target molecule.

In contrast to widely used inhibitors, catalytic proteases do not necessarily have to target the active site of proteins. Any part of the protein can be established as recognition site to gain specificity. High affinity binding is not necessary if the cleavage process is fast enough. The requirements for an artificial protease targeting pathogenic proteins are:

- high activity at physiological conditions
- specific cleavage
- low dosage, i.e. *via* catalytic cleavage
- low toxicity
- high effectivity

1.7 Micelles and aggregates for pharmaceutical applications

Micelles are aggregates of amphiphilic molecules. These molecules consist of a hydrophilic headgroup (Fig. 1.11, shown in blue) and a hydrophobic tail (Fig. 1.11, shown in red). At a certain concentration, the so-called critical micellar concentration (cmc), the amphiphilic molecules self-aggregate in solution. In water the hydrophilic moieties form a shell which interacts with water molecules shielding the hydrophobic residues from these interactions in the core of the micelle.

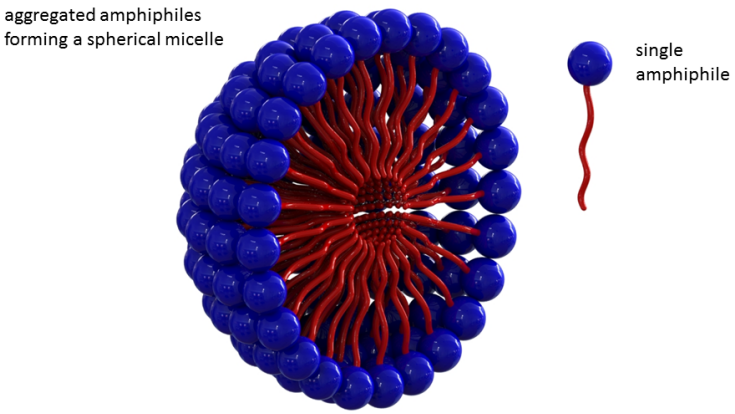

Fig. 1.11: The structure of micelles.

Micelles have been intensively investigated as drug carriers to overcome the insufficient solubility of numerous drugs.[76,77]

The application of micelles not only for the transport of drugs but also as drugs themselves is promising. Multiple examples for the improvement of the hydrolytic activity towards esters, carboxylates. and phosphates due to micelle formation can be found in the literature[78–80] For the hydrolytic cleavage of lipophilic esters micelles from a Zn(II) cyclen derivative were succesfully applied.[81] The group of KÖNIG generated micelles and vesicles (aggregates of amphiphiles with a membrane consisting of a double layer of the molecules) from Zn(II) cyclen amphiphiles for DNA cleavage and were able to show a remarkable increase of the cleavage activity compared to unimolecular non-amphiphilic complexes.[82]

1.8 Motivation

The introduction of cross-linked PCD as scaffold for Cu(II) cyclen complexes was shown to enhance the proteolytic activity.[58] An explanation for this improvement might be the higher local density of catalytic units allowing interaction with each other and the substrate. Another explanation would be the increase of polar interactions due to the hydrophobicity of the PCD backbone and the ability of hydrophobic moieties to mimic the hydrophobic microenvironment many enzymes exploit in their active sites.[41,80,83] Moreover, the proteolytic activity could be increased with multinuclear Cu(II) cyclen units connected to the PCD moiety. Tetranuclear moieties exhibited a 100-fold increase of the proteolytic activity compared to mononuclear derivatives.[41].

In this context it has to be mentioned that numerous natural hydrolases are multinuclear, which supports the assumption that the interaction of catalytic units is beneficial for their activity, e.g. by stabilisation transition states.[41]

The influence of micelle formation on the proteolytic activity of artificial proteases has, to my knowledge, not been investigated yet. Exploiting self-aggregation of amphiphilic molecules for protein cleavage is comparable to the approach of using PCD as scaffold for proteases. In both concepts the cleavage agent consists of hydrophobic and hydrophilic moieties and a high local density of catalytic units is given.

The cyclen moiety was chosen as scaffold for amphiphilic metal complexes because several artificial proteases with outstanding activity based on this macrocycle are already known.[59,60] Cu(II) and Co(III) complexes were shown to be particularly active whereas cyclen complexes from Pd(II), Pt(II), Ce(IV), Fe(III) and Hf(IV) did not show any proteolytic activity.[84]

The aim of this work was to investigate the particle formation behavior and protein cleavage ability of simple amphiphilic Cu(II) and Co(III) complexes based on the cyclen moiety. The central question of this thesis is, if the formation of aggregates, particularly micelles, influences the cleavage of proteins as it does for DNA model systems.[78,82]

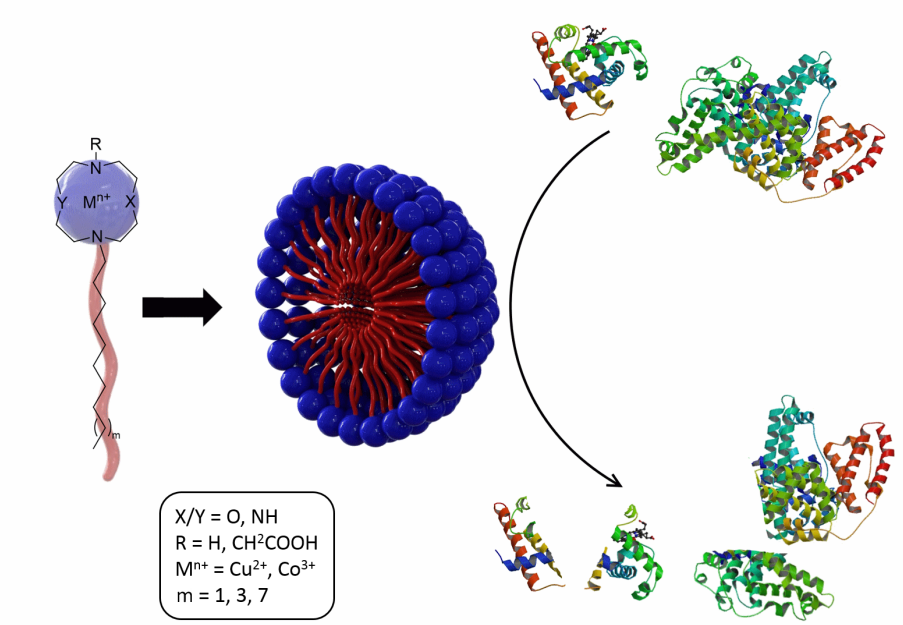

Fig. 1.12: Goals for the thesis at a glance.

I have already synthesized the Cu(II) and Co(III) complexes of 1-dodecylcyclen in the scope of my master thesis and was able to show that the cleavage could be remarkably increased compared to the corresponding complexes of the bare macrocycle.

For the present thesis I firstly wanted to investigate the influence of the alkyl chain length on proteolytic activity and aggregation behavior. Therefore, the synthesis of monoalkylated cyclen complexes with varying chain length was planned.

Secondly, the synthesis of monoalkylated oxacyclen and dioxacyclen species was planned. Regarding the improved protein cleavage of oxacyclen complexes compared to cyclen complexes, the additional substitution of another amino group with an oxygen atom might improve the proteolytic activity even further.

The introduction of a carboxyl group at the amino group oposing to the alkyl chain was planned to investigate the influence of the increased hydrophilicity of the headgroup on the aggregation behavior.

CHAPTER 2

Results and Discussion

2.1 Cyclen and its dervatives

Cyclen (1,4,7,10-tetraazacyclododecane) was first synthesized by Stetter and Mayer in 1960 and has been in the focus of many research interests due to its ability to chelate numerous metal cations since then.[85] The most prominent derivative ist DOTA (1,4,7,10-tetraazacyclododecane-1,4,7,10-tetraacetic acid) (Fig. 2.1). Gd^{3+} complexes of this macrocycle are established contrast agents for magnetic resonance imaging.

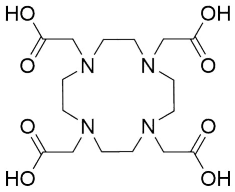

Fig. 2.1: DOTA – 1,4,7,10-tetraazacyclododecane-1,4,7,10-tetraacetic acid.

Moreover, cyclen derivatives can be installed as fluorescent and luminescent probes, antibacterial agents and as RNA, DNA and protein cleavers.[86–90] Not only cyclen itself but also the oxa and dioxa derivatives have proven interesting properties for some of these. applications[57,91,92]

For the *N*-functionalization of those macrocycles three different strategies can be found in the literature: synthesis from acyclic building blocks, alkylation of the amino groups or reaction with acylation or sulfonylation reagents.[93] For the building

block approach the macrocycle is synthesized from two compounds in a 2+2, 3+1 or 4+0 cyclization reaction where the numbers represent the heteroatoms each block contributes to the ring (Fig. 2.2).

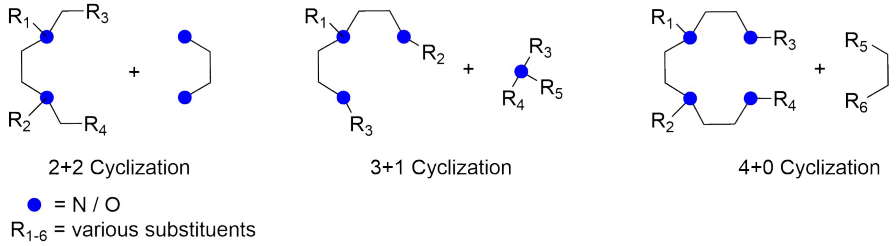

Fig. 2.2: Building block strategies for the synthesis of cyclen derivatives.

In most cases protecting groups are necessary for the ring-closing reactions to avoid polymerization and to afford the macrocycle regioselectively. The tosyl group is most commonly used as protecting group for cyclen derivatives. The final deprotection is, in general, the most critical step in the synthesis of cyclen derivatives and often poor to moderate yields are obtained. Different strategies to cleave the tosyl groups have been developed: acidic deprotection was performed with sulfuric acid or HBr in glacial acetic acid with or without phenol.[89,94,95] Reductive cleavage was conducted with lithium aluminium hydride or sodium amalgam.[96,97] For each derivative a suitable strategy has to be found to avoid side reactions and to obtain the product in a good yield.

2.2 Ligand synthesis

2.2.1 Synthesis of monoalkylated cyclen

The monoalkylation of cyclen was performed with decyl, dodecyl and hexadecyl chains to determine the influence of the chain length on the proteolytic activity and particle formation behavior of the corresponding complexes (Scheme 2.1).

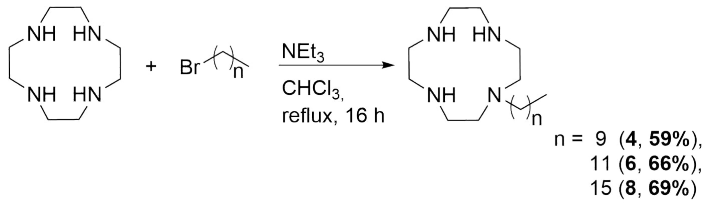

Scheme 2.1: Synthesis of 1-alkyl-4,7,10-triazacyclododecane ligands **4**,**6** and **8**.

The synthesis was performed according to Massue *et al.* with a fourfold excess of cyclen.[98] In order to remove traces of cyclen precipitation as a hydrochloride salt and recrystallization from ethanol were necessary.[99] In spite of the extended work-up the yields were comparable with the literature. Unreacted cyclen can be regained after the synthesis which is important to consider regarding the high costs for this compound (Sigma-Aldrich: 674 €/g).

2.2.2 Synthesis of monoalkylated oxacyclen

Oxacyclen derivatives, which are mono-functionalized at position 7 of the macrocycle, are usually synthesized in a 3+1 cyclization reaction to generate the product regioselectively.[94] The first building block bears the functional group, an alkyl chain in this case, and the second block bears the ether group of the macrocycle (Scheme 2.2).

Building block **14** with the alkyl chain was synthesized in a three step approach. Ethanolamine was ditosylated to create a good leaving group for the subsequent intramolecular ring-closing reaction. For the recrystallization of **11** ethanol was applied instead of carbon tetrachloride, as suggested in the literature, to minimize toxicity.

To prevent further polymerization of the highly reactive aziridine **12** *tert*-butylcatechol was added after the reaction to the crude product.[100] Since recrystallization from DCM and hexane was not successful, the crude product was applied for the subsequent reaction with hexadecylamine.[101] Regarding the yield of this reaction polymerization could be inhibited and purification of **12** can be neglected.

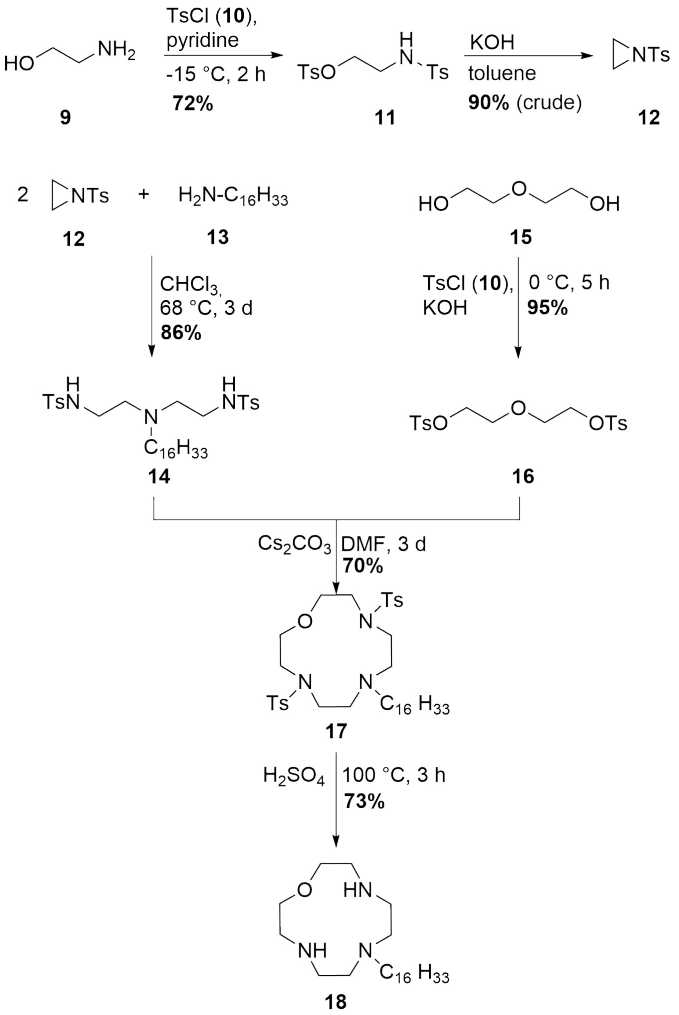

Scheme 2.2: Synthesis of 7-hexadecyl-1-oxa-4,7,10-triazacyclododecane.

Building block **16** with the ether functionality was synthesized by tosylation of diethylene glycol to generate a species with a good leaving group for the macrocycle formation.[102]

The conditions for the cyclization reaction were adapted from Morrow *et al.*.[89] Detosylation was performed with sulfuric acid and the product could be obtained in a comperatively good yield.[94]

2.2.3 Synthesis of monoalkylated dioxacyclen

Regarding the succesful synthesis of **18** a similar approach was planned for monoalkylated dioxacyclen. Applying the same 3+1 building block strategy for both macrocycles would enable a wide range of oxa and dioxa derivatives with a small set of starting materials for the cyclization reaction.

For the introduction of two oxa groups into the macrocycle diethanolamine was alkylated for the first building block and tritosylated for the second building block (Scheme 2.3).

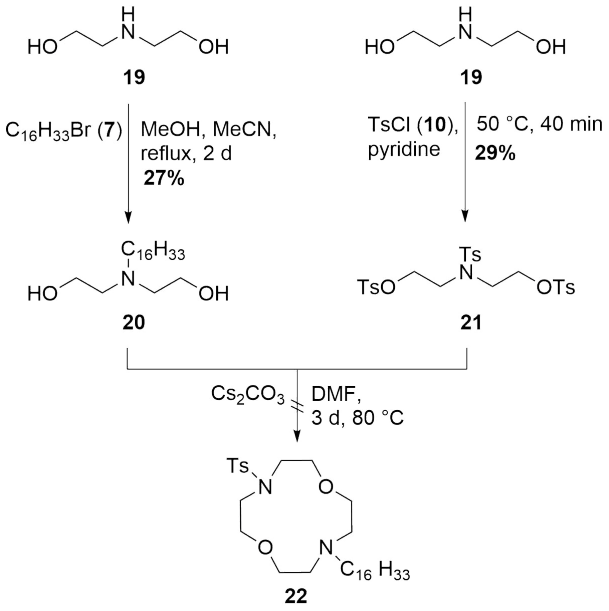

Scheme 2.3: Synthesis strategy for 1-hexadecyl-4,10-dioxacyclen.

The reaction of both building blocks under the same conditions applied for oxacyclen **18** did not afford the tosylated macrocycle **22**.

The template effect of the cesium cation from the corresponding carbonate on the formation of cyclen and oxacyclen derivatives might not be given for dioxacyclen due to conformational differences.[103] No example was found in the literature for the synthesis of dioxacyclen derivatives applying cesium carbonate although it is the base of choice for the formation of oxacyclen derivatives. The building block approach was therefore resigned.

As an alternative synthesis strategy the direct alkylation of dioxacyclen with an excess of the macrocycle was examined. This pathway has already proven succesful for the corresponding cyclen derviatives discussed in this chapter. Dioxacyclen was synthesized according to Borjesson and Welch starting from 2-(2-chloroethoxy)ethanol **23** and tosylamide **24** (Scheme 2.4).

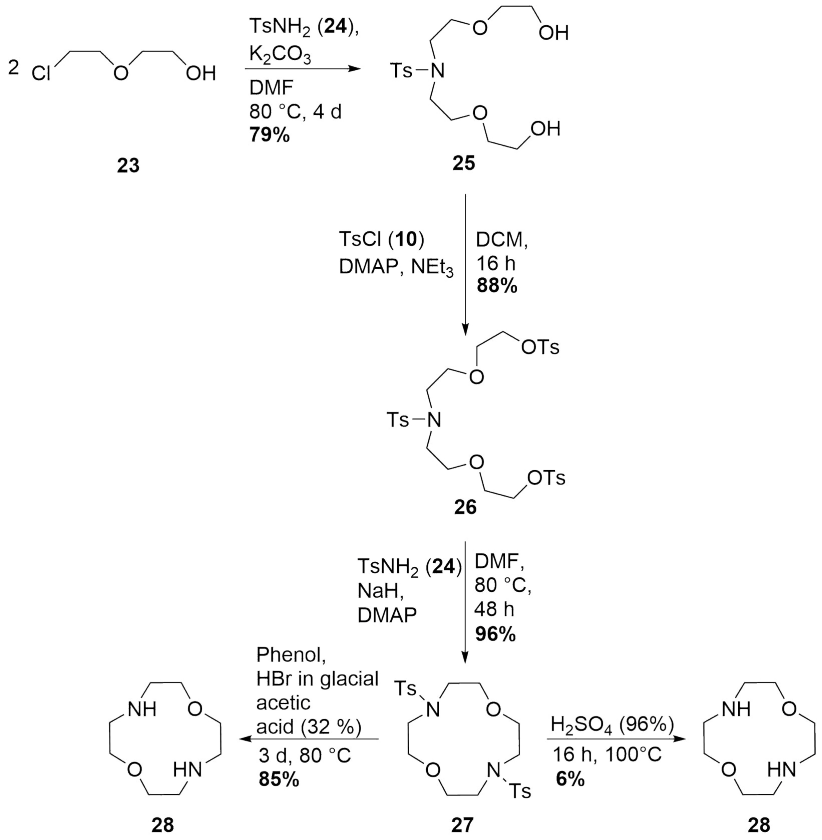

Scheme 2.4: Synthesis of dioxacyclen.

The diol **25** obtained from their reaction was ditosylated to give compound **26**. For the ring-closing reaction with tosylamide a remarkably good yield of 96% compared to 50% in the literature could be obtained. Column chromatography, as suggested by the literature procedure, was not necessary to purify the product. For the deprotection step two different strategies were compared.

The deprotection with sulfuric acid, as performed with the corresponding oxacyclen derivative **17**, resulted in a very poor yield of 6% whereas from deprotection with

phenol and HBr in glacial acetic acid the product could be obtained with a yield of 85%.

The macrocycle could be synthesized with a good overall yield of 42% over 4 steps.

Attempts to alkylate the macrocycle were conducted under the same conditions applied for cyclen with a twofold and fourfold excess of cyclen (Scheme 2.5).

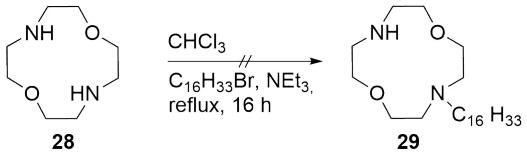

28 29

Scheme 2.5: Alternative synthesis strategy for 1-hexadecyl-4,10-dioxacyclen.

In both cases only the dialkylated derivative could be isolated. This problem might be avoided with a higher dilution of the starting materials for the reaction.

Another strategy for the synthesis of compound **29** is the introduction of the alkyl chain in the course of the ring formation in an alternative 3+1 cyclization reaction (Scheme. 2.6). The introduction of the hexdecyl chain to **26** with the corresponding amine was successful but the yield was poor (Scheme 2.6)

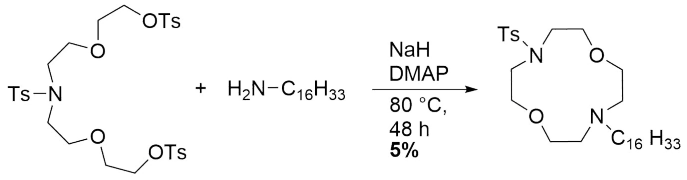

26 13 22

Scheme 2.6: Alternative synthesis strategy for 1-hexadecyl-4,10-dioxacyclen from **26**.

A drastic increase of the yield was possible by substituting **26** with its dimesylated analog **31**.[96] This might be explained with the sterical demand of the two tosyl groups which could prevent the attack of the nucleophilic amine.(Scheme 2.7).

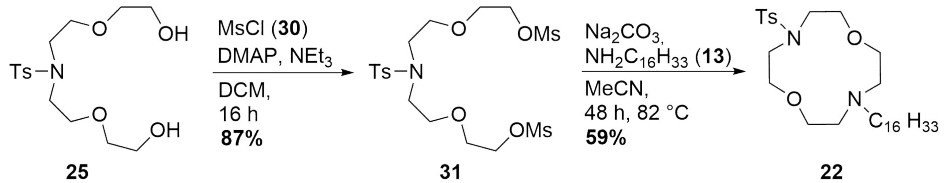

25 31 22

Scheme 2.7: Alternative synthesis strategy for 1-hexadecyl-dioxacyclen from **31**.

For the deprotection of **22** two methods were compared (Scheme. 2.8).

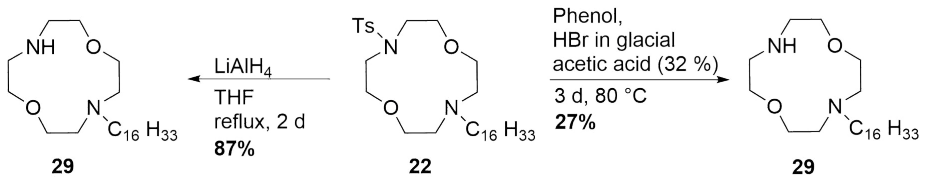

Scheme 2.8: Synthesis of **29**.

Detosylation with HBr in glacial acetic acid and phenol resulted in a moderate yield of 27%, whereas from deprotection with lithium aluminium hydride according to Echegoyen *et al.* the product could be obtained in a good yield of 87%.[96]

These results are in accordance with studies from Raßhöfer and Vögtle suggesting ether cleavage as side reaction for acidic tosyl deprotection of macrocylces with an increased number of oxygen atoms.[104]

In summary it can be said that the 3+1 cyclization according to Echegoyen *et al.* is superior to the other synthesis strategies presented in this section to generate compound **29**.

2.2.4 Synthesis of 1-(2-hydroxyhexadecyl)cyclen

Compound **32** was synthesized according to Griffith *et al.* in a one-step synthesis from 1,2-epoxyhexadecane with a tenfold excess of cyclen (Scheme. 2.9).

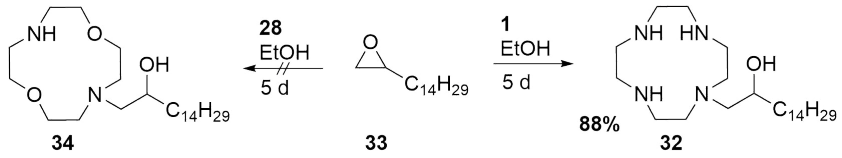

Scheme 2.9: Synthesis strategy for **32** and **34**.

Instead of distillation as suggested by the literature procedure, recrystallization from water was conducted to isolate the product. Attempts to purify the product via kugelrohr distillation failed. This might be explained with the increased chain length compared to the literature procedure where the synthesis of the corresponding tetradecyl derivative was described.

The same reaction was performed with dioxacyclen **28** but the product could not be isolated in this case.

2.2.5 Introduction of a carboxyl group to monoalkylated cyclen

Not only the chain length of the hydrophobic tail but also the increased hydrophilicity of the headgroup might influence micelle formation. Hence, the introduction of a carboxyl group at the nitrogen atom opposing to the nitrogen atom bearing the alkyl chain was planned. To generate such a species regioselectively cyclen **1** was diprotected with Boc in position 1 and 7 (Scheme 2.10).[105]

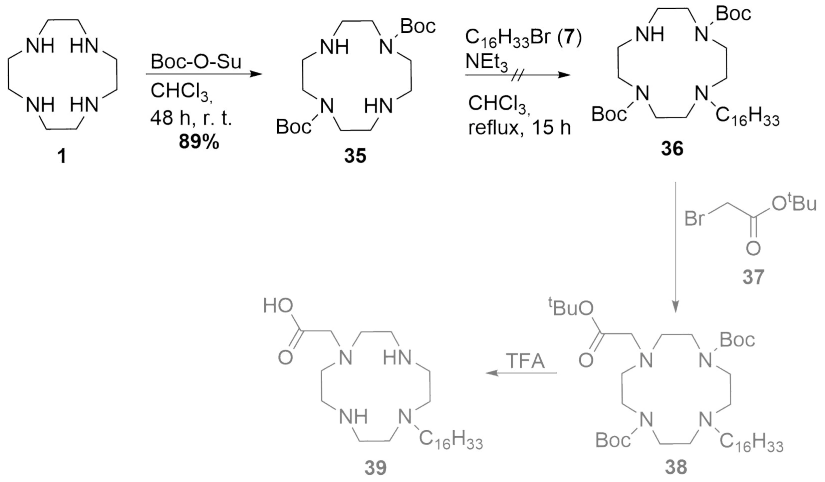

Scheme 2.10: Synthesis strategy for amphiphile **39**.

Approaches to alkylate **35** under the same conditions applied for cyclen were not successful.[98] The sterical demanding Boc groups might hinder the attack of the alkyl compound. Hence, the introduction of a carboxyl group via *tert*-butyl-acetate to **36** and the deprotection of **38** could not be performed. An alternative pathway for the synthesis of **39** needs to be found.

2.3 Complex formation

The exchange inertness of Co(III) complexes is a very interesting factor regarding *in vivo* applications.[106] The investigation of Cu(II) complexes, however, is of interest regarding the metal hypothesis of AD. The sequestration of copper ions from Aβ plaques was shown to cause decomposition of the plaques and constitutes a bimodal approach for the treatment of AD.[36]

Two strategies were followed for the generation of the Co(III) macrocycle complexes presented in this work. $Na_3[Co(CO_3)_3]\cdot 3\ H_2O$ is a much-cited Co(III) source for macrocyclic complexes and was applied for the Co(III) complex of **8**.[107–109] For complexation of ligand **29** this strategy was not successful. Instead, the complex was isolated after oxidation of Co(II) under air from $CoCl_2$.

The corresponding Cu(II) complex could be isolated from an equimolar solution of the ligand **29** and $Cu(NO_3)_2$. For the Cu(II) complexes of **4**, **6** and **8** changing the metal salt to $Cu(ClO_4)_2$ was necessary for the precipitation of the pure complex. As counterions for these three complexes one perchlorate ion and one chloride ion, generated from perchlorate, were found according to CHN analysis. This finding has already been reported for another Cu(II) complex of cyclen in the literature.[32]

In spite of the long alkyl chain crystals suitable for X-ray crystallography could be generated from Cu(II) hexadecylcyclen (Fig. 2.3).

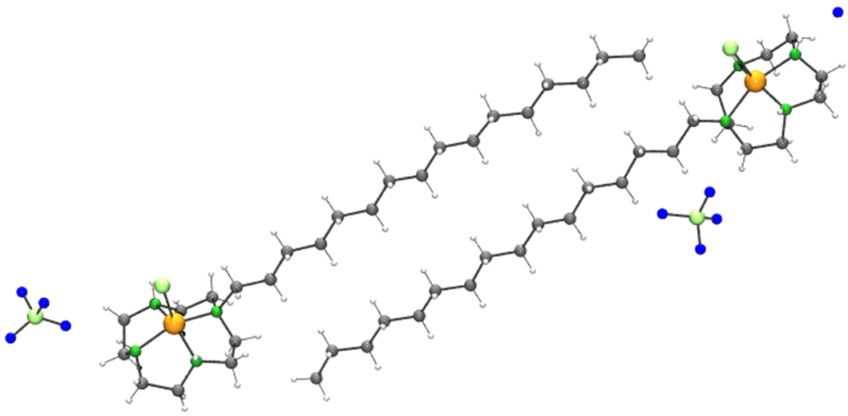

Fig. 2.3: POV-Ray ball-and-stick model of Cu(II) **8** with perchlorate and chloride as counterions.

With highly branched crystals generated *via* diffusion from methanol and hexane the resolution of the crystal structure is poor so that all atoms except for copper and chloride were kept isotropic. Hence, a detailed analysis will not be given here but the distorted square pyramidal structure with the square base formed by the nitrogen

atoms from the macrocycle and a chloride ion as tip can clearly be observed from the structure. The copper ion is located above the plane constituted by the four nitrogen atoms. This conformation is similar to the structure reported for Cu(II) cyclen with one nitrate ion coordinated to the complex and one as counterion.[110]

With a decreasing number of nitrogen atoms in the ring the color intensity of the Cu(II) complexes in solution also decreases (Fig. 2.4).

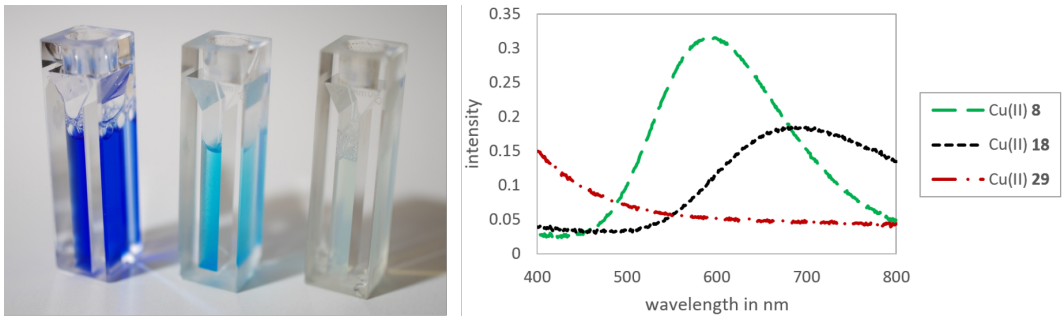

Fig. 2.4: Cu(II) complexes of monoalkylated cyclen derivatives **8**, **18** and **29** in water (10 mM, left) and the corresponding UV/Vis spectra (1 mM).

The 10 mM aqueous solution of Cu(II) **8** is deep blue whereas the corresponding complex of **29** is almost colorless.

The UV/Vis spectra show a drastic decrease of the extinction with an increase of oxygen atoms in the macrocycle. Going from Cu(II) **8** to Cu(II) **18** (and potentially Cu(II) **29** for which no absorption within the visible region of the spectrum was detected) the observed red shift of the absorption might be explained with the spectrochemical series according to which oxygen species like H_2O and OH^- produce a smaller d-orbital splitting compared to nitrogen species like NH_3. Hence, the exchange of nitrogen atoms with oxygen leads to a decrease of the excitation energy necessary for d-d transitions of the Cu(II) complexes causing a drastic change of the samples' color as indicated by the UV/Vis spectra.

A comparable observation was made for the corresponding Co(III) complexes. The complex of **8** exhibits a deep purple color in solution whereas Co(III) **29** is lightly pink (Fig. 2.5). Co(III) **8** has a dinstinct maximum at 533 nm, whereas only a very weak extinction can be observed for Co(III) **29** between 500 and 800 nm. The Co(III) complex of **18** was not available.

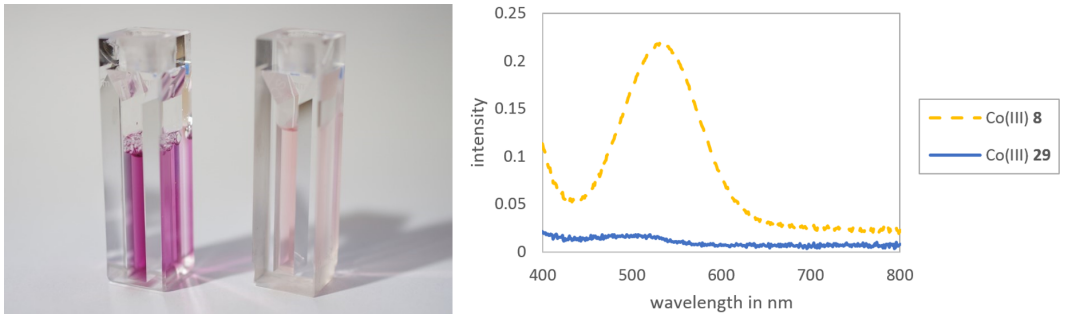

Fig. 2.5: Co(III) complexes of monoalkylated cyclen derivatives **8** (left) and **29** (right) in water (10 mM, left) and the corresponding UV/Vis spectra (1 mM)..

The moderate yields of all complexes presented in this work might be caused by the excellent solubility of all complexes in almost all available solvents as stated by GRIFFITH *et al.* for 1-(2-hydroxytetradecyl)cyclen.[111] The generation and properties of the Cu(II) and Co(III) complexes of ligand **18** will be discussed in another thesis.

2.4 Protein cleavage experiments

2.4.1 SDS-PAGE

Sodium dodecyl sulfate polyacrylamide gel elecrophoresis (SDS-PAGE) is a technique to separate proteins and peptides between 1 – 500 kDa in an electrical field according to their molecular weight.[112] *For this semi-quantitative method SDS is added to the sample solution to denature the proteins and to cover their charge. The anionic detergent imparts a homogenous negative charge to the protein proportional to its relative molecular mass. β-mercaptoethanol is added if the cleavage of disulfide bridges is desired. The samples are loaded onto a porous gel made from polyacrylamide and bisacrylamide (the latter is added for cross-linking of two polyacrylamide molecules). The gel is placed in a buffer solution and an electrical field is applied. The proteins migrate to the anode due to the negative charges derived from SDS. Small biomolecules can pass the pores faster. Hence, a mixture of proteins differing in size can be separated (Fig. 2.6).*

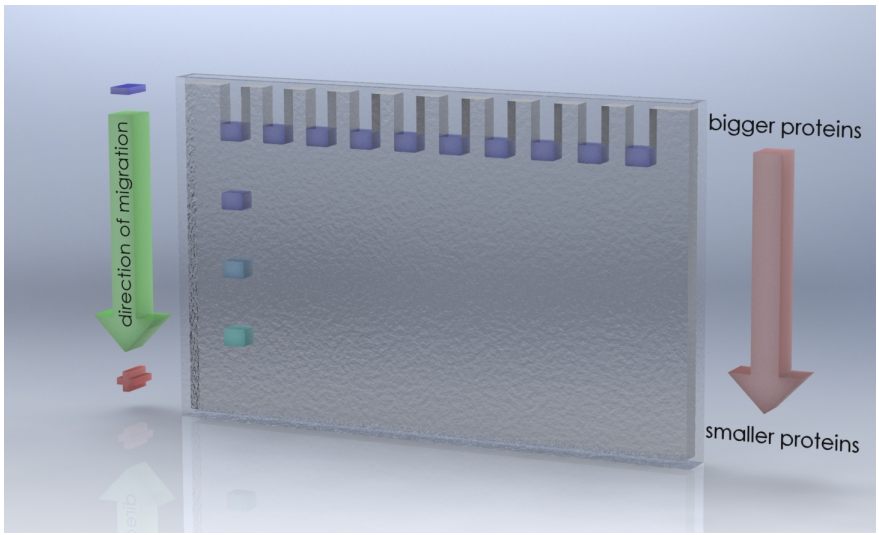

Fig. 2.6: *Principle of SDS-PAGE.*

Cleavage of a single protein can be monitored by intensity loss of the protein band compared to a reference sample of the uncleaved protein of the same concentration.

To investigate the influence of the alkyl chain length on the proteolytic activity electrophoresis experiments were performed with the *in situ* formed Cu(II) and Co(III) complexes of 1-decyl, dodecyl and hexadecylcyclen. BSA, myoglobin, lysozyme, cytochrome c, ovalbumin and horseradish peroxidase were chosen as model proteins to compare the activity with other known artificial proteases.[38,56]

A strong dependence of the cleavage activity from the alkyl chain length is clear to see from the gels presented in Fig. 2.7 (blue triangles below the figures illustrate the band intensity and therefore the cleavage activity qualitatively).

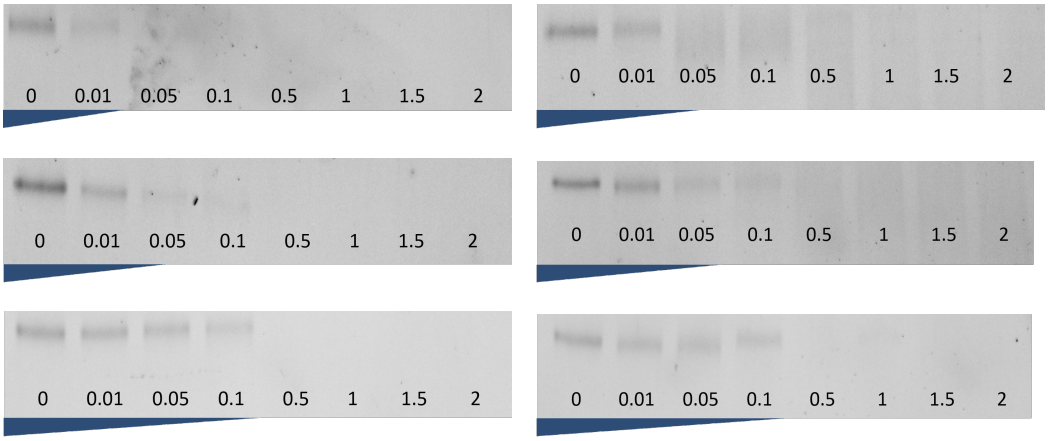

Fig. 2.7: SDS-PAGE, concentration-dependent cleavage of BSA with the complexes of **8**, **6** and **4** (from top to bottom, Co(III) on the left, Cu(II) on the right). Incubation for 48 h at 50 °C and pH 9. Complex concentrations given in the figure are mM.

For the complexes of **4**, the compound with the shortest alkyl chain, full cleavage of the protein can be observed by the absence of the characteristic protein band at a complex concentration of 0.5 mM.

For the other four complexes a lower concentration of 0.05 or 0.1 mM is required for complete cleavage of BSA. The increased activity of the complexes of **8** compared to **6** is not as obvious as for the shortest analog but a minor improvement can be detected regarding the intensity of the electrophoretic bands. The cobalt complexes exhibit a marginally better activity compared to the corresponding copper complexes.

All six complexes exhibit a drastically improved proteolytic activity towards BSA compared to Cu(II) (Fig. 2.8) and Co(III) cyclen (not shown).[113]

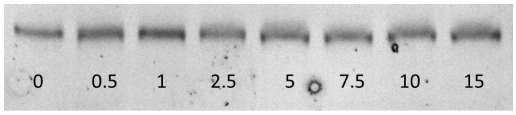

Fig. 2.8: SDS-PAGE, concentration-dependent cleavage of BSA with Cu(II) **1**. Incubation for 48 h at 50 °C and pH 9. Complex concentrations given in the figure are mM.

No cleavage at all can be detected for the copper complex of the bare macrocycle at concentrations between 0.5 and 15 mM whereas the protein is completely cleaved applying 0.05 mM Co(III) **6** or Co(III) **8**. For the Co(III) complex of cyclen a weak proteolytic activity could be observed at complex concentrations of 2 mM but the activity of the alkylated derivatives is much higher[113].

To make sure that cleavage originates from the complexes SDS-PAGE was conducted with the precipitated and redissolved complexes of **8** discussed in section 2.3 (Fig. 2.9).

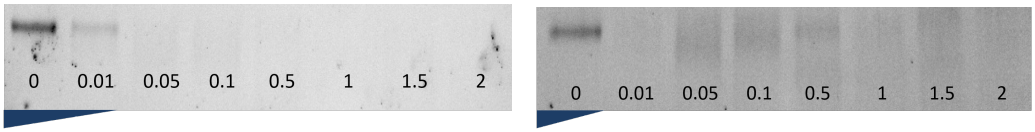

Fig. 2.9: SDS-PAGE, concentration-dependent cleavage of BSA with the precipitated and redissolved complexes of **8** (Co(III) on the left, Cu(II) on the right). Incubation at 50 °C and pH 9 for 48 h. Complex concentrations given in the figure are mM.

Since the activity is comparable to the *in situ* generated complexes, any impurities and free metal ions can be excluded as active species.

Additionally, the activity of the metal salts applied for *in situ* complex formation - $Cu(NO_3)_2 \cdot 3\ H_2O$ and $CoCl_2 \cdot 6\ H_2O$ was investigated. The cobalt salt exhibits no proteolytic activity at all, whereas for the copper salt a weak proteolytic activity was observed, much lower than for the corresponding cyclen complexes (Fig. 2.10). These results confirm the complexes as active species in the cleavage process.

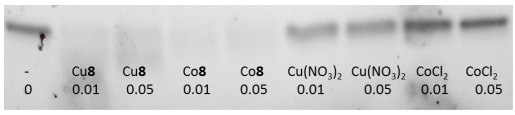

Fig. 2.10: SDS-PAGE, BSA cleavage with Cu(II) **8**, Co(III) **8**, $Cu(NO_3)_2 \cdot 3\ H_2O$ and $CoCl_2 \cdot 6\ H_2O$, respectively. Incubation at 50 °C and pH 9 for 48 h. Complex concentrations given in the figure are mM.

Numerous artificial proteases are only active under relatively harsh conditions. Activity under physiological conditions is a necessity for *in vivo* applications. Therefore electrophoresis experiments were performed with Cu(II) **8** at 37 °C and pH 7.4 (Fig. 2.11).

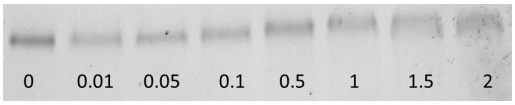

Fig. 2.11: SDS-PAGE, concentration-dependent cleavage of BSA with Cu(II) **8**. Incubation at 37 °C and pH 7.4 for 48 h. Complex concentrations given in the figure are mM.

Although the proteolytic activity is drastically decreased cleavage was still detectable under physiological conditions even at the lowest protease concentration of 0.01 mM.

Time-dependent electrophoresis experiments with BSA revealed that for Co(III) **8** only 16 h of incubation were necessary to completely cleave the protein at a complex concentration of 0.05 mM whereas 39 h were necessary for Cu(II) **8** (Fig. 2.12).

Although most of the protein is already cleaved after 4 h a very faint protein band is still detectable after 8 and 24 h, respectively. These incubation periods are comparable to other artificial proteases reported in literature.[41,60]

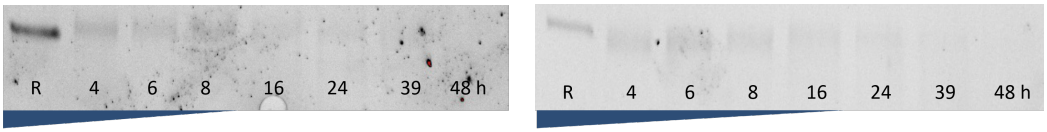

Fig. 2.12: SDS-PAGE, time-dependent cleavage of BSA with the complexes of **8**, (0.05 mM, Co(III) on the left, Cu(II) on the right). Incubation at 50 °C and pH 9 for 48 h. Complex concentrations given in the figure are mM.

To make sure that the proteases do not specifically cleave BSA the experiments were repeated with several other proteins. For the heme protein myoglobin the cleavage behavior of Co(III) **8** is comparable to the activity towards BSA. For the corresponding Cu(II) complex the protein is completely cleaved at 0.01 mM but, suprisingly, cleavage is declining with increasing complex concentrations.

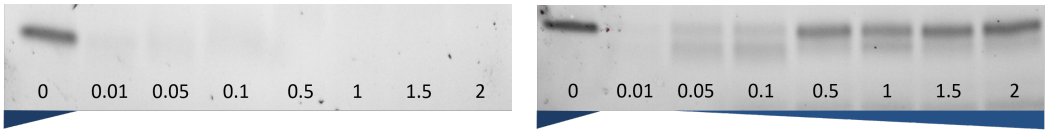

Fig. 2.13: SDS-PAGE, concentration-dependent cleavage of myoglobin with the complexes of **8** (Co(III) on the left, Cu(II) on the right). Incubation at 50 °C and pH 9 for 48 h. Complex concentrations given in the figure are mM.

To further investigate this unexpected finding a comparison between the proteolytic activity of heme-containing and heme-free proteins was drawn with Cu(II) **8**.

For the complexes of **8** this remarkable cleavage behavior is also observable with the heme proteins cytochrome c and peroxidase (Fig. 2.15). The Co(III) complexes of **8** exhibit a proteolytic activity increasing with its concentration, whereas the activity of the corresponding Cu(II) complex decreases after the protein is fully cleaved at 0.1 mM for cytochrome c and 0.01 mM for peroxidase.

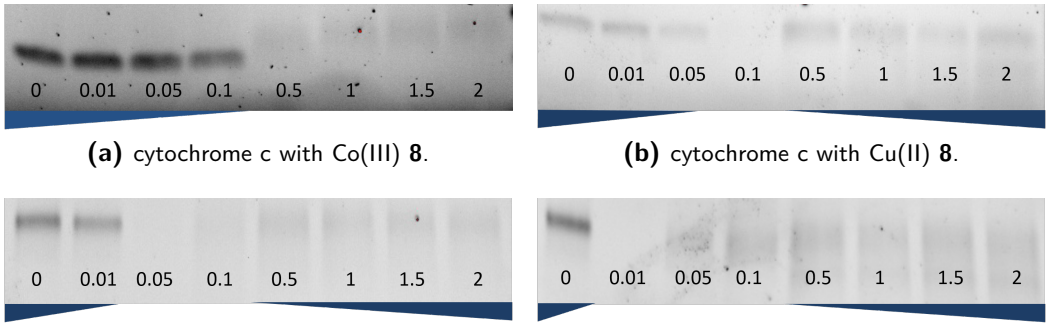

(a) cytochrome c with Co(III) **8**.

(b) cytochrome c with Cu(II) **8**.

(c) peroxidase with Co(III) **8**.

(d) peroxidase with Cu(II) **8**.

Fig. 2.14: SDS-PAGE, concentration-dependent cleavage of heme proteins with Cu(II) and Co(III) **8**. Incubation for 48 h at 50 °C and pH 9. Complex concentrations given in the figure are mM.

For lysozyme and ovalbumin, proteins without a heme group, cleavage increases consistently with the complex concentration as it was shown for BSA.

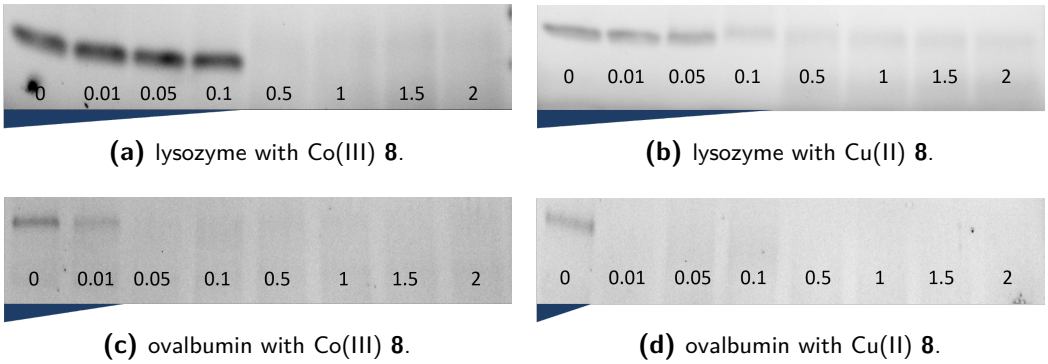

(a) lysozyme with Co(III) **8**. **(b)** lysozyme with Cu(II) **8**.

(c) ovalbumin with Co(III) **8**. **(d)** ovalbumin with Cu(II) **8**.

Fig. 2.15: SDS-PAGE, concentration-dependent cleavage of non-heme proteins with Cu(II) and Co(III) **8**. Incubation for 48 h at 50 °C and pH 9. Complex concentrations given in the figure are mM.

When the activity of ligand **8** alone was investigated, surprisingly, a proteolytic activity comparable to the corresponding Cu(II) and Co(III) complexes was observed (Fig. 2.16). Since metal ions are proposed to play a crucial role in the cleavage mechanism, these findings were unexpected and metal contaminations were assumed to be the cause for this activity.

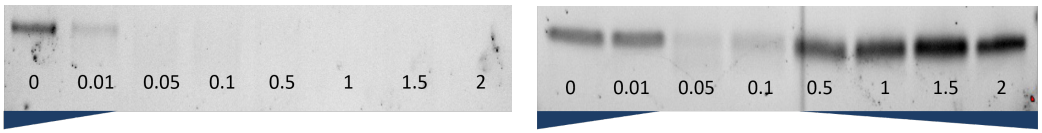

Fig. 2.16: SDS-PAGE, concentration-dependent cleavage of BSA (left) and myoglobin (right) with ligand **8** Incubation at 50 °C and pH 9 for 48 h. Ligand concentrations given in the figure are mM.

A remarkable result was the inhibition of myoglobin cleavage at higher cleavage agent concentrations as it was observed for Cu(II) **8** as well.

Treatment of BSA and buffer solution with Chelex®, a chelating ion exchange resin predominantly binding divalent ions, did not influence the cleavage activity of **8** (not shown).

Ligands **4** and **6** also exhibit a comparable activity to the corresponding complexes towards BSA (Fig. 2.17).

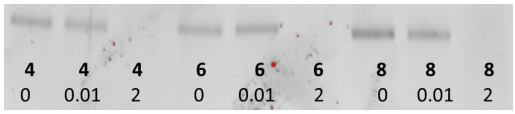

Fig. 2.17: SDS-PAGE with BSA and **4**, **6** and **8**. Incubation at 50 °C and pH 9 for 48 h. Concentration of ligands given in the figure are mM.

EDTA, a chelator for divalent cations, was added to the incubation solution with Cu(II) **8** and ligand **8** (Fig. 2.18).

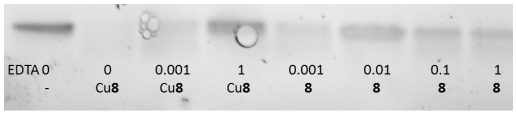

Fig. 2.18: SDS-PAGE, cleavage of myoglobin with **8**, Cu(II) **8** (0.5 mM) and EDTA. Incubation at 50 °C and pH 9 for 48 h. Concentration of EDTA given in the figure are mM.

The cleavage activity of Cu(II) **8** could be inhibited with EDTA suggesting a sequestration of copper ions from **8**. The activity of the ligand could also be inhibited with EDTA but a lower intensity of the protein band can be detected for **8** at the highest EDTA concentration suggesting a less strong inhibition of the proteolytic activity.

For the experiments presented in Fig. 2.18 a disodium salt of EDTA was applied. A comparison of this salt with the tracemetal free corresponding acid is shown in Fig. 2.19.

Two concentrations of myoglobin were compared for these experiments. For both concentrations cleavage increases at a $(Na)_2$EDTA concentration of 0.1 mM and decreases at higher concentrations (Fig. 2.19, left). This effect cannot be observed for the acid (Fig. 2.19, right).

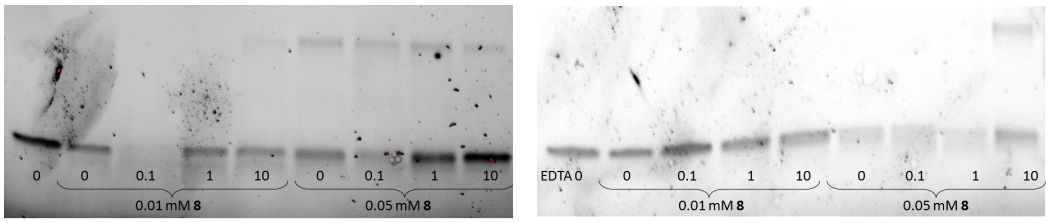

Fig. 2.19: SDS-PAGE, cleavage of myoglobin with ligand **8** and EDTA ($(Na)_2$EDTA on the left, EDTA on the right). Incubation at 50 °C and pH 9 for 48 h. Ligand and EDTA concentrations given in the figure are mM.

With the trace metal free EDTA no cleavage at all was detected for the low ligand concentration which is in accordance with the experiments presented in Fig. 2.16. At a ligand concentration of 0.05 mM cleavage can be observed but applying 10 mM EDTA inhibits the cleavage to some extent. These findings suggest that either sodium is the origin of the proteolytic activity of **8** or trace metals present in the EDTA sodium salt and in one of the components of the incubation solution for SDS experiments.

On the gels presented in Fig. 2.19 not only the electrophoretic band characteristic for myoglobin can be observed but at higher concentrations of ligand and EDTA a second band for a species with a molecular weight between 27 and 34.6 kDa, approximately twice the weight of myoglobin, can be observed. For EDTA this band can be detected only for the highest concentration of chelator and ligand whereas with Na_2EDTA it can be observed for all chelator concentrations at a myoglobin concentration of 0.05 mM.

The propensity of myoglobin to form dimers has already been thoroughly investigated[114,115]. In this case the band might represent aggregates of two myoglobin molecules with EDTA and **8**. A relation between the appearance of the second band and the intensity loss of the myoglobin band is not observable.

EDTA does not have any influence on the cleavage of Cu(II) **8** and **8** towards BSA (Fig. 2.20).

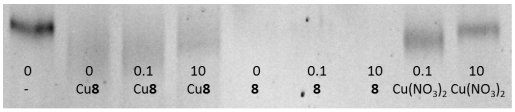

Fig. 2.20: SDS-PAGE, concentration-dependent cleavage of BSA with Cu(II) **8** (0.05 mM) and **8** (0.05 mM). Incubation at 50 °C and pH 9 for 48 h. EDTA concentrations given in the figure are mM. $Cu(NO_3)_2$ was added equimolar to EDTA.

BSA is known to have a very strong binding site for copper itself which might form a strong complex with Cu(II) **8**[116]. These results show that this process is highly dependent on the protein structure. For the last two lanes of the gel presented in Fig. 2.20 copper nitrate was added to illustrate that copper complexes of EDTA have a much weaker cleavage activity compared to cyclen complexes.

Two different buffer systems are utilized for SDS-PAGE with proteins and peptides. The glycine system is usually applied for proteins between 30 and 100 kDa whereas

the tricine gel system is used for the detection of proteins < 30 kDa[112]. In contrast to all other gels presented in this work the one in Fig. 2.21 was performed with tricine to detect cleavage products of myoglobin.

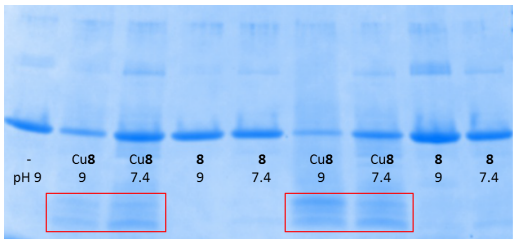

Fig. 2.21: SDS-PAGE (tricine), myoglobin (22.5 µM) cleavage with Cu(II) **8** and **8** Incubation at 50 °C and pH 9 for 48 h. Cleavage agent concentrations given in the figure are mM.

For Cu(II) **8** fragments could be observed with a molecular weight of approximately 4-6 kDa. A particularly high protein concentration was neccesary to detect fragments suggesting their concentration is rather low. An explanation for this finding might be cleavage into fragments even smaller than 1 kDa. Fragments could not be observed in the presence of ligand **8**.

Cu(II) **32** is a literature known compound but the proteolytic activity of this amphiphile has not been investigated yet. The complex exhibits a comparable proteolytic activity towards BSA to Cu(II) **8** (Fig. 2.22). The introduction of the hydroxyl group does not seem to influence protein cleavage activity.

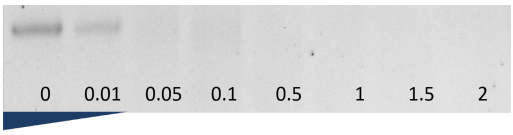

Fig. 2.22: SDS-PAGE, concentration-dependent cleavage of BSA with Cu(II) **32**. Incubation at 50 °C and pH 9 for 48 h. Complex concentrations given in the figure are mM.

A comparison of the electrophoretic experiments conducted for the complexes of **29** (Fig. 2.23) with the results obtained for the complexes of **8** (Fig. 2.7) shows a comparable activity for the Co(III) complexes and a marginally lower activity for Cu(II) **29**. The expected improvement for the dioxacyclen derivatives could not be observed.

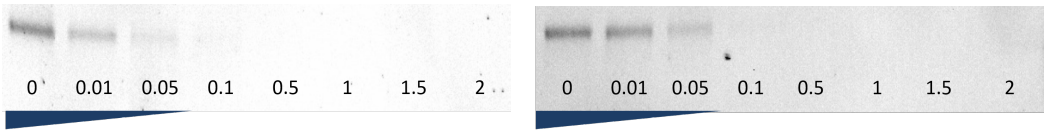

Fig. 2.23: SDS-PAGE, concentration-dependent cleavage of BSA with the complexes of **29** (Co(III) on the left, Cu(II) on the right). Incubation at 50 °C and pH 9 for 48 h. Complex concentrations given in the figure are mM.

A direct comparison of the Cu(II) complexes of **8**, **18** (generously offered by Sebastian Hinojosa) and **29** made sure that the proteolytic activity decreases with an increase of oxygen atoms in the macrocycle (Fig. 2.24).

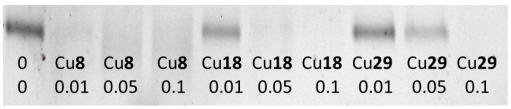

Fig. 2.24: SDS-PAGE, concentration-dependent cleavage of BSA. Comparison of the proteolytic activity of the Cu(II) complexes of **8**, **18** and **29**. Incubation at 50 °C and pH 9 for 48 h. Complex concentrations given in the figure are mM.

In contrast to results reported in the literature for the complexes of **1** an exchange of nitrogen with oxygen is not beneficial for the proteolytic activity of monoalkylated cyclen analoga.[57]

Summarizing the results obtained from the comparison of all SDS-PAGE experiments the Co(III) and Cu(II) complexes of **8** exhibit the highest proteolytic activity towards BSA. All complexes synthesized for this thesis outperform the activity of Cu(II) cyclen by at least two orders of magnitude. The cleavage activity of the ligands and the remarkable cleavage decrease with heme proteins at higher complex concentrations need further investigations.

2.4.2 Determination of protein fragments

> *Matrix-assisted laser desorption/ionisation (MALDI) is a mass spectometry technique applied to detect biomolecules (e.g. proteins, peptides and DNA) which would be fragmented with stronger ionisation methods. This method requires co-crystallization of the sample with a matrix. The matrix, consisting of small organic molecules, is applied in a 100 to 100 000 fold excess. A pulsed laser is applied to irradiate the matrix, triggering desorption and ionization of sample and matrix molecules. The mechanism of ionisation is not completely understood to date. TOF (Time-of-flight) mass spectrometry is frequently used in combination with the MALDI technique to determine the ionized species.*

MALDI-TOF experiments were performed to characterize the fragments observed *via* tricine SDS-PAGE (Fig. 2.21).

Incubation conditions were adapted from SDS-PAGE experiments. At pH 9 fragments could not be detected supporting the theory of a high concentration of fragments too small for detection *via* gel electrophoresis or MALDI mass spectrometry. Hence, incubation was conducted at physiological pH. For the protein without cleavage agent fragments could not be observed (Fig. 2.25, top). With Cu(II) **8** numerous fragments between 4 and 7.5 kDa could be detected (Fig. 2.25, bottom). The bold numbers in the figure represent the assigned position of the fragment in the amino acid sequence of myoglobin.

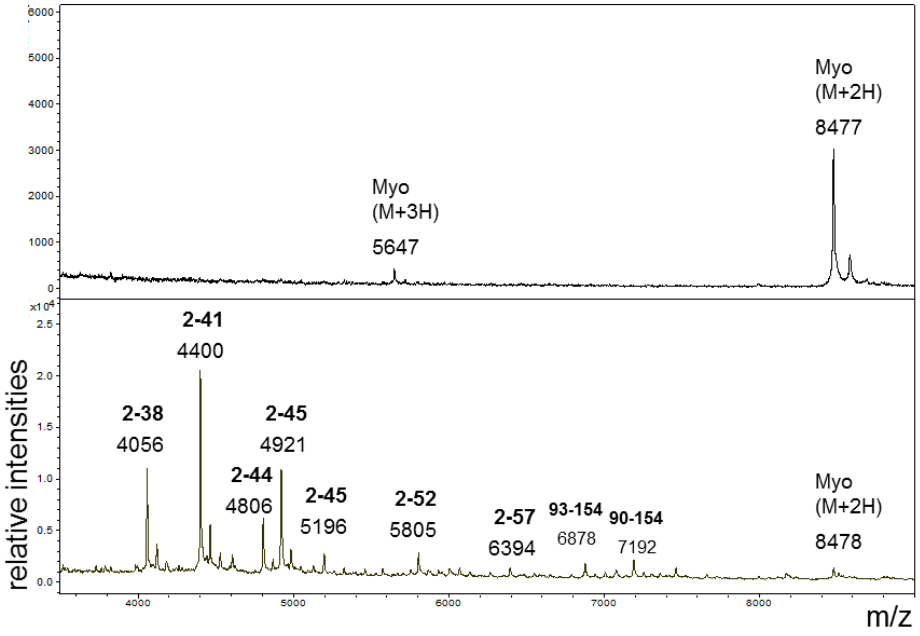

Fig. 2.25: MALDI-TOF MS, myoglobin (2.25 μM) treated with Cu(II) hexadecylcyclen (0.01 mM) (bottom) vs. an untreated sample (top). Incubation at 50 °C and pH 9 for 48 h. Average masses and amino-acid positions of the fragments are given; numbering refers to the database entry SwissProt P68082 for horse myoglobin.

Particularly remarkable is the peak at 6878 Da reflecting cleavage between glutamic acid (92) and serine (93) (see Fig. 2.26). This myoglobin fragment has been reported before for cleavage with a PCD cyclen derivatives and other Cu(II) complexes and was identified as cleavage site in proximity to the heme group. Histidine (96) and the carboxylate of the heme group were proposed as anchoring sites for the complexes.[41,117] A promotion of the cleavage activity by the tyrosine residue in position 146 acting as general acid has been suggested.[60]

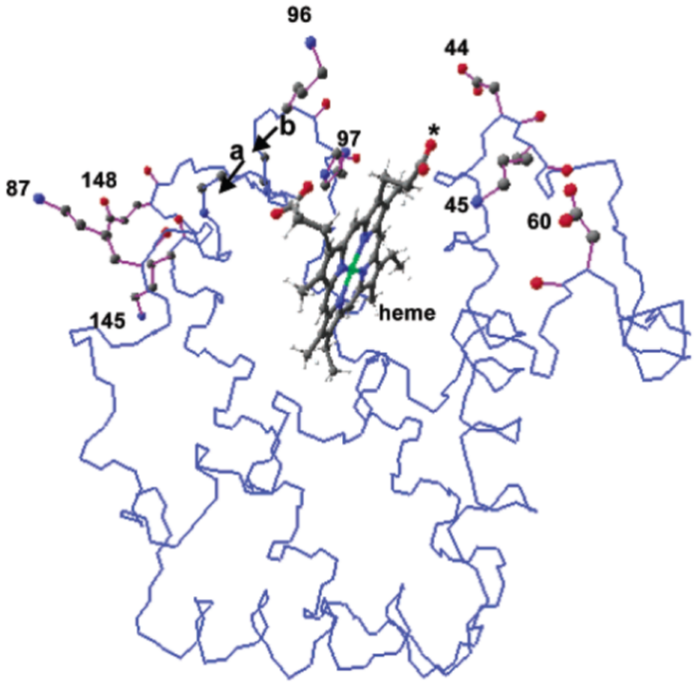

Fig. 2.26: Model of myoglobin. The initial cleavage site is marked with "a". The heme carboxylate is marked with * and His(96) is marked with 97 due to a different numbering. Reprintend with permission from Yoo, C. E.; Chae, P. S.; Kim, J. E.; Jeong, E. J.; Suh, J. *J. Am. Chem. Soc*, **2005**, *125*, 14580.

The results presented here support the theory of initial cleavage close to the heme group reported in the literature.[41,117] To detect the second fragment generated by the initial cleavage time-dependent measurements could be performed. Cleavage of this fragment at 10 094 Da was reported in the literature to be remarkably fast.[60]

Regarding the results obtained from MALDI studies for myoglobin and from SDS-PAGE of heme proteins a key role for the heme group in the cleavage process can be suggested. With the heme group of myoglobin, cytochrome c and peroxidase located in a hydrophobic pocket, hydrophobic interaction of the alkyl chains might be crucial for the approach of the protease to the protein.[79,118,119] The decreased cleavage of heme proteins at higher Cu(II) complex concentrations might be explained with the clogging of the hydrophobic pockets with the highly flexible alkyl chains of the complexes. A different conformation of the Co(III) complexes might prevent the protease from entering into the hydrophobic pocket.

Another explanation could be the tight binding of the complexes to specific fragments inhibiting the catalytic cleavage of the protein. Moreover, the catalysis of autoxidation of heme proteins by Cu(II) complexes is literature-known and might result in species less prone for interaction with the proteases.[120] However, the high complex concentrations necessary to inhibit cleavage suggest a non-catalytic mechanism. To identify the origin for the inhibition of cleavage molecular modeling studies are underway.

To get further insights into the proteolytic activity observed for the monoalkylated cyclen ligands MALDI-TOF experiments were performed with **8** and myoglobin (Fig. 2.27).

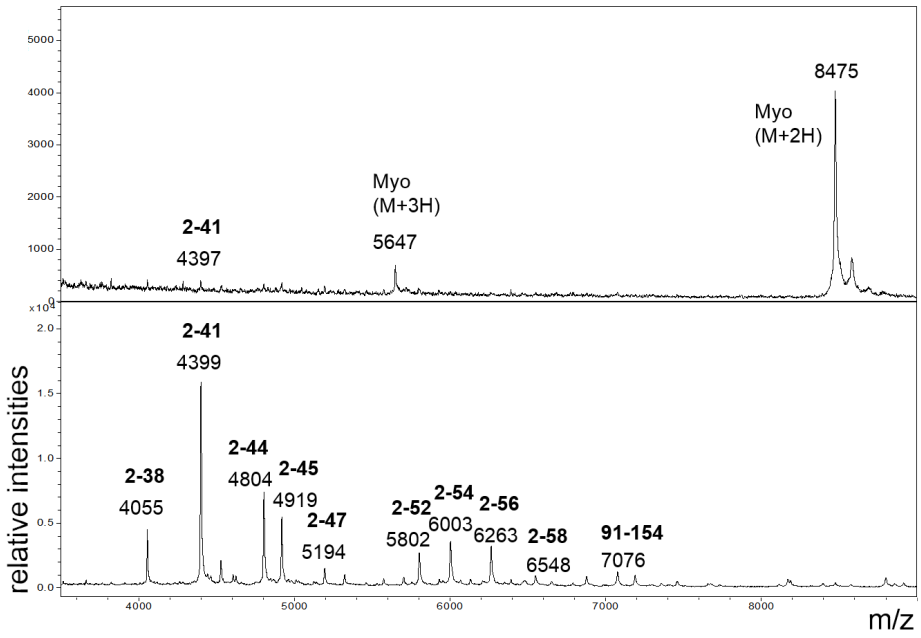

Fig. 2.27: MALDI-TOF MS, myoglobin (2.25 μM) treated with 0.01 mM (bottom) and 0.1 mM **8** (top). Incubation at 50 °C and pH 9 for 48 h. Average masses and amino-acid positions of the fragments are given; numbering refers to the database entry SwissProt P68082 for horse myoglobin.

At the cleavage agent concentration applied for Cu(II) **8** no fragment could be observed, whereas at a concentration of 0.1 mM, fragments could be detected. This is in accordance with the corresponding SDS-PAGE experiments (see Fig. 2.16 and

2.13). All fragments observed for **8** were also found for the complex suggesting the same mechanism of cleavage for both compounds.

ICP-MS measurements were conducted with Na, Mg, Al, Ca, Cr, Mn, Fe, Ni, Zn, Ba and Sr. For none of these metals a concentration comparable to the ligand concentrations in the cleavage experiments were detected. Nickel and aluminum were found with relatively high concentrations of 0.4 and 1.5 μM in the buffer solution but these concentrations are at least 1-2 orders of magnitude below the concentrations applied for SDS-PAGE studies. Either one of the contaminants generates a complex with the ligands, much more active than the Cu(II) and Co(III) complexes or another metal contaminates the incubation samples in higher concentrations. An alternative explanation would be that the proteolytic activity originates from the ligands without any metal but cyclen derivatives were not reported in the literature yet to exhibit proteolytic activity. In general, only few examples can be found for metal-free protein cleavage.[37–39]

Purification of all reactants present in the incubation solutions of MALDI and SDS-PAGE studies, e.g. via ion-exchange chromatography, are necessary to investigate the origin of the proteolytic activity observed for the ligands **4**, **6** and **8**.

2.5 Cytotoxicity studies

The MTT (3-(4,5-dimethylthiazol-2-yl)-2,5-diphenyltetrazolium bromide) assay is a high-throughput colorimetric assay frequently used to investigate the cytotoxity of various compounds.

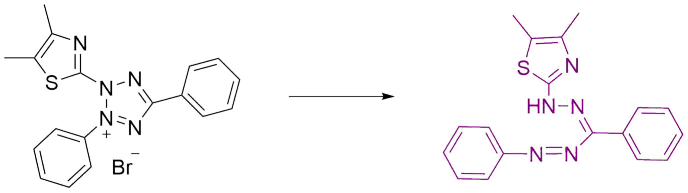

Scheme 2.11: *MTT reduction to formazan.*

MTT is incubated with the cell line of choice and is converted to formazan, a deep purple compound, by viable cells. The cellular mechanism of MTT reduction is not fully understood to date but the involvement of NADH or other cellular

reducing agents is proposed. The absorption of formazan at 570 nm is directly proportional to the number of living cells.

For the MTT assay A549 lung epithelial cancer cells were chosen. Cu(II) and Co(III) complexes of **1** and **6** were applied for the assay. From Fig. 2.28 it can be seen that the complexes of **6** are far more cytotoxic compared to the complexes of **1**.

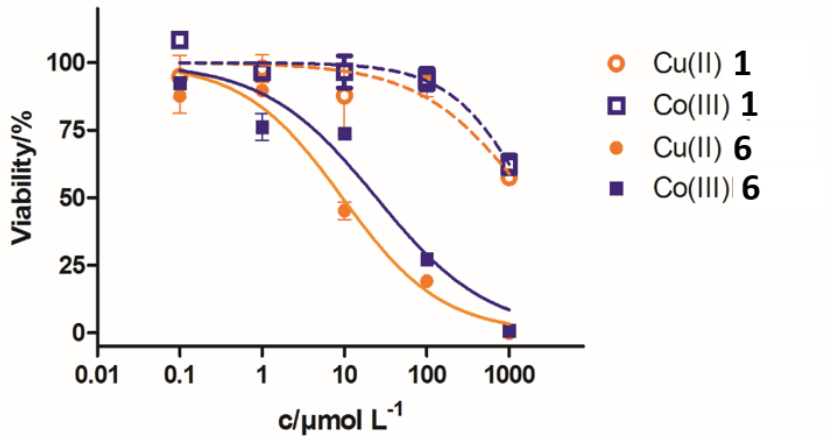

Fig. 2.28: Cytotoxicity profiles of the Cu(II) and Co(III) complexes of **1** and **6** as determined *via* MTT assay on A549 lung cancer cells. Error bars are +/- SEM

The IC_{50} values calculated from these data can bee seen in table 2.1.

Table 2.1: IC_{50} values for complexes of **1** and **6**.

Complex	**IC_{50}**
Cu(II) **1**	1.7 mM
Co(III) **1**	1.7 mM
Cu(II) **6**	9.5 μM
Co(III) **6**	2.25 μM

Although the values are about 100 times lower for the alkylated species their toxicity is comparable to other compounds investigated for AD treatment. The much-cited compounds resveratrol and curcumin have an IC_{50} value of 15.1 and 13.3 μM respectively.[121] The enhanced toxicity might originate from interactions of the alkyl chains with cell membranes. Therefore the cytotoxicity of the corresponding complexes of **8** might be even higher. These complexes were not available when the

present data were collected. Hence, the ideal chain length regarding effectivity and cytotoxicity has yet to be found.

2.6 Determination of the critical micellar concentration

Surface active agents or surfactans are amphiphilic molecules with a hydrophilic head group and a hydrophobic tail. Above a specific concentration, the so-called critical micellar concentration (cmc), surfactants begin to form micelles or other aggregates. In aqueous solutions below the cmc surfactant molecules are mostly located at the surface of the solvents to avoid interactions of the hydrophobic moiety with the solvent. In micelles the hydrophilic moieties shield the hydrophobic core from interactions with the aqueous solvent (Fig. 2.12).

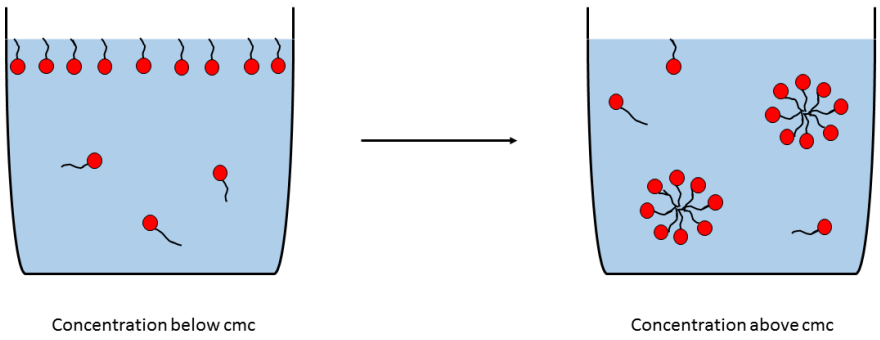

Scheme 2.12: Surfactant distribution in aqueous solution below and above cmc.

Various physical properties of surfactants in solution change above the cmc. Hence, different strategies were developed for the determination of the cmc. Frequently used are techniques measuring surface tension. Below the cmc, the number of surfactants at the surface increases with increasing concentration causing a decrease of the surface tension. Above the cmc, the surface tension is relatively constant. The cmc can be validated regarding this concentration-dependent change.[122]

Moreover, conductometry and viscosity are properties changing above the cmc, allowing the concentration-dependent measurement of particle formation.[123]

Another method for examining the cmc is isothermal titration calorimetry. This method exploits the change of the dilution enthalpy arising from micelle formation

above the cmc. The heat flow is measured during titration of a highly concentrated surfactant solution to a solvent of choice compared to a reference solution of the same solvent in a seperate vessel. Both vessels are kept at the same temperature in an adiabatic environment. The measured heat flux is a direct measure of the dilution enthalpy, which is decreasing with micelle formation. The concentration-dependent detection of the dilution enthalpy allows the determination of the cmc.[124]

For the complexes presented in this work a method was applied based on the fluorescence of pyrene which has been frequently described in the literature.

The "pyrene 1:3 ratio" method exploits the differences in fluorescence the aromatic compound exploits in hydrophobic and hydrophilic environments. The first vibronic peak (I_1) is the largest peak in water, whereas the third peak (I_3) exceeds in unpolar solvents like heptane (Fig. 2.29).

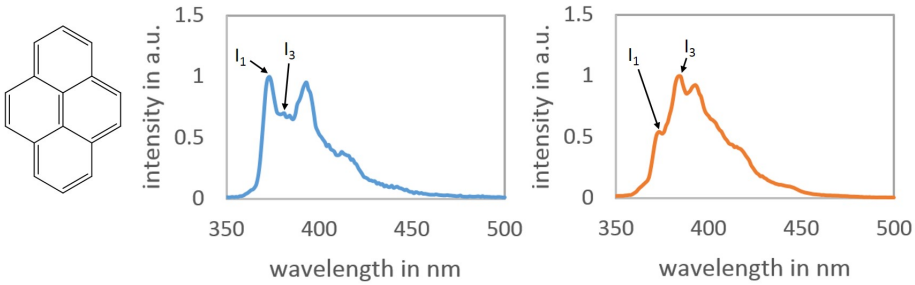

Fig. 2.29: Pyrene structure (left), fluorescence spectrum of pyrene dissolved in water (middle) and heptane (right).

An explanation for this effect could not be given to date but solute-solvent-dipole-dipole coupling appears to play a key role.[125] *The ratio I_1/I_3 is examined for the determination of the cmc. With increasing concentrations of a surfactant in aqueous solutions the ratio decreases. Pyrene is proposed to be enclosed in the hydrophobic core of micelles exposed to a more hydrophobic environment above cmc. This change from a hydrophilic to a hydrophobic environment can be observed in pyrene's fluorescence spectrum as shown in Fig. 2.29 for water and heptane.*

All seven complexes synthesized in the scope of this thesis were investigated according to the "pyrene 1:3 ratio" method. Pyrene was dissolved in 50 mM Tris-HCl buffer (pH 9) to give a 0.4 μM solution of the fluorescent probe. Varying

concentrations of the complex were added to the buffer solution and fluorescence spectra were recorded.

Throughout this titration the fluorescence intensity decreases drastically. This behavior can be explained with fluorescence quenching of Cu(II) and Co(II)/Co(III) which has been described in the literature.[126,127]

A very small distance of the fluorescent probe, the pyrene molecule, and the quenching agent, the metal ion in the head group of the surfactant, would be required according to FRET (Förster resonance energy transfer) for fluorescence quenching.[128,129] This implies that pyrene is, at least partly, solubilized at the outer shell of the micelle. A solubilization of the fluorescent probe at the outer sphere of the micelle has been proposed for small micelles.[127]

To obtain the cmc in spite of the decreasing fluorescence intensity with increasing complex concentration the slit width was changed from 5 to 10 nm throughout the experiment. Regarding the spectra obtained for the different concentrations of Co(III) **8** the change of the slit width is clear to see in a drastic increase of the intensities as can be seen for the dotted black and green curves in Fig. 2.30. Utilizing solely the ratio of two points from each spectrum, this adjustment should be negligible for the determination of the cmc.

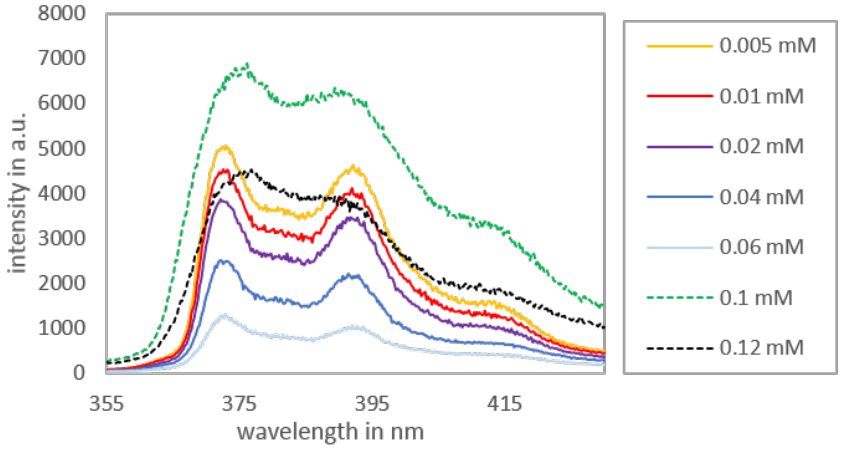

Fig. 2.30: Fluorescence spectra for different concentrations of Co(III) **8**.

For all the measurements conducted according to the "pyrene 3:1 ratio" method a peak for I_3 could never be clearly observed. For the determination of the I_1/I_3

ratio the fluorescence intensity at 385 nm was applied. This value was found in the literature for I_3.[123]

A sigmoidal graph was obtained plotting the I_1/I_3 ratio against the complex concentration.

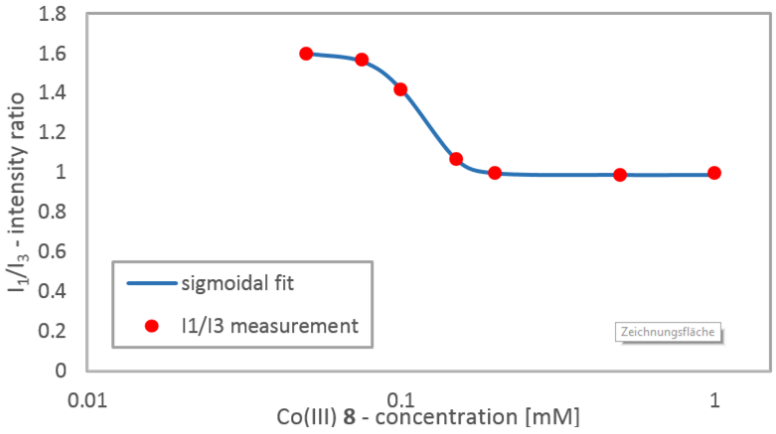

Fig. 2.31: Plot of the 1/3 ratio vs. logarithmic concentration of Co(III)**8**.

The cmc for all complexes could be obtained from the inflection point of the curve and can be found in table 2.2.

Table 2.2: Critical micellar concentrations.

Complex	cmc [mM]
Cu(II) **4**	0.47
Cu(II) **6**	0.18
Cu(II) **8**	0.08
Cu(II) **29**	0.04
Cu(II) **32**	0.46
Co(III) **8**	0.12
Co(III) **29**	0.05

With increasing chain length the cmc decreases due to an increase in hydrophobicity of the complexes.[130] According to Griffith *et al.* the introduction of a CH_2 unit cuts the cmc in half for ionic surfactants.[111] The values obtained from the fluorescence experiments do not reflect these findings. The introduction of four additional CH_2 groups from Cu(II) **6** to Cu(II) **8** resulted in a decrease of approximately 50% for the cmc.

A distinct relation between the proteolytic activity of the complexes and the cmc cannot be observed. For all complexes but Cu(II) **32** BSA was already completely cleaved at concentrations below the cmc whereas lysozyme and cytochrome c are cleaved at concentrations above the cmc of Cu(II)/Co(III) **8**. The complexes of **29** exhibit the lowest cmc but their proteolytic activity is not improved compared to the complexes of **8**. Moreover, the Cu(II) complexes exhibit a lower cmc value but also a lower proteolytic activity compared to the corresponding Co(III) complexes.

The values for the cmc were determined at room temperature whereas samples for SDS-PAGE experiments were incubated at 50 °C.[131,132] However, it was found for numerous ionic surfactants that the cmc has a minimum at concentrations close to room temperature and increases at higher concentrations. Therefore the cmc is expected to increase under the conditions chosen for the cleavage experiments.

Regarding the fluorescence quenching and the indistinct peak for I_3, another method for the determination should be used to validate the values for the cmc, e.g. ITC.

Comparing the cmc data presented in this section with the results from protein cleavage studies, micelle formation does not seem to be the origin of the improved proteolytic activity compared to complexes of cyclen. Interactions of the alkyl chain with hydrophobic regions of the proteins allowing an approach of the catalytic unit might be an explanation for the remarkable activity of the complexes below the cmc.

However, a decrease of the proteolytic activity is also not observable above the cmc although the hydrophobic residues should be shielded from interactions with the protein in the core of the micelle. Hydrophobic interactions might be the origin for the improved cleavage below the cmc, whereas above the cmc the local density of catalytic units might be beneficial for the proteolytic activity.

An alternative explanation could be the enhancement of the cmc to concentrations above those applied for the SDS-PAGE studies due to hydrophobic interactions of the complexes with the proteins. In this case hydrophobic interactions would be the single cause for the improved proteolytic activity compared to the complexes of cyclen. Interactions of the hydrophobic moiety of a Co(III) surfactant with albumin have already been observed.[126]

CHAPTER 3

Conclusion

With the finding that cyclen-based micellar species exhibit an increased cleavage activity towards DNA model systems, the question arises if this is also given for protein cleavage. To investigate the influence of micelle formation on the cleavage activity towards proteins, alkyl chains were introduced to cyclen, oxacyclen and dioxacyclen to generate amphiphiles.

The introduction of an alkyl chain to cyclen was accomplished in one step from the corresponding alkyl bromide. Derivatives with a chain length of 10, 12 an 16 carbon atoms were prepared.

Oxacyclen derivative **18** was synthesized from a 3+1 building block approach in seven steps. The final deprotection was accomplished with sulfuric acid. Complexation, proteolytic activity and particle formation studies of **18** will be discussed in the scope of another thesis.

For the synthesis of compound **29** different strategies were tested. From an adjusted building block approach as applied for **18** the product could not be obtained.

The direct alkylation of dioxacyclen only afforded the dialkylated species.

An alternative 3+1 building block approach starting from 2(-2-chloroethoxy)ethanol and tosylamine afforded the product in four steps. For the final step a much better yield was obtained *via* reductive deprotection with lithium aluminum hydride compared to acidic deprotection with HBr in glacial acetic acid and phenol.

The synthesis of compound **32** could be accomplished in one step from the macrocycle in excess with the corresponding alkyl epoxide.

The synthesis of a monoalkylated cyclen derivative with a carboxyl group, was not successful. An alternative synthesis introducing both substituents from two different building blocks might be promising.

The Cu(II) complexes of **29** and **32** were generated with copper nitrate. For the complexes of **4**, **6** and **8** copper perchlorate had to be applied for precipitation.

The Co(III) complex of **29** could be isolated with $CoCl_2$ and subsequent oxidation under air. For ligand **8** the complex could not be isolated with a Co(II) salt. $Na_3[Co(CO_3)_3]$ was used as a source for Co(III) ions. All complexes were isolated in moderate yields due to their excellent solubility in most solvents.

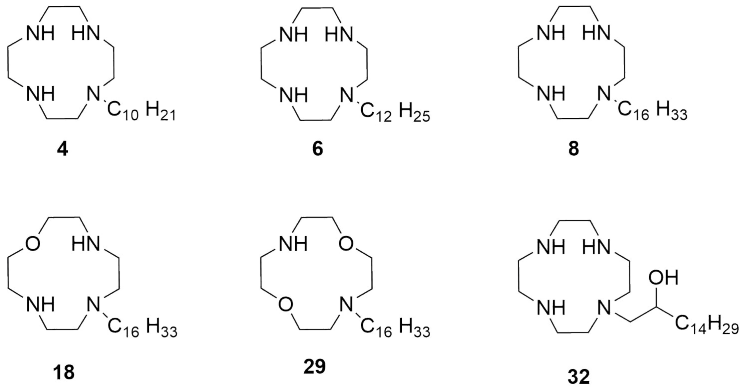

Fig. 3.1: Ligands synthesized in the scope of the present thesis.

For the determination of the proteolytic activity SDS-PAGE was performed with all complexes and various proteins. A comparison of the Cu(II) and Co(III) complexes of cyclen with a decyl, dodecyl and hexadecyl chain clearly showed a dependence of the proteolytic activity on the chain length. For complexes of the hexadecyl derivative **8** the highest activity towards BSA was detected.

Cu(II) **8** exhibited a remarkable proteolytic behavior towards heme proteins. The three heme proteins investigated for this thesis were all completely cleaved at a certain concentration. At higher concentrations, surprisingly, the proteolytic activity decreased again. For non-heme proteins the activity increases consistently with the complex concentrations.

An unexpected finding was the proteolytic activity of the ligands. Although the metal plays a key role in the cleavage mechanism proposed for cyclen complexes, the ligands exhibited a comparable activity to the complexes. ICP-MS studies suggest

nickel or aluminum contaminations in the buffer solution as source for the observed proteolytic activity

The proteolytic activity of oxacyclen complexes was reported to exceed the activity of cyclen complexes drastically. However, the oxa and dioxa species Cu(II) **18** and Cu(II) **29** were observed to cleave BSA less effectively than the cyclen derivative Cu(II) **8**.

All seven complexes, Cu(II) **4**, Cu(II) **6**, Cu(II) **8**, Co(III) **8**, Cu(II) **29**, Co(III) **29** and Cu(II) **32**, exhibit a proteolytic activity exceeding the parent compound Cu(II) **1** by at least two orders of magnitude. In general, the cleavage efficiency of the Co(III) complexes was slightly higher compared to the Cu(II) complexes.

To characterize fragments of the cleavage reaction MALDI-TOF mass spectra were recorded from myoglobin samples. Various fragments between 4 and 7.5 kDa were detected. One of the fragments has been reported before as product of the initial cleavage of a cyclen derivative near the heme group.

In context with the particular cleavage properties observed for Cu(II) **8** towards heme proteins, these findings suggest a key role of the heme group in the cleavage process. Since the heme groups of all proteins examined in these studies can be found in hydrophobic pockets, a strong interaction of the alkyl chain with the amino acids in proximity to the heme group might be possible allowing the approach of the catalytic group.

MALDI experiments with ligand **8** afforded the same fragments detected for Cu(II) **8**. This implicates that both compounds cleave myoglobin according to the same mechanism.

To investigate if the enhanced cleavage activity of the monoalkylated complexes is related to aggregation of the amphiphilic complexes the cmc was determined. The "pyrene 1:3 ratio" method was applied, a technique observing the changes in the fluorescence spectrum of pyrene in hydrophilic and hydrophobic environments. A drastic decrease of the fluorescence intensity at higher complex concentrations might originate from fluorescence quenching of the metal ions. The evaluation of the ratio of the first and third vibronic peak was complicated due to the overlapping of the peaks. The third peak was never clearly distinguishable. Hence, validation of the cmc values with another technique, e. g. ITC, is suggested.

Comparing the values for the cmc obtained from the pyrene method with the results from SDS-PAGE experiments, no distinct relation can be observed. In table

3.1 the cmc of Co(III) is compared to the lowest concentration necessary for complete cleavage of all proteins investigated here.

Table 3.1: Comparison of the cmc of Co(III) **8** with the lowest concentration necessary for complete protein cleavage according to SDS-PAGE experiments (myo = myoglobin, cyt = cytochrome c).

	Co(III) **8** conc. necessary for full protein cleavage [mM]					
cmc Co(III) **8**	BSA	cyt.	lysozyme	myo.	ovalbumin	peroxidase
0.12 mM	0.05	0.5	0.5	0.01	0.05	0.05

For lysozyme and cytochrome c cleavage is only observed above the cmc, whereas the four other proteins are completely cleaved below. These ambiguous results were also observed for other complexes.

Hydrophobic interactions might be an alternative explanation for the improved proteolytic activity of the amphiphilic complexes compared to Cu(II) **1**. However, those interactions would be inhibited by micelle formation due to the shielded hydrophobic residues in the core of the micelle. Since a decrease of the cleavage activity above the cmc is not observed for all complexes a combination of hydrophobic interaction below cmc and increased catalytic activity above cmc might explain the excellent proteolytic activity of the complexes presented in this thesis. Another theory would be a shift of the cmc to higher concentrations (above the concentrations applied for SDS-PAGE) in the presence of the proteins due to hydrophobic interactions. Therefore, the influence of the hydrophobic alkyl chain on the proteolytic activity should be further examined. Investigation of the cleavage sites of various proteins with hydrophobic regions via MALDI mass spectrometry might give insight into the origin of the enhanced proteolytic activity of complexes of monoalkylated cyclen derivatives.

Regarding the hydrophobic sites of the Aβ peptide, the introduction of an alkyl residue to a selective artificial protease could promote the proteolytic activity.[133]

The cytotoxicity of the complexes of **1** and **6** was examined with an MTT assay. As expected, the long alkyl chain caused a drastic increase of the cytotoxicity compared to the complexes of the bare macrocycle. Compared to other compounds currently under investigation for AD treatment the cytotoxicity of the complexes of **6** is moderate.

In summary it can be said, that seven complexes with a remarkable proteolytic activity were synthesized in the scope of this thesis. No clear relation between the proteolytic activity and particle formation could be found.

To study the nature and the size of the aggregates formed by the complexes, transmission electron microscopy and dynamic light scattering can be applied.

Regarding the requirements for artificial proteases established in section 1.6 the complexes presented in this thesis exhibit a high effectivity and a moderate toxicity. If the proposed mechanism presented in section 1.5 can be applied for these complexes a low dosage would be possible due to the catalytic mode of action. To enhance the activity under physiological conditions and to cleave pathogenic peptides specifically, the proteases need to be further modified.

The complexes presented in this work exhibit an excellent proteolytic activity with a very simple modification of the macrocycles compared to other known artificial proteases. Hence, they might serve as scaffold for such proteases for the treatment of a protein misfolding diseases or one of the numerous other applications for hydrolytic protein cleavage species.

CHAPTER 4

Experimental Section

4.1 Materials and methods

Nuclear magnetic resonance: ^{1}H NMR spectra were recorded on a JEOL JNM-LA 400 FT-NMR spectrometer at 399.65 MHz. ^{13}C NMR spectra were recorded on a BRUKER AMX 500 NMR spectrometer at 125 MHz. Chemical shifts are referenced to external TMS.

Mass spectrometry: ESI mass spectra were recorded on an AGILENT 6210 ESI TOF. The flow rate was 4 µL/min and the spray voltage was 4 kV.

SDS-PAGE: All gel electrophoreses were accomplished with a BIO-RAD Mini-PROTEAN® Tetra Cell. For the glycine system all chemicals but the gels were purchased from CARL ROTH. As reducing loading buffer Roti®-Load 1 was used. For electrophoreses "any kD" BIO-RAD Mini-PROTEAN® TGX Stain Free™ gels were used. LAEMMLI buffer as electrophoresis buffer was prepared from Rotiphorese® 10x SDS-PAGE. The self-fluorescing gels were recorded with a BIO-RAD GEL DOC™ EZ. For the experiments with tricine gels Mini-PROTEAN® Tris-Tricine Precast Gels were applied. Tricine Sample Buffer, β-mercaptoethanol and 10x Tris/Tricine/SDS buffer were purchased from BIO-RAD.

MALDI-TOF MS: MALDI-TOF measurements were prepared and recorded by **Dr. Christoph Weise** from Freie Universität Berlin. An Ultraflex-II TOF/TOF

instrument (Bruker Daltonics, Bremen, Germany) equipped with a 200 Hz solid-state Smart beam™ laser was used for the measurements. The mass spectrometer was operated in the positive linear mode. MS spectra were acquired over a m/z range of 3,000-20,000, and data were analysed using the FlexAnalysis 2.4. software provided with the instrument. Sinapinic acid was applied as matrix and the samples were spotted using the dried-droplet technique (undiluted sample directly from the incubation solution/saturated matrix solution 1:1).

MTT assay: MTT assays were prepared and evaluated by **Dr. Stefanie Wedepohl** from Freie Universität Berlin. The A549 lung epithelial cancer cells (DSMZ – German collection of microorganisms and cell cultures, #ACC 107) were maintained in DMEM medium (Life Technologies) with 10% FBS (FBS Superior, Merck Millipore) and 1% penicillin/streptomycin (Life Technologies) at 37 °C and 5% CO_2. For each MTT assay, 10 000 cells/well were seeded into 96-well plates and grown overnight. The medium was discarded and replaced with 50 μL fresh medium and 50 μL of serial dilutions of the test compounds in triplicates. The samples were incubated for 48 h. The medium was discarded and replaced with 100 μL/well fresh medium and 10 μL/well MTT (Sigma, 5 mg/mL stock solution in PBS) and incubated for another 4 h at 37 °C. The supernatant was discarded and 100 μL/well isopropanol with 0.04 M HCl was added to dissolve formazan dye crystals. Absorbance was read at 570 nm in a microplate reader (Tecan Infinite M200Pro). Absorbance values of untreated cells were set as 100% and relative viabilities were calculated as percentage of 100% control. Errors were calculated (SEM), and nonlinear dose-response curves (log(inhibitor) vs. normalized response - variable slope) were fitted to the data of three independent experiments using GraphPad Prism 5.

X-ray Crystallography: X-ray data were recorded by **Prof. Dr. Dieter Lentz** and solved by **Christian Wende** from Freie Universität Berlin. X-ray diffraction data were collected with a Bruker-AXS SMART CCD system. The structures were solved by direct methods and refined by full-matrix least-squares methods (SHELX-97).

Fluorescence: Fluorescence spectra were recorded with a Hitachi F-4500 fluorescence spectrometer or with a Varian Cary Eclipse fluorescence spectrometer.

ICP-MS: ICP-MS measurements were conducted by **Dr. Larissa Müller** from Bundesanstalt für Materialforschung und -prüfung, division 1.1. The samples were diluted in a 1:10 ratio using 1% HNO_3. For solution analysis an Element XR (Thermo Fisher Scientific, Bremen, Germany) was connected to a MicroMist nebulizer with a Twinnabar cyclonic spray chamber (Glass Expansion, Melbourne, Australia) using a nebulizer gas fow rate of 1.0 L/min argon. A non-matrix-matched one-point-calibration was performed for semi quantitative analysis of the samples.

4.2 Starting materials

Stock: 1-Bromodecane, 1-bromododecane, triethylamine, cobalt(II) chloride hexahydrate, copper(II) nitrate, cyclen, sodium carbonate, phenol, sodium hydride (60% dispersion in mineral oil), millipore water, cobalt(II) nitrate hexahydrate, diethylene glycol, ethylenediaminetetraacetic acid disodium salt dihydrate.

Acros: Pyridine, 4-toluenesulfonamide, dimethylformamide, triethylamine, copper(II) perchlorate hexahydrate.

Alfa Aesar: Methanesulfonyl chloride.

Bio-Rad: Any kD™ Mini-PROTEAN® TGX Stain-Free Protein Gels, Mini-PROTEAN®, Tris/tricine precast gels, tricine sample buffer, 10x Tris/tricine-SDS running buffer, β-mercaptoethanol.

Chempure: 4-Toluenesulfonyl chloride.

Fischer Scientific: Tris, sodium bicarbonate, hydrogen peroxide, potassium carbonate, sulfuric acid ($\geq$ 95%).

Merck: Lithium aluminium hydride, 1-hexadecylamine, hydrogen bromide in glacial acetic acid (32%), 1-bromohexadecane, ethanolamine, DMAP.

New England Biolabs: Protein marker (2-212 kDa).

Roth: BSA, Rotiphorese® 10x SDS-PAGE running buffer, Roti®-Load 1 loading buffer, Roti®-blue staining solution, lysine (chicken egg white).

Sigma Aldrich: 1,2-Epoxyhexadecane, 2-(2-chloroethoxy)ethanol, cesium carbonate, myoglobin (equine sceletal), ovalbumin (chicken egg white), cytochrome c (equine heart), horseradish peroxidase, ethylenediaminetetraacetic acid (99.995% trace metal basis).

VWR: Chloroform.

4.3 Ligand synthesis

4.3.1 General procedure for the preparation of 1-alkyl-1,4,7,10-tetraazacyclododecanes

Four equivalents of 1,4,7,10-tetraazacyclododecane were dissolved in chloroform (15 mL/mmol of alkyl bromide). Triethylamine (1.2 equivalents) and the alkyl bromide (1 equivalent) were added under argon atmosphere and the solution was heated to reflux for 15 h. The mixture was allowed to cool to room temperature and was washed with a sodium hydroxide solution (1 M, 15 mL/mmol of alkyl bromide) three times and three times with water. The organic layer was dried with sodium sulfate and the solvent was evaporated to give a yellow solid. The residue was dissolved in ethanol, HCl (24%) was added until no more precipitate was formed and the mixture was filtered. The precipitate was recrystallized from ethanol. The white powder was dissolved in KOH (20%, 10 mL/mmol of alkyl bromide) and extracted with chloroform. The organic layers were combined, dried over sodium sulfate and the solvent was evaporated.

4.3.2 Synthesis of 1-decyl-1,4,7,10-tetraazacyclododecane

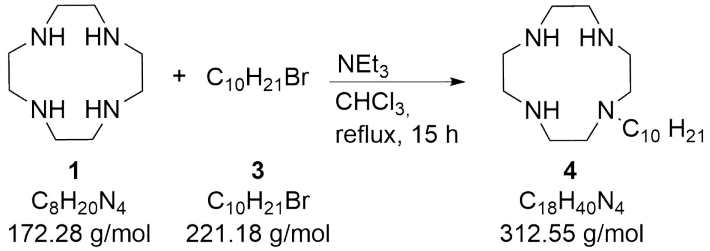

Scheme 4.1: Synthesis of 1-decyl-1,4,7,10-tetraazacyclododecane.

1,4,7,10-Tetraazacyclododecane:	3.11 g	(18.2 mmol)
Triethylamine:	0.54 g	(0.8 mL, 7.2 mmol)
1-Bromodecane:	1.00 g	(0.9 mL, 4.5 mmol)

Compound **4** was synthesized according to the general procedure given above.
Yield: 0.83 g (2.7 mmol), 59%
Appearance: orange oil

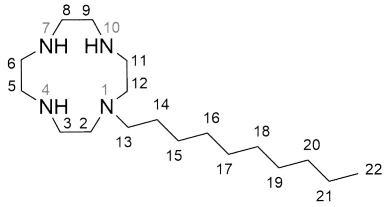

^{1}**H NMR** (400 MHz, $CDCl_3$) δ = 0.85 (t,J = *6.8 Hz*, 3 H, H^{22}), 1.22 (s, 14 H, H^{15-21}), 1.40–1.45 (m, 2 H, H^{14}), 2.36–2.40 (m, 2 H,H^{13}), 2.47–2.51, 2.52–2.55, 2.60–2.62, 2.74–2.79 (m, 16 H, $H^{2,3,5,6,8,9,11,12}$) ppm.

4.3.3 Synthesis of 1-dodecyl-1,4,7,10-tetraazacyclododecane

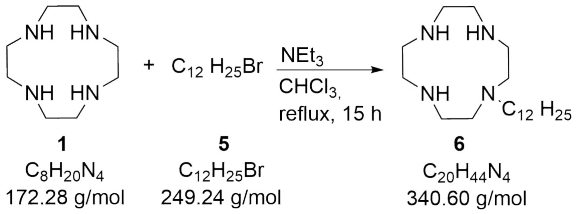

Scheme 4.2: Synthesis of 1-dodecyl-1,4,7,10-tetraazacyclododecane.

1,4,7,10-Tetraazacyclododecane:	4.14 g	(24.0 mmol)
Triethylamine:	0.73 g	(1.0 mL, 7.2 mmol)
1-Bromododecane:	1.33 g	(1.24 mL, 5.3 mmol)

Compound **6** was synthesized according to the general procedure given above.

Yield: 1.20 g (3.5 mmol), 66%
Appearance: orange solid

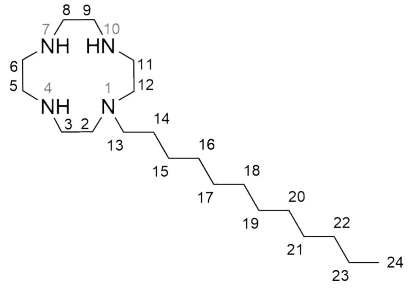

^{1}**H NMR** (400 MHz, $CDCl_3$) δ = 0.85 (m, 3 H, H^{24})), 1.22 (s, 18 H, H^{15-23})), 1.41–1.47 (m, 2 H, H^{14})), 2.35–2.39 (m, 2 H, H^{13}), 2.47-2.50, 2.52-2.55, 2.60–2.62, 2.73–2.78 (m, 4 H, $H^{2,3,5,6,8,9,11,12}$) ppm.

4.3.4 Synthesis of 1-hexadecyl-1,4,7,10-tetraazacyclododecane

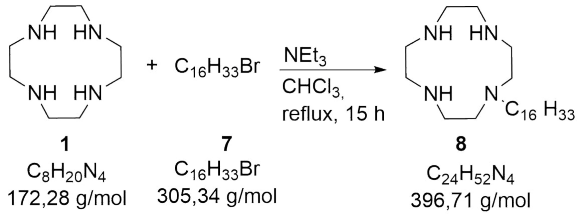

Scheme 4.3: Synthesis of 1-hexadecyl-1,4,7,10-tetraazacyclododecane.

1,4,7,10-Tetraazacyclododecane:	2.07 g (12.0 mmol)
Triethylamine:	0.37 g (0.5 mL, 3.6 mmol)
1-Bromohexadecane:	0.96 g (0.9 mL, 3.8 mmol)

Compound **8** was synthesized according to the general procedure given above.

Yield: 1.04 g (2.6 mmol), 69%
Appearance: yellow solid

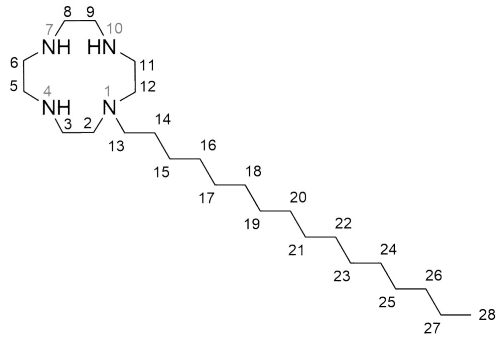

^{1}H NMR (400 MHz, $CDCl_3$) δ = 0.85 (t, J = 6.8 Hz, 3 H, H^{28}), 1.23 (s, 25 H, H^{15-27}), 1.40–1.48 (m, 2 H, H^{14}), 2.36–2.40 (m, 2 H, H^{13}), 2.48–2.51 , 2.53–2.56, 2.60–2.62 , 2.74–2.79 (m, 4 H, $H^{2,3,5,6,8,9,11,12}$) ppm.

4.3.5 Synthesis of 1-(2-hydroxyhexadecyl)-1,4,7,10-tetraazacyclododecane

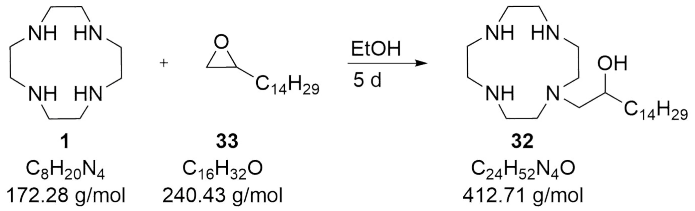

Scheme 4.4: Synthesis of 1-(2-hydroxyhexadecyl)-1,4,7,10-tetraazacyclododecane.

1,4,7,10-Tetraazacyclododecane:	5.51 g	(32.0 mmol)
1,2-Epoxyhexadecane:	0.77 g	(0.3 mmol)

Cyclen and the epoxide were dissolved in 55 mL of degassed ethanol. The solution was stirred for 5 days. The clear colorless solution was evaporated and recrystallized from water.

Yield: 1.16 g (0.3 mmol), 88% Lit: quantitative[134]
Appearance: white powder

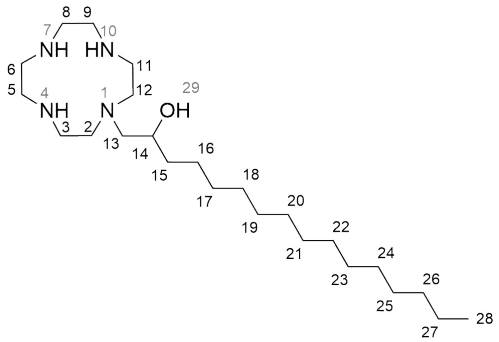

^{1}**H NMR** (400 MHz, $CDCl_3$) δ = 0.88 (t, J = *6.9 Hz*, 3 H, H^{28}), 1.25 (s, 26 H, H^{15-27}), 2.34–2.86 (m, 18 H, CH^{2-12}), 3.68 (m, 1 H, H^{14}) ppm.

4.3.6 Synthesis of 2-((4-methylphenyl)sulfonamido)ethyl-4-methylbenzenesulfonate

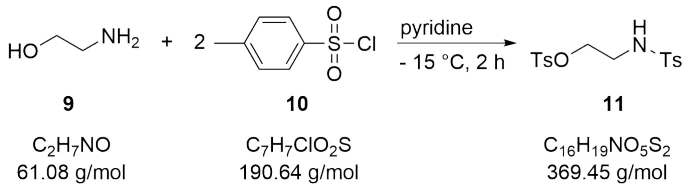

Scheme 4.5: Ditosylation of ethanolamine.

p-Toluenesulfonyl chloride:	40.30 g	(211.0 mmol)
Ethanolamine:	6.10 g	(100.0 mmol)
Pyridine:	35 mL	

p-Toluenesulfonyl chloride was added to 25 mL of pyridine and cooled to -15 °C. Over a period of 30 minutes a pre-cooled solution (0 °C) of ethanolamine in 10 mL of pyridine was added dropwise. The yellow mixture was stirred for 2 h at -15 °C and then for 5 h at 0 °C. The mixture was kept at -20 °C for two days. Ice water was added and the solid was filtered off. The residue was dissolved in 250 mL of $CHCl_3$, washed with water three times and dried over sodium sulfate. The solution was evaporated and the yellow solid was recrystallized from ethanol.

Yield: 26.60 g (72.0 mmol), 72%
Appearance: cream colored powder

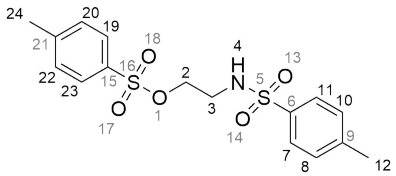

^{1}H NMR (400 MHz, $CDCl_3$) δ = 2.43 (s, 3 H), 2.46 (s, 3 H), 3.20 –3.24 (m, 2 H), 4.04 (t,*J = 5.4 Hz*, 1H), 4.86 (t, *J = 6.5 Hz*, 1 H, NH), 7.29 –7.36 (m, 4 H, $H^{8,10,20,22}$), 7.68–7.75 (m, 4 H, $H^{7,11,19,23}$) ppm.

4.3.7 Synthesis of *N*-(*p*-tolylsulfonyl)aziridine

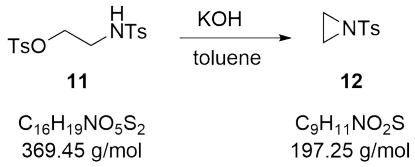

Scheme 4.6: Synthesis of *N*-(*p*-Tolylsulfonyl)aziridine.

Compound **11**:	7.50 g	(20 mmol)
KOH (aqueous solution, 20%):	30.0 mL	

Compound **11** was added to 160 mL of dry toluene. KOH was added rapidly to the stirred solution. The orange mixture was stirred for 40 minutes. The mixture was washed with water three times and was dried with sodium sulfate. Catalytic amounts of 4-*tert*-butylcatechol were added to prevent polymerization before the solvent was removed under vacuum. The crude product was isolated as a brown oil. Crystallization of the brown oil with DCM and hexane as described in the literature was not successful.

Yield: 3.605 g (18.3 mmol), 90% (crude) Lit: 93%[100]
Appearance: brown oil

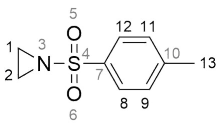

^{1}H NMR (400 MHz, $CDCl_3$) δ = 2.37 (s, 4 H, $H^{1,2}$), 2.45 (s, 3 H, H^{13}), 7.35 (d, 2 H, *J = 7.8 Hz* $H^{9,11}$), 7.83 (d, *J = 7.8 Hz*, 2 H, $H^{8,12}$) ppm.

4.3.8 Synthesis of *N,N''*-(bis(*p*-tolylsulfonyl)diethylentriamine

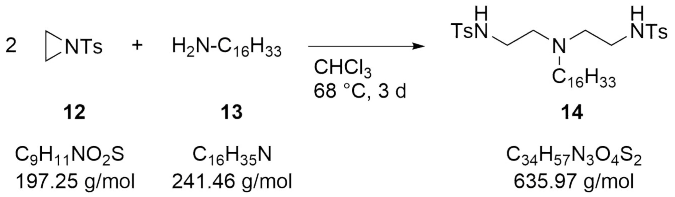

Scheme 4.7: Synthesis of *N,N''*-(bis(*p*-tolylsulfonyl)diethylenetriamine.

Compound **12**:	5.04 g	(25.6 mmol)
1-Hexadecylamine:	3.09 g	(12.1 mmol)

Compound **12** and 1-hexadecylamine were heated to reflux in 50 mL of chloroform for 56 h. The solution was allowed to cool to room temperature and the solvent was evaporated. The brown oil was purified *via* column chromatography (SiO_2, DCM/MeOH 98:2).

Yield: 6.959 g (10.7 mmol), 86% Lit: 77%[101]
Appearance: light brown oil

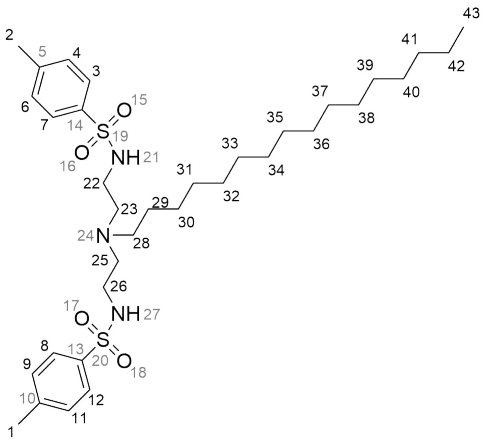

^{1}**H NMR** (400 MHz, $CDCl_3$) δ = 0.88 (t, *J = 6.8 Hz*, 3 H, H^{43}), 1.26 (m, 28 H, H^{29-42}), 2.13–2.19 (m, 2 H, H^{28}), 2.42–2.45 (m, 10 H, $H^{1,2,23,25}$), 2.89 (t, *J = 5.6 Hz*, 4 H, $H^{22,26}$), 7.31 (2 d, *J = 8.5 Hz*, 4 H, $H^{4,6,9,11}$), 7.77 (2 d, *J = 8.2 Hz*, 4 H, $H^{3,7,8,12}$) ppm.

4.3.9 Synthesis of 1,5-bis(tosyloxy)-3-oxapentane

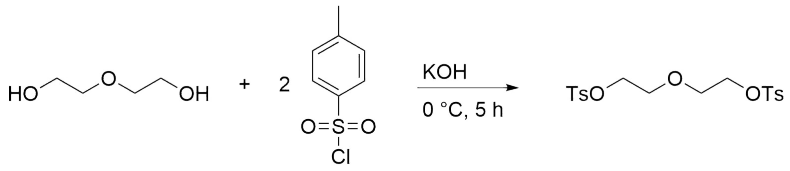

15
$C_4H_{10}O_3$
106.12 g/mol

10
$C_7H_7ClO_2S$
190.64 g/mol

16
$C_{18}H_{22}O_7S_2$
414.49 g/mol

Scheme 4.8: Synthesis of 1,5-bis(tosyloxy)-3-oxapentane.

p-Toluenesulfonyl chloride:	28.62 g	(150.1 mmol)
KOH:	33.10 g	(590.0 mmol)
Diethylene glycol:	7.80 g	(73.5 mmol)

Diethylene glycol and *p*-toluenesulfonyl chloride were added to 75 mL of DCM. The stirred mixture was cooled to 0 °C. Potassium hydroxide was added in small portions keeping the temperature below 5 °C. The suspension was stirred for 3 h at 0 °C. 75 mL of DCM and 90 mL of ice water were added. The aqueous phase was washed with DCM twice and the organic phases were combined, washed with water twice, dried over sodium sulfate and the solvent was evaporated.

Yield: 28.9 g (69.7 mmol), 95% Lit: 98%[102]
Appearance: white powder

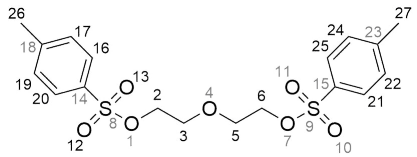

^{1}H NMR (400 MHz, $CDCl_3$) δ = 2.46 (s, 6H, $H^{26,27}$), 3.56–3.65 (m, 4H, $H^{3,5}$) ppm, 4.10–4.06 (m, 4H, $H^{2,6}$), 7.34 (d, *J = 7.6 Hz*, 4H, $H^{17,19,22,24}$), 7.78 (d, *J = 6.9 Hz*, 4H, $H^{16,20,21,25}$) ppm.

4.3.10 Synthesis of 7-hexadecyl-1-oxa-4,10-ditosyl-4,7,10-triazacyclododecane

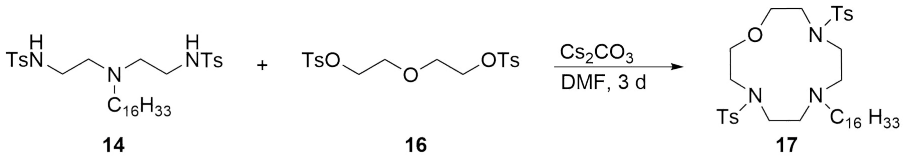

14 $C_{34}H_{57}N_3O_4S_2$ 635.97 g/mol

16 $C_{18}H_{22}O_7S_2$ 414.49 g/mol

17 $C_{38}H_{63}N_3O_5S_2$ 706.06 g/mol

Scheme 4.9: Synthesis of macrocycle **17**.

Compound **14**:	6.70 g	(10.5 mmol)
Compound **16**:	4.36 g	(10.5 mmol)
Cesium carbonate:	8.58 g	(26.3 mmol)

Compound **14** and cesium carbonate were added to 160 mL of dry DMF under argon atmosphere. The mixture was stirred for 50 minutes. Compound **16** in 30 mL of dry DMF was added dropwise over a period of 4.5 h. The suspension was stirred for 3 days under argon. Ice water was added and mixture was left at -20 °C overnight. The precipitate was filtered off and recrystallized from DMF.

Yield: 5.19 g (7.3 mmol), 70%
Appearance: brown crystals

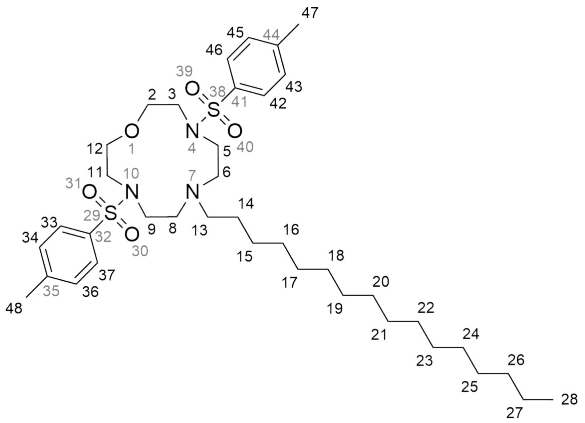

^{1}H NMR (400 MHz, $CDCl_3$) δ = 0.88 (t, *J = 6.6 Hz*, 3H, H^{28}), 1.26 (s, 28 H, H^{14-17}), 2.42 (s, 8H, $H^{13,47,48}$), 2.86 (t, *J = 6.8 Hz*, 4H, $H^{6,8}$), 3.15

(t, J = *6.6 Hz*, 4H, $H^{5,9}$), 3.33–3.25 (m, 4H, $H^{3,11}$), 3.66–3.56 (m, 4H, $H^{2,12}$), 7.30 (d, J = *8.0 Hz*, 4H, $H^{34,36,43,45}$), 7.66 (d, J = *8.2 Hz*, 4H), 7.30 (d, J = *8.0 Hz*, 4H) ppm.

^{13}C-NMR (125 MHz, $CDCl_3$) δ = 143.48 ($C^{35,44}$), 135.78 ($C^{32,41}$), 129.37 ($C^{33,37,42,46}$), 127.37 ($C^{34,36,43,45}$), 71.82 ($C^{2,12}$), 55.25 (C^{13}), 51.86 ($C^{macrocycle}$), 50.03 ($C^{macrocycle}$), 47.77 ($C^{macrocycle}$), 32.04 (C^{14}), 29.83, 29.75, 29.48, 27.44, 22.80 (C^{15-27}), 21.61 ($C^{47,48}$), 14.24 (C^{28}) ppm.

ESI-MS: $^{m}/_{z}$ = 706.2205 [**17**+H]$^+$ (calculated: 706.4282)

4.3.11 Synthesis of 7-hexadecyl-1-oxa-4,7,10-triazacyclododecane

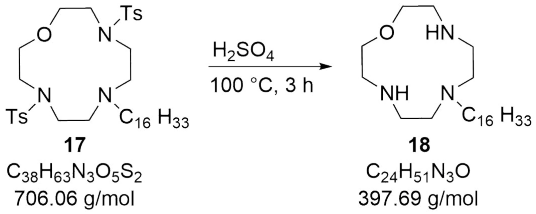

17
$C_{38}H_{63}N_3O_5S_2$
706.06 g/mol

18
$C_{24}H_{51}N_3O$
397.69 g/mol

Scheme 4.10: Synthesis of 7-hexadecyl-1-oxa-4,7,10-triazacyclododecane.

Compound **17**:	0.48 g	(0.7 mmol)
Sulfuric acid (96%):	53.0 mL	

Compound **17** was added to sulfuric acid and the solution was stirred at 100 °C for 3 h. The mixture was cooled to 0 °C and 1.3 mL of ethanol and 1.1 mL of diethyl ether were added slowly. The solution was kept at -20 °C overnight. A black solid was filtered off and was dried under vacuum. The residue was dissolved in 2 mL of a 1 M sodium hydroxide solution and was washed three times with 1 mL of chloroform. The organic layers were combined, dried over sodium sulfate and the solvent was evaporated.

Yield: 0.20 g (0.5 mmol), 73%
Appearance: light yellow powder

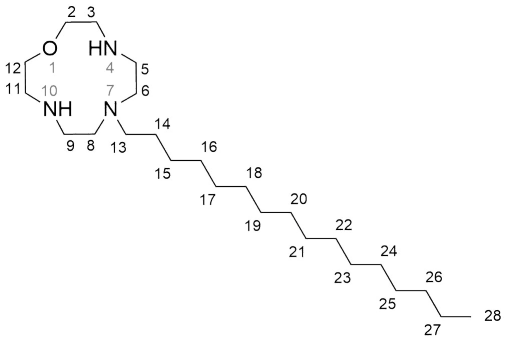

^{1}H NMR (400 MHz, $CDCl_3$) δ = 0.88 (t, *J = 6.7 Hz*, 3H, H^{28}), 1.25 (s, 28 H, H^{14-28}), 2.44–2.37 (m, 2H, H^{13}) 2.55–2.52 (m, 4H, $H^{6,8}$), 2.64–2.60 (m, 4H, $H^{5,9}$), 2.79–2.76 (m, 4H, $H^{3,11}$), 3.63–3.59 (m, 4H, $H^{2,12}$) ppm.

^{13}C-NMR (125 MHz, $CDCl_3$) δ = 68.15 ($C^{2,12}$), 52.45 ($C^{3,5,6,8,9,11,12}$), 32.06, 29.83, 29.82, 29.79, 29. 78, 29.77, 29.70, 29.49, 27.66, 27.44, 22.82 (C^{13-27}), 14.24 (C^{28}) ppm.

ESI-MS: $^{m}/_{z}$ = 398.4102 [**18**+H]$^{+}$ (calculated: 398.4105)

4.3.12 Synthesis of 2,2'-(hexadecylazanediyl)bis(ethan-1-ol)

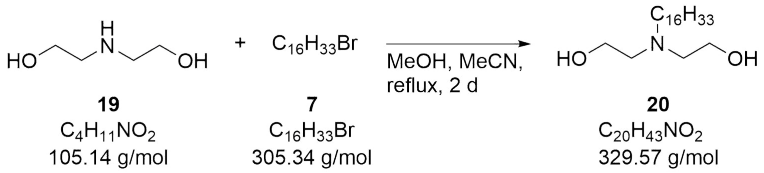

19
$C_4H_{11}NO_2$
105.14 g/mol

7
$C_{16}H_{33}Br$
305.34 g/mol

20
$C_{20}H_{43}NO_2$
329.57 g/mol

Scheme 4.11: Synthesis of 2,2'-(hexadecylazanediyl)bis(ethan-1-ol.

Diethanolamine:	542 mg	(5.2 mmol)
Hexadecyl bromide :	1.6 mL	(5.2 mmol)

To a solution of diethanolamine in 30 mL of a methanol/acetonitrile solvent mixture (3:7) hexadecyl bromide was added. The solution was heated to reflux for 48 h. The solvent was evaporated and the residue was cooled to 5 °C. The white solid was washed with diethyl ether and dried under vacuum. The residue was dissolved in water and the pH was adjusted to 14 with potassium hydroxide. The precipitate was filtered off and was washed with diethyl ether three times. The organic layers were combined, dried over sodium sulfate and the solvent was evaporated.

Yield: 470 mg (1.4 mmol), 27% Lit: 63%[135]
Appearance: yellow powder

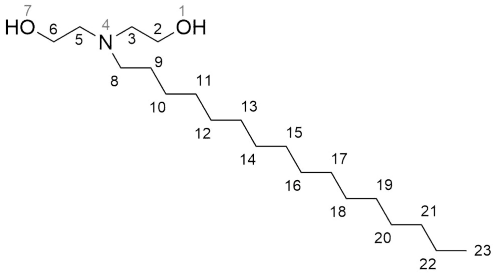

^{1}H NMR (400 MHz, $CDCl_3$) δ = = 0.88 (t, *J = 6.8 Hz*, 3 H, H^{23}), 1.25 (brs, 28 H, H^{9-22}), 2.61–2.51 (m, 2 H, H^8), 2.70 (t, *J = 5.4 Hz,* 4 H, $H^{3,5}$), 3.64 (t, *J = 5.4 Hz*, 4 H, $H^{2,6}$) ppm.

4.3.13 Synthesis of *N*-*O*-*O'*-tris(*p*-tolylsulfonyl)-diethanolamine

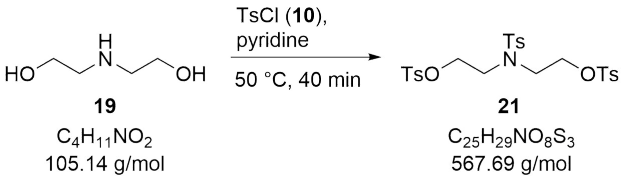

Scheme 4.12: Synthesis of*N*-*O*-*O'*-tris(*p*-tolylsulfonyl)-diethanolamine.

Diethanolamine:	7.7 g	(73.2 mmol)
p-Toluenesulfonyl chloride:	41.7 g	(219.0 mmol)
Pyridine:	120 mL	

To a solution of *p*-toluenesulfonyl chloride in 100 mL of pyridine was added diethanolamine in 20 mL of pyridine dropwise over a period of 40 minutes keeping the temperature below 50 °C. The mixture was stirred for 40 minutes at 50 °C and was then cooled to 0 °C. 90 mL of water were added to the yellow suspension and it was stirred for 16 h. The mixture was cooled to 0 °C, a pale yellow solid was filtered off and was washed with cold ethanol. The yellow powder was purified *via* column chromatography (SiO_2, hexane/ethyl acetate/DCM 4:1:5).

Yield: 12.21 g (21.5 mmol), 29% Lit: 60%[136]
Appearance: white powder

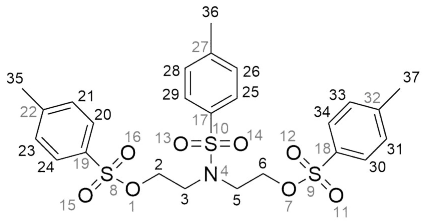

^{1}H NMR (400 MHz, $CDCl_3$) δ = = 2.43 (s, 3 H, H^{36}), 2.46 (s, 6 H, $H^{35,37}$), 3.37 (t, *J = 6.0 Hz*, 4 H, $H^{3,5}$), 4.11 (t, *J = 5.9 Hz*, 4 H, $H^{2,6}$), 7.29 (dd, *J = 7.6, 0.8 Hz*, 2 H, $H^{26,28}$), 7.36 (dd, *J = 7.7, 0.9 Hz*, 4 H, $H^{21,23,31,33}$), 7.61 (dd, *J = 8.3, 1.7 Hz*, 2 H, $H^{25,29}$), 7.76 (dd, *J = 8.4, 1.7 Hz*, 4 H, $H^{20,24,30,34}$) ppm.

4.3.14 Synthesis of *N,N*-bis(2-(2-Hydroxyethoxy)ethyl)-4-methylbenzenesulfonamide

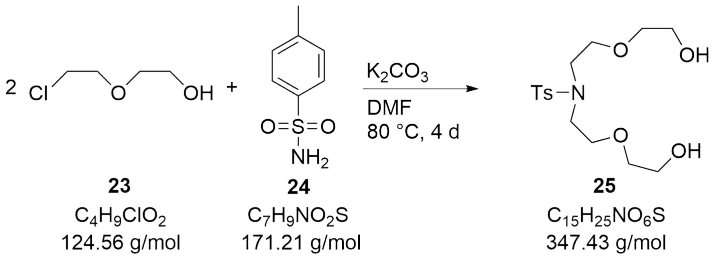

Scheme 4.13: Synthesis of diol **25**.

4-Toluenesulfonamide:	21.14 g	(0.1 mol)
2-(2-Chloroethoxy)ethanol:	34.0 mL	(0.2 mol)
Potassium carbonate:	86.69 g	(0.6 mol)

All reactants were added to 300 mL of DMF and the mixture was heated to reflux for 4 days under vigorous stirring. The mixture was cooled to room temperature and was filtered. The precipitate was washed with DCM (2 x 50 mL). The filtrate and the washing solution were combined and the solvent was evaporated *in vacuo*. The product was purified *via* column chromatography (ethylacetate, ethylacetate/methanol 95:5).

Yield: 33.92 g (97.6 mmol), 79% Lit: 77%[137]
Appearance: yellow oil

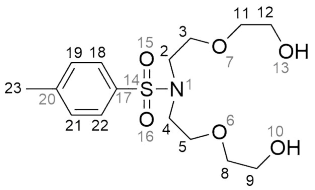

^{1}H NMR (400 MHz, $CDCl_3$) δ = 2.42 (s, 3 H, H^{23}), 3.34–3.36, 3.53–3.55, 3.67 – 3.70 (m, 16 H, $H^{2,3,4,5,8,9,11,12}$), 7.3 (m, *J = 8.2 Hz*, 2 H, $H^{19,21}$), 7.69 (d,*J = 8.2 Hz*, 2 H, $H^{18,22}$) ppm.

4.3.15 Synthesis of *N,N*-bis(2-(2-Hydroxyethoxy)ethyl)-4-methylbenzenesulfonamide

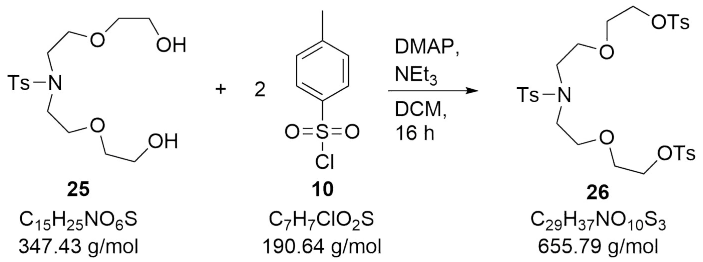

25
$C_{15}H_{25}NO_6S$
347.43 g/mol

10
$C_7H_7ClO_2S$
190.64 g/mol

26
$C_{29}H_{37}NO_{10}S_3$
655.79 g/mol

Scheme 4.14: Synthesis of diol **25**.

Compound **25**:	10.93 g	(31.5 mmol)
p-Toluenesulfonyl chloride:	18.00 g	(94.4 mmol)
Triethylamine:	26.5 mL	(190.0 mmol)
DMAP:	7 mg	(0.1 mmol)

Compound **25**, DMAP and *p*-toluenesulfonyl chloride were dissolved in 300 mL of DCM under argon and cooled to 0 °C. *p*-Toluenesulfonyl chloride was dissolved in 200 mL of DCM and was added dropwise over a period of 2.5 h at 0 °C. The mixture was stirred overnight and was washed with saturated sodium hydrogencarbonate solution (2 x 150 mL). The aqueous layer was washed with DCM (3 x 100 mL). The combined organic phases were dried with sodium sulfate and evaporated in vacuo. The pure product was obtained by column chromatography (SiO_2, DCM).

Yield: 18.06 g (27.6 mmol), 88% Lit: 65%[95]
Appearance: yellow oil

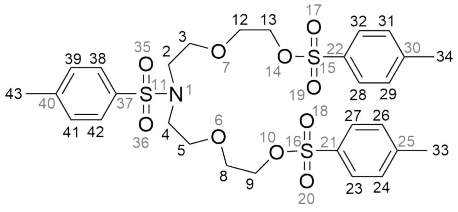

^{1}**H NMR** (400 MHz, $CDCl_3$) δ = 2.42 (s, 3 H, H^{43}), 2.44 (s, 6 H, $H^{33,34}$), 3.3 (t, *J = 5.8 Hz*, 4 H, $H^{2,4}$), 3.53–3.59 (m, 8 H, $H^{3,5,8,12}$), 4.08–4.10 (m, 4 H, $H^{9,13}$), 7.3 (d, *J = 8.2 Hz*, 2 H, $H^{39,41}$), 7.35 (d, *J = 8.3 Hz*, 4 H, $H^{24,26,29,31}$), 7.68 (d, *J = 8.2 Hz*, 2 H, $H^{39,41}$), 7.78 (d, *J = 8.3 Hz*, 4 H, $H^{38,42}$) ppm.

4.3.16 Synthesis of 4,10-ditosyl-1,7-dioxa-4,10-diazacyclododecane

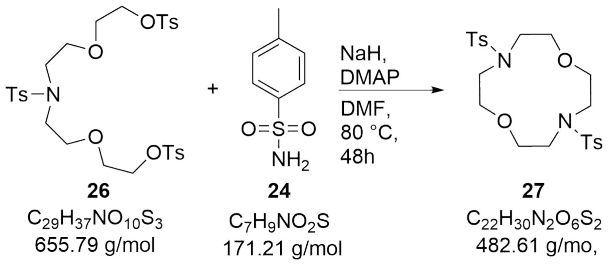

Scheme 4.15: Synthesis of 4,10-ditosyl-1,7-dioxa-4,10-diazacyclododecane.

Compound **26**:	6.36 g	(9.7 mmol)
p-Toluenesulfonamide:	1.66 g	(9.6 mmol)
Sodium hydride (60% dispersion in mineral oil):	0.88 g	(22.1 mmol)

p-Toluenesulfonamide was dissolved in 450 mL of dry DMF under argon. Sodium hydride was added to the solution under stirring. The mixture was heated to 80 °C for 2.5 h. Compound **26** was dissolved in 30 mL of dry DMF and was added dropwise over a period of 5.5 h at the same temperature. The yellow solution was stirred at 80 °C overnight and then cooled to room temperature. 300 mL of a saturated sodium hydrogencarbonate solution were added and the mixture was extracted with DCM (4 x 150 mL). The organic layers were combined, dried over sodium sulfate and the solvent was evaporated. The residue was recrystallized from DCM and ethanol.

Yield: 4.49 g (9.3 mmol), 96% Lit: 50%[95]
Appearance: yellow oil

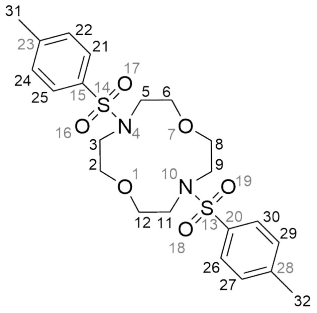

^{1}**H NMR** (400 MHz, $CDCl_3$) δ = 2.41 (s, 6 H, $H^{31,32}$), 3.22–3.24 (m, 8 H, $H^{3,5,9,11}$), 3.73–3.75 (m, 8 H, $H^{2,6,8,12}$), 7.32 (d, J = *8.3 Hz*, 4 H, $H^{22,24,26,30}$), 7.69 (d, J = *8.3 Hz*,4 H, $H^{21,25,26,30}$) ppm.

4.3.17 Synthesis of 1,7-dioxa-4,10-diazacyclododecane

Method 1

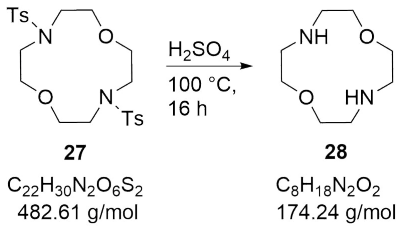

Scheme 4.16: Detosylation of **27** with H_2SO_4.

Compound **27**:	2.00 g	(11.5 mmol)
H_2SO_4 (96%):	23.0 mL	

Compound **27** was added to H_2SO_4 and the mixture was stirred for 16 h at 100 °C. The solution was cooled to room temperature and 100 mL of water were added. The solution was extracted with DCM (3 x 50 mL) and the pH of the aqueous phase was adjusted to 14 with KOH. The mixture was filtered and the filtrate was extracted with DCM (4 x 100 mL), dried with sodium sulfate and the solvent was evaporated.

Yield: 44 mg (0.3 mmol), 6%

Method 2

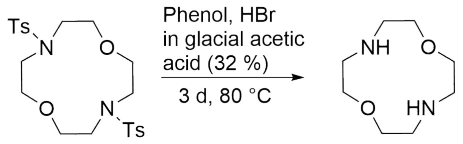

27
$C_{22}H_{30}N_2O_6S_2$
482.61 g/mol

28
$C_8H_{18}N_2O_2$
174.24 g/mol

Scheme 4.17: Detosylation of **27** with HBr/glacial acetic acid and phenol.

Compound **27**:	2.76 g	(5.7 mmol)
Phenol:	3.27 g	(34.7 mmol)
HBr in glacial acetic acid (32%):	180.0 mL	

Compound **27** and phenol were added to HBr in glacial acetic acid and the mixture was heated to 80 °C for 3 d. The solvent was removed *via* distillation and traces of the acid were removed by distillation of the dark brown residue with ethanol. The residue was dissolved in 150 mL of water and was extracted with DCM (2 x 150 mL). The aqueous phase was filtered and the filtrate was adjusted to pH 14 with KOH. The mixture was extracted with DCM (5 x 100 mL). The organic phases were combined, dried over sodium sulfate and the solvent was evaporated.

Yield: 0.85 g (4.9 mmol), 85% Lit: quantitative[95]
Appearance: white powder

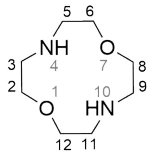

^{1}**H NMR** (400 MHz, $CDCl_3$) δ = 2.80–2.83 (m, 8 H, $H^{3,5,9,11}$), 3.62–3.64 (m, 8 H, $H^{2,6,8,12}$) ppm.

4.3.18 Synthesis of (4-[(Methylphenyl)sulfonyl]- 6-aza-1,11-undecanediol bis(methanesulfonate)

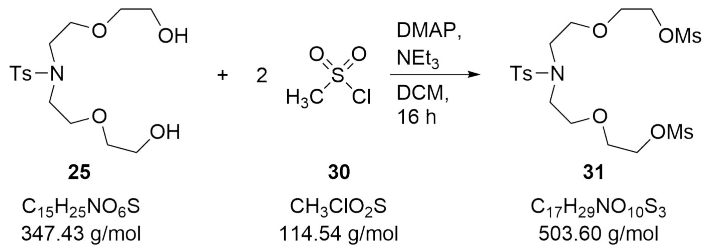

Scheme 4.18: Dimesylation of diol **25**.

Compound **25**:	9.89 g	(26.3 mmol)
Methanesulfonyl chloride:	6.05 g	(52.9 mmol)
Pyridine:	44.0 mL	

Methanesulfonyl chloride was added dropwise to compound **25** dissolved in pyridine over a period of 30 minutes with the reaction temperature beeing kept below 0 °C. The yellow mixture was stirred for 2 h at 0 °C and was kept in the refrigerator overnight. It was poured on 100 g of ice with 50 mL of HCl (30%) and extracted with DCM (3 x 40 mL). The organic phases were combined, washed with brine (2 x 25 mL) and dried over sodium sulfate. Evaporation of the solvent afforded the product as a yellow oil.

Yield: 18.06 g (27.6 mmol), 89% Lit: 50%[137]
Appearance: yellow oil

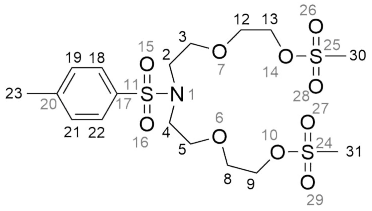

^{1}**H NMR** (400 MHz, $CDCl_3$) δ = 2.42 (s, 3 H, H^{23}), 3.04 (s, 6 H, $H^{30,31}$), 3.35–3.38 (m, 4 H, $H^{2,4}$), 3.64–3.70 (m, 8 H, $H^{3,5,8,12}$), 4.30–4.32 (m, 4 H, $H^{9,13}$), 7.31 (d, *J = 8.1 Hz*, 2 H, $H^{19,21}$), 7.69 (d, *J = 8.2 Hz*, 2 H, $H^{18,22}$) ppm.

4.3.19 Synthesis of 4-hexadecyl-10-(4'-methylbenzenesulfonyl)-4,10-diaza-1,7-dioxacyclododecane

Method 1

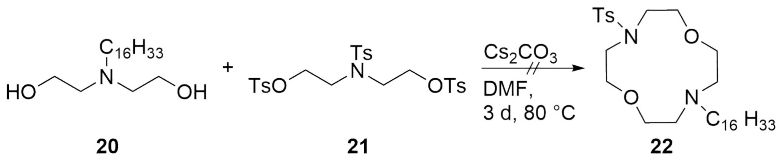

20 $C_{20}H_{43}NO_2$ 329.57 g/mol

21 $C_{25}H_{29}NO_8S_3$ 567.69 g/mol

22 $C_{31}H_{56}N_2O_4S$ 552.86 g/mol

Scheme 4.19: Synthesis of dioxacyclen **22** from **20** and **21**.

Compound **21**:	1.00 g	(3.0 mmol)
Compound **20**:	1.72 g	(3.0 mmol)
Cesium carbonate:	1.98 g	(6.1 mmol)

Compound **20** was dissolved in 20 mL of dry DMF under argon. Cesium carbonate was added and the suspension was allowed to stir for 2 h at 80 °C. Compound **21** in 10 mL of dry DMF was added dropwise over a period of 5 h. The reaction mixture was stirred for three days under argon at 80 °C. The suspension was cooled to room temperature, poured over 100 g of ice and kept at 0 °C for 2 h. 15 mL of 1 M NaOH were added and the mixture was extracted with chloroform (3 x 50 mL). The organic layers were combined, dried over sodium sulfate and the solvent was evaporated. The product could not be isolated.

Method 2

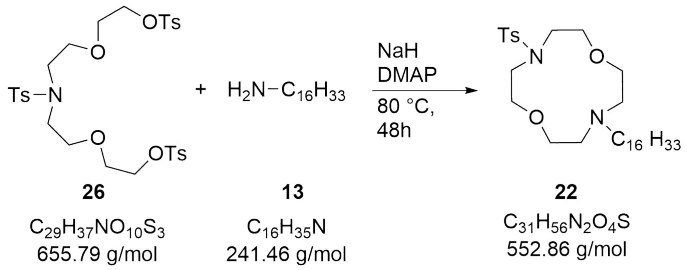

26 $C_{29}H_{37}NO_{10}S_3$ 655.79 g/mol

13 $C_{16}H_{35}N$ 241.46 g/mol

22 $C_{31}H_{56}N_2O_4S$ 552.86 g/mol

Scheme 4.20: Synthesis of dioxacyclen **22** from **26**.

Compound **26**:	3.00 g	(4.4 mmol)
Hexadecylamine:	1.11 g	(4.6 mmol)
Sodium hydride (60% dispersion in mineral oil):	0.42 g	(10.4 mmol)
DMAP:	0.01 g	(0.1 mmol)

Hexadecylamin was added to 180 mL of dry DMF under argon. Sodium hydride and DMAP were added and the mixture was stirred for 2.5 h at 80 °C. Compound **26** dissolved in 24 mL of dry DMF was added dropwise over a period of 8 h. The mixture was stirred for 2 d at 80 °C. The solvent was evaporated and the residue was purified *via* column chromatography (SiO_2, ethyl acetate/isopropylamine 95:5).

Yield: 124 mg (0.2 mmol), 5%
Appearance: white powder

Method 3

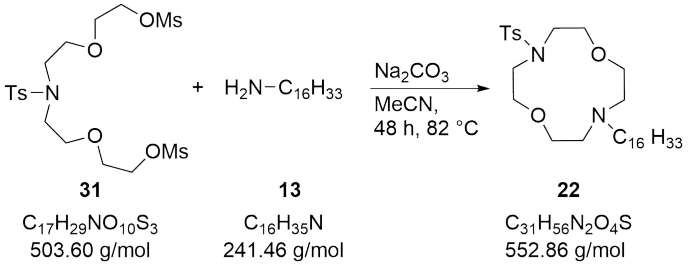

31 $C_{17}H_{29}NO_{10}S_3$ 503.60 g/mol

13 $C_{16}H_{35}N$ 241.46 g/mol

22 $C_{31}H_{56}N_2O_4S$ 552.86 g/mol

Scheme 4.21: Synthesis of dioxacyclen **22** from **31**.

Compound **31**:	8.3 g	(16.5 mmol)
Hexadecylamine:	5.6 g	(23.2 mmol)
Sodium carbonate:	9.4 g	(0.3 mmol)

All reactants were added to 500 mL of dry acetonitrile under argon and were heated to reflux for 48 h under stirring. After cooling to room temperature the mixture was filtered. The precipitate was washed with acetonitrile (200 mL) and DCM (200 mL). The collected filtrates were evaporated and the residue was purified *via* column chromatography (Al_2O_3, ethylacetate/hexane 1:1, ethylacetate 100%).

Yield: 5.41 g (9.8 mmol), 59%
Appearance: white powder

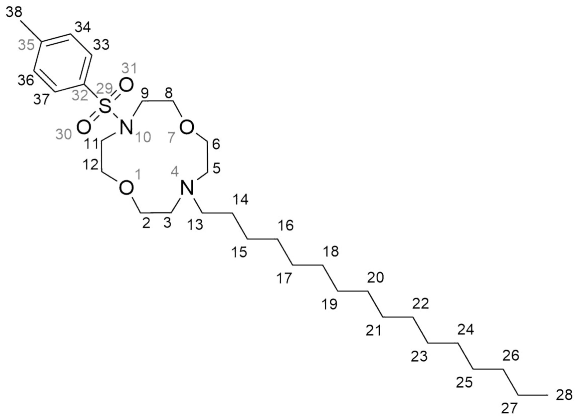

^{1}H NMR (400 MHz, $CDCl_3$) δ = 0.88 (t, 3 h, H^{28}), 1.24 (s, 26 H, H^{15-27}), 1.39–1.50 (m, 2 H, H^{14}), 2.38–2.46 (m, 5 H, $H^{13,38}$), 2.58–2.65 (m, 4 H, $H^{3,5}$), 2.75 (t, *J = 5.2 Hz*, 4 H, $H^{9,11}$), 3.51–3.55 (m, 4 H, $H^{2,6}$), 3.6 (t, *J = 5.2 Hz*, 4 H, $H^{8,12}$), 7.28 (d, *J = 8.2 Hz*, 2 H, $H^{34,36}$), 7.68 (d, *J = 8.2 Hz*, 2 H, $H^{33,37}$) ppm.

^{13}C-NMR (125 MHz, $CDCl_3$) δ = 143.3 (C^{35}), 136.17 (C^{32}), 129.26 ($C^{33,37}$), 127.44 ($C^{34,36}$), 70.44 ($C^{8,12}$), 69.4 ($C^{2,6}$), 57.36 ($C^{9,11}$), 55.8 ($C^{3,5}$), 50.7 (C^{13}), 32.06 (C^{14}), 29.83, 29.8, 29.73, 29.49, 27.83, 27.61, 22.82 (C^{15-27}), 21.62 (C^{38}), 14.25 (C^{28}) ppm.

ESI-MS: m/z = 553.4255 [**22**+H]$^+$ (calculated: 553.4034)
m/z = 399.3936 [**22**–Ts+H]$^+$ (calculated: 399.3945)

4.3.20 Synthesis of 4-hexadecyl-1,7-dioxa-4,10-diazacyclododecane

Method 1

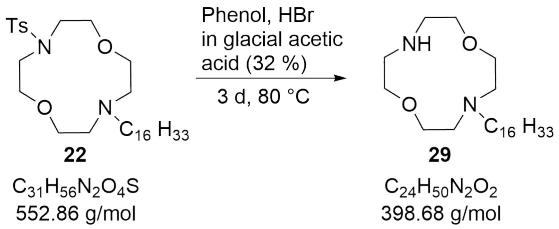

Scheme 4.22: Synthesis of dioxacyclen **29** with phenol and HBr in glacial acetic acid.

Compound **22**:	4.88 g	(31.5 mmol)
Phenol:	2.23 g	(23.7 mmol)
HBr in glacial glacial acetic acid (32%)	300 mL	

Compound **22** and phenol were dissolved in HBr in glacial glacial acetic acid and the solution was stirred for 3 d at 80 °C. The glacial glacial acetic acid was removed *via* distillation at 140 °C. Ethanol was added (2 x 100 mL) and distilled to remove traces of the acid. The brown residue was dissolved in 100 mL of water and washed with DCM (2 x 100 mL). The pH of the aqueous phase was adjusted to 14 with KOH and the orange solution was extracted with DCM (3 x 100 mL). The organic phases were combined, dried over sodium sulfate and the solvent was evaporated. Column chromatography (Al_2O_3, ethylacetate/hexane 1:1, ethylacetate, ethylacetate/methanol 9:1) afforded a yellow solid. The product was dissolved in 50 mL of ethanol and HCl was added (10 mL, 24%). Since the hydrochloride did not form a precipitate the solvent was evaporated and the residue was dissolved in 50 mL of DCM. Extraction with KOH (1 mM, 3 x 50 mL) afforded the pure product.

Yield: 0.98 g (2.5 mmol), 27%
Appearance: yellow solid

Method 2

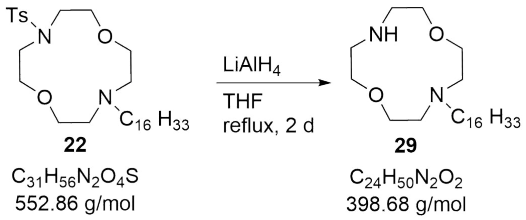

Scheme 4.23: Synthesis of dioxacyclen **29** with $LiAlH_4$.

Compound **22**:	0.56 g	(1.0 mmol)
$LiAlH_4$:	0.99 g	(26.1 mmol)

$LiAlH_4$ was added to 60 mL of dry THF under argon. Compound **22** dissolved in 50 mL of dry THF was added dropwise over a period of 2 h. The mixture was heated to reflux for 40 h and was cooled to room temperature. 100 mL of ethylacetate and 15 mL of ice water were added and the suspension was filtered through celite. The filter cake was washed with DCM, the filtrates were combined and the solvent was evaporated. The yellow solid was dissolved in water and extracted with DCM (3 x 50 mL). The combined organic phases were dried over sodium sulfate and evaporated. Column chromatography was conducted for purification (Al_2O_3, ethylacetate/hexane 5:1, ethylacetate/hexane 1:1, ethylacetate, ethylacetate/methanol 9:1).

Yield: 0.34 g (0.9 mmol), 85%
Appearance: yellow solid

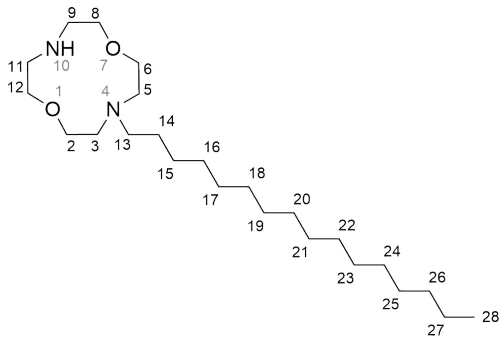

^{1}**H NMR** (400 MHz, $CDCl_3$) δ = 0.84 (t, *J = 6.9 Hz*, 3 H, H^{28}), 1.22 (s, 26 H, H^{15-27}), 1.39–1.44 (m, 2 H, H^{14}), 2.45–2.49 (m, 2 H, H^{13}), 2.6 (t,*J = 4.8 Hz*, 4 H, $H^{2,5}$), 2.75 (t, *J = 4.8 Hz*, 4 H, $H^{9,11}$), 3.51 (t,*J = 4.8 Hz*, 4 H, $H^{3,6}$), 3.59–3.61 (m, 4 H, $H^{8,12}$) ppm.

^{13}**C-NMR** (125 MHz, $CDCl_3$) δ = 66.25, 65.48 ($C^{2,6,8,12}$), 51.3, 48.82 ($C^{3,5,9,11}$), 32.05, 29.82, 29.80, 29.79, 29. 78, 29. 76, 29.74, 29.69, 29.58, 29,48 (C^{13-27}),f 14.24 (C^{28}) ppm.

CHN-Analysis: Calculated for $C_{24}H_{50}N_2O_2 \cdot 4.5\ HCl \cdot 1\ C_2H_5OH$: C, 51.3; H, 10.14; N, 4.60. Found: C, 51.29; H, 10.02; N, 4.60.

ESI-MS: $m/z = 399.4265$ [**29**+H]$^+$ (calculated: 399.3945)

4.4 Complex synthesis

4.4.1 Synthesis of sodium tris-carbonatocobaltate(III) trihydrate

Cobalt(II) nitrate hexahydrate:	2.91 g	(10.0 mmol)
Sodium bicarbonate:	4.20 g	(50.0 mmol)
Hydrogen peroxide (< 30%):	1.2 mL	

Sodium bicarbonate was added to 5 mL of water. The suspension was cooled to 0 °C and a solution of cobalt(II) nitrate hexahydrate in hydrogen peroxide (1.2 mL, 30%) and 1 mL of water was added dropwise. The mixture was stirred at 0 °C for one hour. The moss green precipitate was filtered off, washed with ice water, ethanol and diethyl ether and dried under vacuum.

Yield: 3.30 g (9.1 mmol), 91% (crude) Lit: 92%[138]
Appearance: moss green powder

4.4.2 Synthesis of Co(III)-1-hexadecyl-1,4,7,10-tetraazacyclododecane

Sodium tris-carbonatocobaltate(III) trihydrate:	159 mg	(0.4 mmol)
Compound **8**:	155 mg	(0.4 mmol)

Compound **8** was dissolved in 1.2 mL of HCl (1.2 M) and sodium tris-carbonatocobaltate(III) trihydrate was added. The purple solution was heated to 66 °C for 5 minutes, filtered and 90 mL of acetone were added to te filtrate. The mixture was kept in the refrigerator overnight and a purple precipitate was filtered off and dried under vacuum.

Yield: 127 mg (0.2 mmol), 40%
Appearance: purple powder

^{1}H NMR (700 MHz, D_2O) $\delta = 0.89$ (m, 3 H, CH_3), 1.30 (brs, 28 H, CH_2^{alkyl}), 1.67 (brs, 1 H, NH), 1.78 (brs, 1 H, NH), 2.64–3.44 (m, 18 H, C$H_2^{cyclen,alkyl}$) ppm.

CHN-Analysis: Calculated for $C_{25}H_{52}ClCoN_4O_3 \cdot 7\ H_2O \cdot 4$ HCl: C, 36.48; H, 8.57; N, 6.81. Found: C, 36.67; H, 8.58; N, 6.92.

ESI-MS:
$m/z = 515.3975$ [Co(III) **8**+CO_3]$^+$ (calculated: 515.3366)
$m/z = 489.3138$ [Co(III) **8**–H+Cl]$^+$ (calculated: 489.3129)
$m/z = 453.3712$ [Co(III) **8**–2H]$^+$ (calculated: 453.3362)

4.4.3 Synthesis of Co(III)-4-hexadecyl-1,7-dioxa-4,10-diazacyclododecane

Compound **29**:	50 mg	(0.1 mmol)
$CoCl_2 \cdot 6\ H_2O$:	62 mg	(0.3 mmol)

Compound **29** was dissolved in 3 mL of methanol and $CoCl_2 \cdot 6\ H_2O$, dissolved in 3 mL of methanol, was added. The mixture was heated to 50 °C for 1 h and was kept at -20 °C overnight. A purple precipitate was filtered off and was dried under vacuum.

Yield: 31 mg (0.1 mmol), 45%
Appearance: purple powder

CHN-Analysis: Calculated for $C_{25}H_{50}ClCoN_2O_5$: C, 54.29; H, 9.11; N, 5.09.
Found: C, 54.19; H, 9.28; N, 5.09.

ESI-MS: $m/z = 492.2895$ [Co(II) **29**+Cl]$^+$ (calculated: 492.2887)

4.4.4 General procedure for the preparation of Cu(II) complexes of 1-alkyl-1,4,7,10-tetraazacyclododecanes

Monoalkylated 1,4,7,10-tetraazacyclododecane was added to 5 mL of methanol and $Cu(ClO_4)_2 \cdot 6\ H_2O$ was added. The mixture was heated to 50 °C and was kept at -20 °C overnight.

4.4.5 Synthesis of Cu(II) 1-decyl-1,4,7,10-tetraazacyclododecane

Compound **4**:	169 mg	(0.5 mmol)
$Cu(ClO_4)_2 \cdot 6\ H_2O$:	200 mg	(0.5 mmol)

The complex was generated according to the general procedure given above. Cold diethyl ether was added to the blue solution. The mixture was filtered, washed with cold diethyl ether and the precipitate was dried under vacuum.

Yield: 149 mg (0.3 mmol), 44%
Appearance: blue powder

CHN-Analysis: Calculated for $C_{18}H_{40}Cl_2CuN_4O_8 \cdot 1\ CH_3OH \cdot 1\ H_2O$: C, 36.51; H, 8.96; N, 7.42. Found: C, 36.74; H, 8.96; N, 7.42.

ESI-MS:
$m/z = 374.2602$ [Cu(II) **4**–H]$^+$ (calculated: 374.2465)
$m/z = 410.2379$ [Cu(II) **4**+Cl]$^+$ (calculated: 410.2232)
$m/z = 474.2204$ [Cu(II) **4**+ClO_4]$^+$ (calculated: 474.2029)

4.4.6 Synthesis of Cu(II) 1-dodecyl-1,4,7,10-tetraazacyclododecane

Compound **6**:	200 mg	(0.59 mmol)
$Cu(ClO_4)_2 \cdot 6\ H_2O$:	222 mg	(0.6 mmol)

The complex was generated according to the general procedure given above. Cold diethyl ether was added to the blue solution. The precipitate was filtered off, was washed with cold diethyl ether and dried under vacuum.

Yield: 201 mg (0.3 mmol), 53%
Appearance: blue powder

CHN-Analysis: Calculated for $C_{20}H_{44}Cl_2CuN_4O_8 \cdot 1.5\ CH_4O$: C, 39.66; H, 7.74;N, 8.81. Found: C, 39.54; H, 7.78; N, 8.61.

ESI-MS:

$m/z = 402.2912$ [Cu(II) **6**–H]$^+$	(calculated: 402.2778)
$m/z = 438.2689$ [Cu(II) **6**+Cl]$^+$	(calculated: 438.2545)
$m/z = 504.2511$ [Cu(II) **6**+ClO_4]$^+$	(calculated: 502.2342)

4.4.7 Synthesis of Cu(II) 1-hexadecyl-1,4,7,10-tetraazacyclododecane

Compound **8**:	113 mg	(0.3 mmol)
$Cu(ClO_4)_2 \cdot 6\ H_2O$:	100 mg	(0.3 mmol)

The complex was generated according to the general procedure given above. The blue precipitate was filtered off and was recrystallized from DCM and hexane.

Yield: 111 mg (0.2 mmol), 55%
Appearance: blue powder

CHN-Analysis: Calculated for $C_{24}H_{52}Cl_2CuN_4O_8 \cdot 2\ CH_3OH$: C, 43.18; H, 8.36; 7.75. Found: C, 43.31; H, 8.05; N, 7.75.

ESI-MS:
$^{m}/_{z} = 558.3032$ [Cu(II) **8**+ClO_4]$^+$ (calculated: 558.2968)
$^{m}/_{z} = 494.3235$ [Cu(II) **8**+Cl]$^+$ (calculated: 494.3172)
$^{m}/_{z} = 458.3463$ [Cu(II) **8**+H]$^+$ (calculated: 458.3404)

4.4.8 Synthesis of Cu(II) 4-hexadecyl-1,7-dioxa-4,10-diazacyclododecane

Compound **29**:	150 mg	(0.4 mmol)
$Cu(NO_3)_2 \cdot 3\ H_2O$:	90 mg	(0.4 mmol)

Both compounds were dissolved in 5 mL of methanol and were heated to 50 °C for 1 h. The turqoise solution was kept at -20 °C overnight. The precipitate was filtered off, was washed with cold hexane and dried under vacuum.

Yield: 111 mg (0.2 mmol), 50%
Appearance: turqoise powder

CHN-Analysis: Calculated for $C_{24}H_{50}CuN_4O_8$: C, 49.17; H, 8.6; N, 9.53. Found: C, 49.26; H, 8.69; N, 9.56.

ESI-MS: $^{m}/_{z} = 460.3090$ [Cu(II) **29**–H]$^+$ (calculated: 460.3090)
$^{m}/_{z} = 496.2854$ [Cu(II) **29**+Cl]$^+$ (calculated: 496.2857)

4.4.9 Synthesis of Cu(II) 1-(2-hydroxyhexadecyl)-1,4,7,10-tetraazacyclododecane

Compound **32**:	115 mg	(0.3 mmol)
$Cu(NO_3)_2 \cdot 3\ H_2O$:	70 mg	(0.3 mmol)

Compound **32** and $Cu(NO_3)_2 \cdot 3\ H_2O$ were dissolved in 13 mL of methanol and the solution was heated to reflux for 10 minutes. The deep blue solution was kept at -20 °C overnight. The precipitate was filtered off, was washed with cold hexane and dried under vacuum.

Yield: 72 mg (0.1 mmol), 43%
Appearance: deep blue powder

CHN-Analysis: Calculated for $C_{24}H_{52}CuN_6O_6 \cdot 0.5\ CH_3OH \cdot 1\ H_2O$: C, 46.39; H, 8.9; N, 13.25 . Found: 46.57; H, 8.71; N, 13.15.

ESI-MS: $^{m}/_{z} = 474.3443$ [Cu(II) **32**–H]$^+$ (calculated: 474.3353)
$^{m}/_{z} = 537.3412$ [Cu(II) **32**+NO_3]$^+$ (calculated: 537.3310)

4.5 Performance of SDS-PAGE experiments

The concentration of the proteins in the incubation solution was chosen according to their molecular weight for ideal intensities of the reference bands for SDS-PAGE and can be taken from table 4.1.

Table 4.1: Protein concentration for SDS-PAGE.

Protein	**Concentration [µM]**
BSA	0.75
Cytochrome c	2.25
Lysozyme	2.25
Myoglobin	2.25
Ovalbumin	1.5
Peroxidase	1.5

For the glycine gels 3.3 μL of reducing loading buffer were added to 10 μL of the incubated samples and the solution was heated to 85 °C for 5 minutes for denaturation of the proteins and their fragments. 10 μL of this solution were loaded onto the gel. The gel electrophoresis was accomplished in 35 minutes for BSA and 30 min for all other proteins at 200 V. The stain-free protein gels were activated and recorded with a Bio-Rad Gel Doc™ EZ system.

For the tricine gels 4.75 μL of tricine sample buffer and 0.5 μL of β-mercaptoethanol were added to 10 μL of the sample after incubation. The mixture was heated to 70 °C for 10 minutes and loaded onto the gel. The electrophoresis was performed in 85 minutes at 100 V. The tricine gels were dyed with the Roti-Blue® staining solution according to the instructions of the manufacturer. The gels were recorded with a Bio-Rad Gel Doc™ EZ system.

Bibliography

[1] R. A. R. Bryant, D. E. Hansen, *J. Am. Chem. Soc.* **1996**, *118*, 5498.

[2] R. M. Smith, D. E. Hansen, *J. Am. Chem. Soc.* **1998**, *120*, 8910.

[3] A. Radzicka, R. Wolfenden, *J. Am. Chem. Soc.* **1996**, *118*, 6105.

[4] H.-C. Tai, E. M. Schuman, *Nat. Rev. Neurosci.* **2008**, *9*, 826.

[5] S. M. Molineaux, *Clin. Cancer. Res.* **2012**, *18*, 15.

[6] C. López-Otín, J. S. Bond, *J. Biol. Chem.* **2008**, *283*, 30433.

[7] J. Kubelka, J. Hofrichter, W. A. Eaton, *Curr. Opin. Struct. Biol.* **2004**, *14*, 76.

[8] U. Schubert, L. C. Antón, J. Gibbs, C. C. Norbury, J. W. Yewdell, J. R. Bennink, *Nature* **2000**, *404*, 770.

[9] J. J. Yerbury, E. M. Stewart, A. R. Wyatt, M. R. Wilson, *EMBO reports* **2005**, *6*, 1131.

[10] B. Alies, C. Hureau, P. Faller, *Metallomics* **2013**, *5*, 183.

[11] W. L. Klein, W. B. Stine, D. B. Teplow, *Neurobiol. Aging* **2004**, *25*, 569.

[12] C. M. Dobson, *Science* **2004**, *304*, 1259.

[13] P. Hammarström, R. L. Wiseman, E. T. Powers, J. W. Kelly, *Science* **2003**, *299*, 713.

[14] T. M. Ryan, B. R. Roberts, G. McColl, D. J. Hare, P. A. Doble, Q.-X. Li, M. Lind, A. M. Roberts, H. D. T. Mertens, N. Kirby, C. L. L. Pham, M. G. Hinds, P. A. Adlard, K. J. Barnham, C. C. Curtain, C. L. Masters, *J. Neurosci.* **2015**, *35*, 2871.

[15] F. Chiti, M. Stefani, N. Taddei, G. Ramponi, C. M. Dobson, *Nature* **2003**, *424*, 805.

[16] A. K. Ghosh, H. L. Osswald, *Chem. Soc. Rev.* **2014**, *43*, 6765.

[17] B. Tate, T. D. McKee, R. M. B. Loureiro, J. A. Dumin, W. Xia, K. Pojasek, W. F. Austin, N. O. Fuller, J. L. Hubbs, R. Shen, J. Jonker, J. Ives, B. S. Bronk, *Int. J. of Alzheimers Dis.* **2012**, *2012*, 1.

[18] R. B. DeMattos, K. R. Bales, D. J. Cummins, J. C. Dodart, S. M. Paul, D. M. Holtzman, *Proc. Natl. Acad. Sci.* **2001**, *98*, 8850.

[19] Y. Okuda, K. Takasugi, *Arthritis Rheum.* **2006**, *54*, 2997.

[20] W. W. Barker, C. A. Luis, A. Kashuba, M. Luis, D. G. Harwood, D. Loewenstein, C. Waters, P. Jimison, E. Shepherd, S. Sevush, N. Graff-Radford, D. Newland, M. Todd, B. Miller, M. Gold, K. Heilman, L. Doty, I. Goodman, B. Robinson, G. Pearl, D. Dickson, R. Duara, *Alz. Dis. Assoc. Disord.* **2002**, *16*, 203.

[21] M. Prince, A. Wimo, M. Guerchet, A. Gemma-Claire, Y.-T. Wu, M. Prina, *World Alzheimer Report 2015: The Global Impact of Dementia - An analysis of prevalence, incidence, cost And trends*, Alzheimer's Disease International, London, **2015**, S. 1–6.

[22] C. Vigo-Pelfrey, D. Lee, P. Keim, I. Lieberburg, D. B. Schenk, *J. Neurochem.* **1993**, *61*, 1965.

[23] K. N. Dahlgren, *J. Biol. Chem.* **2002**, *277*, 32046.

[24] J. T. Jarrett, E. P. Berger, P. T. Lansbury, *Biochem.* **1993**, *32*, 4693.

[25] D. B. Milne, P. E. Johnson, *Clin. Chem.* **1993**, *39*, 883.

[26] A. I. Bush, R. E. Tanzi, *Neurotherapeutics* **2008**, *5*, 421.

[27] M. A. Lovell, J. D. Robertson, W. J. Teesdale, J. L. Campbell, W. R. Markesbery, *J. Neurol. Sci.* **1998**, *158*, 47.

[28] A. I. Bush, W. H. Pettingell, G. Multhaup, M. d. Paradis, J. P. Vonsattel, J. F. Gusella, K. Beyreuther, C. L. Masters, R. E. Tanzi, *Science* **1994**, *265*, 1464.

[29] C. S. Atwood, R. D. Moir, X. Huang, R. C. Scarpa, N. M. Bacarra, D. M. Romano, M. A. Hartshorn, R. E. Tanzi, A. I. Bush, *J. Biol. Chem.* **1998**, *273*, 12817.

[30] P. W. Mantyh, J. R. Ghilardi, S. Rogers, E. DeMaster, C. J. Allen, E. R. Stimson, J. E. Maggio, *J. Neurochem.* **1993**, *61*, 1171.

[31] R. A. Cherny, J. T. Legg, C. A. McLean, D. P. Fairlie, X. Huang, C. S. Atwood, K. Beyreuther, R. E. Tanzi, C. L. Masters, A. I. Bush, *J. Biol. Chem.* **1999**, *274*, 23223.

[32] K. M. Lincoln, P. Gonzalez, T. E. Richardson, D. A. Julovich, R. Saunders, J. W. Simpkins, K. N. Green, *Chem. Commun.* **2013**, *49*, 2712.

[33] X. Huang, C. S. Atwood, M. A. Hartshorn, G. Multhaup, L. E. Goldstein, R. C. Scarpa, M. P. Cuajungco, D. N. Gray, J. Lim, R. D. Moir, R. E. Tanzi, A. I. Bush, *Biochem.* **1999**, *38*, 7609.

[34] V. Conte, K. Uryu, S. Fujimoto, Y. Yao, J. Rokach, L. Longhi, J. Q. Trojanowski, V. M.-Y. Lee, T. K. McIntosh, D. Praticò, *J. Neurochem.* **2004**, *90*, 758.

[35] G. P. Lim, T. Chu, F. Yang, W. Beech, S. A. Frautschy, G. M. Cole, *J. Nerusci.* **2001**, *21*, 8370.

[36] K. M. Lincoln, T. E. Richardson, L. Rutter, P. Gonzalez, J. W. Simpkins, K. N. Green, *ACS Chem. Neurosci.* **2012**, *3*, 919.

[37] H. Kim, M.-S. Kim, H. Paik, Y.-S. Chung, I. S. Hong, J. Suh, *Bioorg. Med. Chem. Lett.* **2002**, *12*, 3247.

[38] J. Suh, S. Oh, *J. Org. Chem.* **2000**, *65*, 7534.

[39] A. Suzuki, M. Hasegawa, M. Ishii, S. Matsumura, K. Toshima, *Bioorg. Med. Chem. Lett.* **2005**, *15*, 4624–4627.

[40] J. Suh, *Acc. Chem. Res.* **1992**, *25*, 273.

[41] C. E. Yoo, P. S. Chae, J. E. Kim, E. J. Jeong, J. Suh, *J. Am. Chem. Soc.* **2003**, *125*, 14580.

[42] J. Gallagher, O. Zelenko, A. D. Walts, D. S. Sigman, *Biochem.* **1998**, *37*, 2096.

[43] E. Bamann, H. Trapmann, A. Rother, *Chem. Ber.* **1958**, *91*, 1744.

[44] H. Kroll, *J. Am. Chem. Soc.* **1952**, *74*, 2036.

[45] L. Meriwether, F. H. Westheimer, *J. Am. Chem. Soc.* **1956**, *78*, 5119.

[46] K. B. Grant, M. Kassai, *Curr. Org. Chem.* **2006**, *10*, 1035.

[47] D. A. Buckingham, J. P. Collman, D. A. R. Happer, L. G. Marzilli, *J. Am. Chem. Soc.* **1967**, *89*, 1082.

[48] A. Schepartz, B. Cuenoud, *J. Am. Chem. Soc.* **1990**, *112*, 3247.

[49] T. M. Rana, C. F. Meares, *J. Am. Chem. Soc.* **1990**, *112*, 2457.

[50] L. Zhu, N. M. Kostic, *J. Am. Chem. Soc.* **1993**, *115*, 4566–4570.

[51] S. Manka, F. Becker, O. Hohage, W. S. Sheldrick, *J. Inorg. Biochem.* **2004**, *98*, 1947.

[52] A. Erxleben, *Inorg. Chem.* **2005**, *44*, 1082.

[53] M. Kito, Y. Takenaka, R. Urade, *FEBS Lett.* **1995**, *362*, 39.

[54] E. L. Hegg, J. N. Burstyn, *J. Am. Chem. Soc.* **1995**, *117*, 7015.

[55] B. Jang, J. Suh, *Bull. Korean Chem. Soc.* **2008**, *29*(1), 202.

[56] S. W. Jang, J. Suh, *Org. Lett.* **2008**, *10*, 481.

[57] H. M. Kim, B. Jang, Y. E. Cheon, M. P. Suh, J. Suh, *J. Biol. Inorg. Chem.* **2009**, *14*, 151.

[58] B.-B. Jang, K.-P. Lee, D.-H. Min, J. Suh, *J. Am. Chem. Soc.* **1998**, *120*, 12008.

[59] M.-G. Kim, H.-M. Kim, J. Suh, *Bull. Korean Chem. Soc.* **2011**, *32*, 3113.

[60] S. H. Yoo, B. J. Lee, H. Kim, J. Suh, *J. Am. Chem. Soc.* **2005**, *127*, 9593–9602.

[61] H. Kim, H. Paik, M.-S. Kim, Y.-S. Chung, J. Suh, *Bioorg. Med. Chem. Lett.* **2002**, *12*, 2557.

[62] J. Suh, S. H. Yoo, M. G. Kim, K. Jeong, J. Y. Ahn, M.-s. Kim, P. S. Chae, T. Y. Lee, J. Lee, J. Lee, Y. A. Jang, E. H. Ko, *Angew. Chem. Int. Ed.* **2007**, *46*, 7064.

[63] K. Jeong, W. Y. Chung, Y.-S. Kye, D. Kim, *Bioorg. Med. Chem.* **2010**, *18*, 2598.

[64] W. Chei, H. Ju, J. Suh, *Bioorg. Med. Chem. Lett.* **2012**, *22*, 1533.

[65] W.-H. Wu, P. Lei, Q. Liu, J. Hu, A. P. Gunn, M.-S. Chen, Y.-F. Rui, X.-y. Su, Z.-P. Xie, Y.-F. Zhao, A. I. Bush, Y.-M. Li, *J. Biol. Chem.* **2008**, *283*, 31657.

[66] B. K. Takasaki, J. H. Kim, E. Rubin, J. Chin, *J. Am. Chem. Soc.* **1993**, *115*, 1157–1159.

[67] J. H. Kim, J. Britten, J. Chin, *J. Am. Chem. Soc.* **1993**, *115*, 3618.

[68] W. S. Chei, H. Ju, J. Suh, *J. Biol. Inorg. Chem.* **2011**, *16*, 511.

[69] M. B. Rao, A. M. Tanksale, M. S. Ghatge, V. V. Deshpande, *Microbiol. Mol. Biol. Rev.* **1998**, *62*, 597.

[70] O. Kirk, T. V. Borchert, C. C. Fuglsang, *Curr. Opin. Biotechnol.* **2002**, *13*, 345.

[71] M. Schnolzer, P. Jedrzejewski, W. D. Lehmann, *Electrophoresis* **1996**, *17*, 945.

[72] J. J. Thomas, R. Bakhtiar, G. Siuzdak, *Acc. Chem. Res.* **2000**, *33*, 179.

[73] T. Durek, C. F. W. Becker, *Biomol. Eng.* **2005**, *22*, 153.

[74] D. P. Greiner, K. A. Hughes, A. H. Gunasekera, C. F. Meares, *Proc. Natl. Acad. Sci.* **1996**, *93*, 71.

[75] T. Heyduk, E. Heyduk, K. Severinov, H. Tang, R. H. Ebright, *Proc. Natl. Acad. Sci.* **1996**, *93*, 10162.

[76] H. Ding, X. Wang, S. Zhang, X. Liu, *J. Nanopart. Res.* **2012**, *14*, 1254.

[77] Z. Ahmad, A. Shah, M. Siddiq, H.-B. Kraatz, *RSC Adv.* **2014**, *4*, 17028.

[78] F. Mancin, P. Scrimin, P. Tecilla, U. Tonellato, *Coord. Chem. Rev.* **2009**, *253*, 2150.

[79] F. M. Menger, L. H. Gan, E. Johnson, D. H. Durst, *J. Am. Chem. Soc.* **1987**, *109*, 2800.

[80] J. Zhang, X.-G. Meng, X.-C. Zeng, X.-Q. Yu, *Coord. Chem. Rev.* **2009**, *253*, 2166.

[81] E. Kimura, H. Hashimoto, T. Koike, *J. Am. Chem. Soc.* **1996**, *118*, 10963.

[82] B. Gruber, E. Kataev, J. Aschenbrenner, S. Stadlbauer, B. König, *J. Am. Chem. Soc.* **2011**, *133*, 20704.

[83] J. Suh, *Acc. Chem. Res.* **2003**, *36*, 562.

[84] J. W. Jeon, S. J. Son, C. E. Yoo, I. S. Hong, J. Suh, *Bioorg. Med. Chem.* **2003**, *11*, 2901.

[85] K.-H. Mayer, H. Stetter, *Chem. Ber.* **1960**, *94*, 1410.

[86] S. Aoki, H. Kawatani, T. Goto, E. Kimura, M. Shiro, *J. Am. Chem. Soc.* **2001**, *123*, 1123.

[87] T. Gunnlaugsson, J. P. Leonard, *Chem. Commun.* **2005**, (25), 3114.

[88] S. Li, J.-X. Chen, Q.-X. Xiang, L.-Q. Zhang, C.-H. Zhou, J.-Q. Xie, L. Yu, F.-Z. Li, *Eur. J. Med. Chem.* **2014**, *84*, 677.

[89] C. S. Rossiter, R. A. Mathews, J. R. Morrow, *J. Inorg. Biochem.* **2007**, *101*, 925.

[90] J. Hormann, C. Perera, N. Deibel, D. Lentz, B. Sarkar, N. Kulak, *Dalton Trans.* **2013**, *42*, 4357.

[91] X. Sheng, X. M. Lu, Y. T. Chen, G. Y. Lu, J. J. Zhang, Y. Shao, F. Liu, Q. Xu, *Chem. Eur. J.* **2007**, *13*, 9703.

[92] J. Hormann, M. van der Meer, B. Sarkar, N. Kulak, *Eur. J. Inorg. Chem.* **2015**, 4722.

[93] M. Suchý, R. H. E. Hudson, *Eur. J. Org. Chem.* **2008**, *2008*, 4847.

[94] C. S. Rossiter, R. A. Mathews, I. M. A. del Mundo, J. R. Morrow, *J. Inorg. Biochem.* **2009**, *103*, 64.

[95] L. Borjesson, C. J. Welch, *Acta Chem. Scand.* **1991**, *45*, 621.

[96] L. Echegoyen, R. C. Lawson, C. Lopez, *J. Org. Chem.* **1994**, *59*, 3814.

[97] C. S. Rossiter, R. A. Mathews, J. R. Morrow, *Inorg. Chem.* **2005**, *44*, 9397.

[98] J. Massue, S. E. Plush, C. S. Bonnet, D. A. Moore, T. Gunnlaugsson, *Tetrahedron Lett.* **2007**, *48*, 8052.

[99] W. C. Baker, M. J. Choi, D. C. Hill, J. L. Thompson, P. A. Petillo, *J. Org. Chem.* **1999**, *64*, 2683–2689.

[100] R. Herges, A. Dikmans, U. Jana, F. Kohler, P. G. Jones, I. Dix, T. Fricke, B. König, *Eur. J. Org. Chem.* **2002**, *2002*, 3004.

[101] G. Brand, M. W. Hosseini, R. Ruppert, *Helv. Chim. Acta* **1992**, *75*, 721.

[102] E. Keegstra, J. Zwikker, M. Roest, *J. Org. Chem.* **1992**, *57*, 6678–6680.

[103] F. Vögtle, F. Ley, *Chem. Ber.* **1983**, *116*, 3000.

[104] W. Raßhofer, F. Vögtle, *Liebigs Ann. Chem.* **1977**, 1340.

[105] L. M. De León-Rodríguez, Z. Kovacs, A. C. Esqueda-Oliva, A. D. Miranda-Olvera, *Tetrahedron Lett.* **2006**, *47*, 6937.

[106] S. J. Lippard, J. M. Berg, *Principles of Bioinorganic Chemistry*, University Science Books, Mill Valley, **1994**, S. 28–31.

[107] E. U. Akkaya, A. W. Czarnik, *J. Phys. Org. Chem.* **1992**, *5*, 540.

[108] R. W. Hay, B. Jeragh, *Trans. Met. Chem.* **1979**, *4*, 288.

[109] D. H. Vance, A. W. Czarnik, *J. Am. Chem. Soc.* **1993**, *115*, 12165.

[110] R. Clay, P. Murray-Rust, J. Murray-Rust, *Acta. Cryst.* **1979**, *B35*, 1894.

[111] P. C. Griffiths, I. A. Fallis, C. James, I. R. Morgan, G. Brett, R. K. Heenan, R. Schweins, I. Grillo, A. Paul, *Soft Matter* **2010**, *6*, 1981.

[112] H. Schägger, *Nat. Protoc.* **2006**, *1*, 16.

[113] C. Perera, *Synthese und biologische Evaluation von Cyclen- basierten Metalloproteasen*, Freie Universität, Berlin, Master thesis, **2012**, S. 16.

[114] A. H. van Den Oord, J. J. Wesdorp, A. F. Van Dam, J. A. Verheij, *European J. Biochem.* **1969**, *10*, 140.

[115] S. Nagao, H. Osuka, T. Yamada, T. Uni, Y. Shomura, K. Imai, Y. Higuchi, S. Hirota, *Dalton Trans.* **2012**, *41*, 11378.

[116] Y. Jin, J. A. Cowan, *J. Am. Chem. Soc.* **2005**, *127*, 8408.

[117] L. Zhang, Y. Mei, Y. Zhang, L. Shuan, X. Sun, L. Zhu, *Inorg. Chem.* **2003**, *42*, 492.

[118] N. Mogharrab, H. Ghourchian, M. Amininasab, *Biophys. J.* **2007**, *92*, 1192.

[119] T. P. Lo, M. E. P. Murphy, J. G. Guillemette, M. Smith, G. D. Brayer, *Protein Sci.* **1995**, *4*, 198.

[120] M. A. Augustin, Y. J. K., *Inorg. Chim. Acta* **1979**, 11–18.

[121] K. Rajasekhar, M. Chakrabarti, T. Govindaraju, *Chem. Commun.* **2015**, *51*, 13434.

[122] T. Chakraborty, I. Chakraborty, S. Ghosh, *Arab. J. Chem.* **2011**, *4*, 265.

[123] A. I. Mitsionis, T. C. Vaimakis, *Chem. Phys. Lett.* **2012**, *547*, 110.

[124] K. Bouchemal, F. Agnely, A. Koffi, M. Djabourov, G. Ponchel, *J. Mol. Recognit.* **2010**, *23*, 335.

[125] J. K. Kalyanasundaram, K. Thomas, *J. Am. Chem. Soc.* **1977**, *99*, 2039.

[126] R. S. Kumar, P. Paul, A. Riyasdeen, G. Wagniéres, H. van den Bergh, M. A. Akbarsha, S. Arunachalam, *Colloids Surf., B.* **2011**, *86*, 35.

[127] R. Konuk, J. Cornelisse, S. P. Mcglynn, *J. Phys. Chem.* **1989**, *101*, 7405.

[128] T. Förster, *Ann. Phys. (Berlin)* **1946**, *33*, 166.

[129] H. Sahoo, *J. Photochem. Photobiol., C.* **2011**, *12*, 20.

[130] S. S. Berr, R. R. M. Jones, *J. Phys. Chem.* **1989**, *93*, 2555.

[131] N. Muller, *Langmuir* **1993**, *9*, 96.

[132] H.-U. Kim, K.-H. Lim, *Colloids Surf., A* **2004**, *135*, 121.

[133] C. Soto, M. C. Brahes, J. Alvarez, N. C. Inestrosa, *J. Neurochem.* **1994**, *63*, 1191.

[134] P. C. Griffiths, I. A. Fallis, D. J. Willock, A. Paul, C. L. Barrie, P. M. Griffiths, G. M. Williams, S. M. King, R. K. Heenan, R. Görgl, *Chem. Eur. J.* **2004**, *10*, 2022.

[135] B. K. Mishra, P. Mukherjee, S. Dash, S. Patel, H. N. Pati, *Synthetic Commun.* **2009**, *39*, 2529.

[136] G. Stones, R. Tripoli, C. L. McDavid, K. Roux-Duplâtre, A. R. Kennedy, D. C. Sherrington, C. L. Gibson, *Org. Biomol. Chem.* **2008**, *6*, 374.

[137] P. L. Anelli, F. Montanari, S. Quici, *J. Org. Chem.* **1988**, *53*, 5292.

[138] H. F. Bauer, W. C. Drinkard, *J. Am. Chem. Soc.* **1960**, *82*, 5031–5032.

Appendix — Compound directory

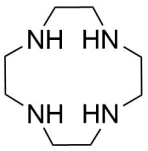

1

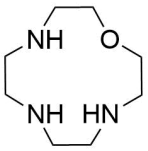

2

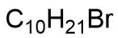

3

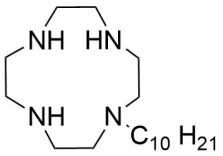

4

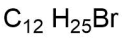

5

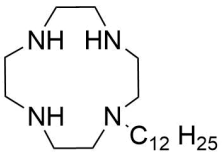

6

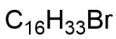

7

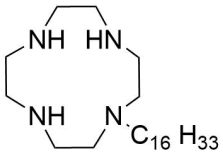

8

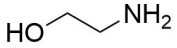

9

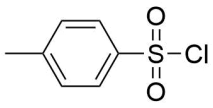

10

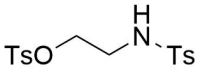

11

12

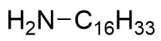

13

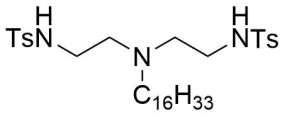

14

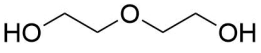

15

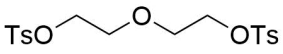

16

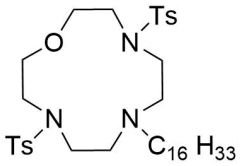

17

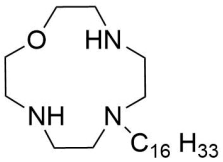

18

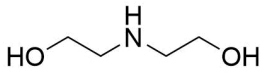

19

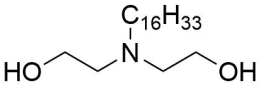

20

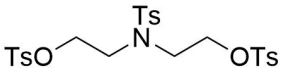

21

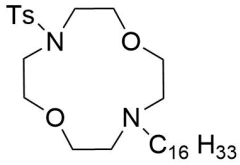

22

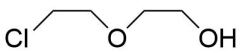

23

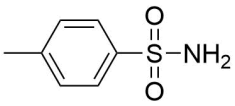

24

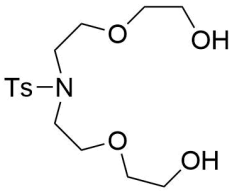

25

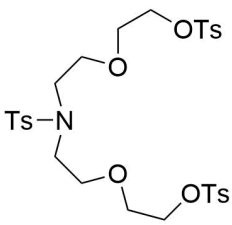

26

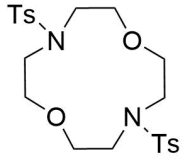

27

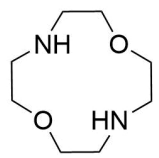

28

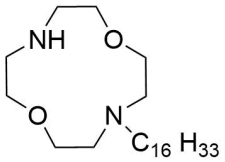

29

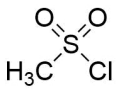

30

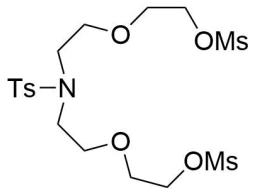

31

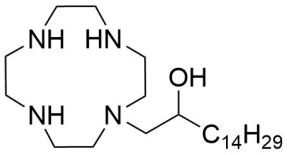

32

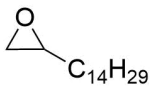

33

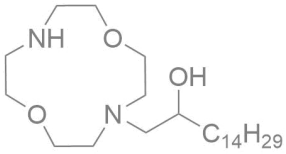

34

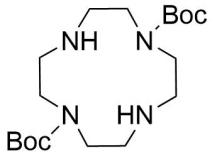

35

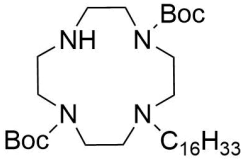

36

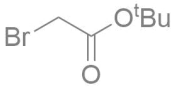

37

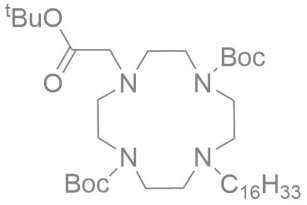

38

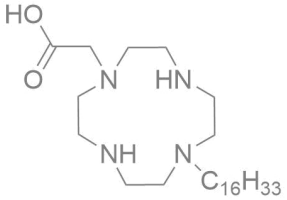

39

Grey compounds could not be synthesized and 12 compounds were commercially available (**1, 3, 5, 7, 9, 10, 13, 15, 19, 23, 24, 30**).